

# Thermal Properties, Sizes, and Size Distribution of Jupiter-Family Cometary Nuclei

Y. R. Fernández<sup>a</sup>, M. S. Kelley<sup>b</sup>, P. L. Lamy<sup>c</sup>, I. Toth<sup>c,d</sup>, O. Groussin<sup>c</sup>, C. M. Lisse<sup>e</sup>,  
M. F. A'Hearn<sup>b</sup>, J. M. Bauer<sup>f</sup>, H. Campins<sup>a</sup>, A. Fitzsimmons<sup>g</sup>, J. Licandro<sup>h</sup>, S. C. Lowry<sup>i</sup>,  
K. J. Meech<sup>j</sup>, J. Pittichová<sup>f</sup>, W. T. Reach<sup>k</sup>, C. Snodgrass<sup>l</sup>, H. A. Weaver<sup>e</sup>

<sup>a</sup> Dept. of Physics, Univ. of Central Florida, 4000 Central Florida Blvd., Orlando, FL 32816-2385, U.S.A. +1-407-823-6939, yan@ucf.edu

<sup>b</sup> Dept. of Astronomy, Univ. of Maryland, College Park, MD 20742-2421, U.S.A.

<sup>c</sup> Aix Marseille Université, CNRS, Laboratoire d'Astrophysique de Marseille UMR 7326, 13388, Marseille, France

<sup>d</sup> Konkoly Observatory MTA CSFK CSI, PO Box 67, H-1525 Budapest, Hungary

<sup>e</sup> Applied Physics Laboratory, Johns Hopkins Univ., 11100 Johns Hopkins Rd., Laurel, MD 20723, U.S.A.

<sup>f</sup> Jet Propulsion Laboratory, California Institute of Technology, 4800 Oak Grove Drive, Pasadena, CA 91109, U.S.A.

<sup>g</sup> Astrophysics Research Centre, School of Physics and Astronomy, Queen's Univ., Belfast BT7 1NN, U.K.

<sup>h</sup> Instituto de Astrofísica de Canarias, c/Via Lactea s/n, 38200 La Laguna, Spain

<sup>i</sup> School of Physical Sciences, Univ. of Kent, Canterbury CT2 7NH, U.K.

<sup>j</sup> NASA Astrobiology Institute, Institute for Astronomy, Univ. of Hawai'i, 2680 Woodlawn Dr., Honolulu, HI 96822, U.S.A.

<sup>k</sup> Stratospheric Observatory for Infrared Astronomy, NASA/Ames Research Center, Moffet Field, CA 94035, U.S.A.

<sup>l</sup> Max-Planck-Institut für Sonnensystemforschung, Max-Planck-Str. 2, 37191 Katlenburg-Lindau, Germany

**To appear in the journal *Icarus*.**

**Accepted July 13, 2013.**

**DOI: 10.1016/j.icarus.2013.07.021**

arXiv preprint version 1 - July 23, 2013

## Abstract

We present results from SEPPCoN, an on-going Survey of the Ensemble Physical Properties of Cometary Nuclei. In this report we discuss mid-infrared measurements of the thermal emission from 89 nuclei of Jupiter-family comets (JFCs). All data were obtained in 2006 and 2007 using imaging capabilities of the Spitzer Space Telescope. The comets were typically 4 to 5 AU from the Sun when observed and most showed only a point-source with little or no extended emission from dust. For those comets showing dust, we used image processing to photometrically extract the nuclei. For all 89 comets, we present new effective radii, and for 57 comets we present beaming parameters. Thus our survey provides the largest compilation of radiometrically-derived physical properties of nuclei to date. We have five main conclusions: (a) The average beaming parameter of the JFC population is  $1.03 \pm 0.11$ , consistent with unity; coupled with the large distance of the nuclei from the Sun, this indicates that most nuclei have Tempel 1-like thermal inertia. Only two of the 57 nuclei had outlying values (in a statistical sense) of infrared beaming. (b) The known JFC population is not complete even at 3 km radius, and even for comets that approach to  $\sim 2$  AU from the Sun and so ought to be more discoverable. Several recently-discovered comets in our survey have small perihelia and large (above  $\sim 2$  km) radii. (c) With our radii, we derive an independent estimate of the JFC nuclear cumulative size distribution (CSD), and we find that it has a power-law slope of around  $-1.9$ , with the exact value depending on the bounds in radius. (d) This power-law is close to that derived by others from visible-wavelength observations that assume a fixed geometric albedo, suggesting that there is no strong dependence of geometric albedo with radius. (e) The observed CSD shows a hint of structure with an excess of comets with radii 3 to 6 km. (f) Our CSD is consistent with the idea that the intrinsic size distribution of the JFC population is not a simple power-law and lacks many sub-kilometer objects.

*Keywords: Comets, nucleus – Comets, dust – Infrared Observations*

## 1. Introduction

While comets are the most-observable, most-pristine remnants leftover from the era of Solar System formation, it is still necessary to understand their subsequent evolution if we are to fully take advantage of what comets can tell us about the compositional and thermophysical conditions of the protoplanetary disk. Jupiter-family comets (JFCs) – also known as ecliptic comets (Levison 1996) – are remnants of the icy planetesimals that existed during the era of planet formation. There is dynamical evidence that today’s JFCs come to the inner Solar System from the scattered disk of objects in the trans-Neptunian region (e.g. Duncan et al. 2004), although the precise origin location of the JFCs is a subject of ongoing dynamical and compositional study (A’Hearn et al. 2012). The relationships between JFCs and trans-Neptunian objects (TNOs), and in particular the scattered disk objects (SDOs), are reviewed in detail elsewhere (e.g. by Lowry et al. (2008)), but suffice to mention here that the objects themselves (as JFCs and as SDOs) have suffered evolutionary processes such as collisions and devolatilization since their formation (see e.g. Farinella and Davis 1996, Kenyon et al. 2008, Meech and Svoreň 2004). The properties of today’s JFC population reflect this history. Thus our overarching goal is to use the JFC population to understand cometary evolution.

To this end, our team initiated SEPPCoN – a “Survey of the Ensemble Physical Properties of Cometary Nuclei” – in 2006 to build up a statistically-significant database of nuclear radii, albedos, shapes, and thermal parameters. SEPPCoN is different from previous surveys in that it makes use of mid-infrared observations of thermal emission in conjunction with non-simultaneous visible-wavelength observations to obtain a clearer picture of the thermophysical properties of cometary nuclei. While we aim to understand individual comets as much as possible, the greater goal is to infer the ensemble properties of nuclei.

One ensemble property that has been discussed extensively recently is the JFC size distribution. It is important to establish the character of the distribution since its shape will depend not only on the original distribution of object properties in the source region but also on the comets’ mass loss since reaching the inner Solar System. The mass loss occurs not only through the ‘typical’ cometary activity but also by the shedding of small (cm-size) and large (meter-size and up) fragments that over time can radically alter a comet’s shape, size, and spin (Boehnhardt 2004, Chen and Jewitt 1994, Fernández 2009, Reach et al. 2007).

In the recent past, there have been several studies of the size distribution of active nuclei (e.g. Lowry et al. 2003, Weissman and Lowry 2003, Lamy et al. 2004, Meech et al. 2004, Tancredi et al. 2006, Fernández and Morbidelli 2006, Snodgrass et al. 2011 Weiler et al. 2011, Fernández and Sosa 2012) and of dormant or extinct comets (e.g. Alvarez-Candal and Licandro 2006, Whitman et al. 2006). All these studies have made use of visible-wavelength magnitudes of objects. Since the magnitude is proportional to the product of the geometric albedo and the square of the effective radius, these studies included an assumption about albedo. With SEPPCoN’s Spitzer observations, we have created an entirely new and independent estimate of the JFC size distribution without the need to make a critical albedo assumption, since for low-albedo objects the mid-IR flux is largely independent of it.

Another important ensemble property to address is the physical structure of the nuclei.

The structure of a nucleus today is a result of both the original cometary aggregation process and the subsequent evolution due to collisions and mass loss. Traditionally it has been difficult to investigate via remote sensing all the details of a nucleus’s structure. The Deep Impact impactor experiment on comet 9P/Tempel 1 provided much insight, showing that, for example, its nucleus must be a highly-porous object (Richardson et al. 2007, Ernst and Schultz 2007). One important quantity that can be investigated remotely is the thermal inertia, i.e. the geometric mean of the thermal conductivity and the volumetric heat capacity, or in other words the thermal memory of a nucleus’s surface. For example, the Deep Impact spacecraft was able to obtain thermal mapping of 9P/Tempel 1’s surface, revealing that the thermal inertia must be low (Groussin et al. 2007), and that in fact there is likely severe thermal decoupling between surface ice and surrounding rock (Sunshine et al. 2006). Deep Impact obtained similar data on comet 103P/Hartley 2, revealing again a low-thermal inertia nucleus (Groussin et al. 2013). These results are consistent with studies of other cometary nuclei that have been done using ground-based mid-IR observations (e.g. Campins et al. 1995, Fernández 1999, Fernández et al. 2006). The survey we present here represents the first systematic investigation of thermal inertia across a large number – dozens – of comets.

Some results on individual nuclei in our survey have appeared already (Groussin et al. 2009, Licandro et al. 2009). In this paper we present results for all of the survey’s sample, and also present the distributions of JFC nucleus size and thermal behavior. In §2, we discuss the observations and reduction, and in §3, we describe the data analysis techniques. We show the distributions in §4 and discuss some interpretations. This paper focusses on the nuclei; a companion paper by Kelley et al. (2013) discusses the observed extended emission from dust and the properties of the grains.

## 2. Observations and Reduction

Our program was approved for observation with the Spitzer Space Telescope (Werner et al. 2004) during General Observer Cycle 3, from July 2006 to July 2007, as program #30908. We used the Multiband Imaging Photometer for Spitzer (MIPS; Rieke et al. 2004) and the InfraRed Spectrograph (IRS; Houck et al. 2004).

SEPPCoN was designed to study a significant fraction of the known JFC population so as to overcome any biases from small-number statistics. In early 2006, when the survey was proposed, there were just over 300 known JFCs, so our goal was to have a sample size logarithmically within half an order of magnitude of this number. For our purposes, we simplistically defined a JFC as any short-period comet with Tisserand invariant  $T_J$  between 2 and 3, excluding active Centaurs. (One Centaur with perihelion  $q$  slightly above the 5.2 AU cutoff was inadvertently included in the sample however.) Our choice of targets was constrained by other conditions: First, the comet had to be greater than 4 AU from the Sun when it would be visible by Spitzer in Cycle 3, since we wanted to minimize the contamination by coma. Second, the nucleus had to have an expected brightness that would require no more than one hour of clock time to detect with MIPS or 2.5 hours of clock time to detect with IRS. Our desired minimum detection threshold was  $5\sigma$ . Third, we excluded comets that were likely to have very poor ephemerides with position uncertainties greater

than a few arcminutes. Fourth, we excluded most comets that had already had their nucleus characterized by other mid-IR observations or by spacecraft visits. While the second and third criteria certainly biased our sample selection, they were necessary to create a feasible sample. Still, it is important to acknowledge that the criteria mean that we would tend to avoid observing relatively small (sub-km) nuclei, exactly the nuclei that would provide the most help in finding the true size distribution.

With these parameters, we found 100 targets, about one-third of the total then known. Currently (at time of writing) there are over 450 known<sup>1</sup>, but our survey still represents a significant fraction, and is still so far the largest study of JFC physical properties in the infrared. The target list is given in Table 1, along with the geometry of each target and the clock time duration of each observation (“astronomical observation request”, or AOR, in Spitzer jargon). Orbital properties of the targets can be found in the companion paper by Kelley et al. (2013) and so are not reproduced here.

**Table 1**

Each comet was observed with either IRS or MIPS. IRS observations made use of peak-up (PU) imaging mode in both the “blue” and “red” channels, corresponding to monochromatic wavelengths of 15.77 and 22.33  $\mu\text{m}$  (after color correction). Those channels throw light onto separate sections of a 128-by-128 pixel Si:As array. The blue section is 44-by-31 pixels (80-by-56 arcsec with 1.8-arcsec wide pixels), and the red section is 46-by-30 pixels (82-by-54 arcsec with same size pixels). Observations in either array made use of a five-point dither pattern to improve image quality. Integration times of individual exposures were 14 seconds, so the total integration time on a particular comet in a single channel was  $14 \times 5 \times n_{cyc}$  seconds, where  $n_{cyc}$  is the number of cycles requested and which ranged from 1 to 50, depending on how bright we anticipated the nucleus would be in the blue or red passbands. During an AOR, the telescope was tracked at the comet’s rate. Having two bands allowed us to identify comets both by the motion and by the color. In all, 64 of the 100 comets were targeted with IRS.

Comets for which the  $3\sigma$  ephemeris uncertainty was thought to be larger than about 30 arcsec were observed instead with MIPS, with its larger field of view. Each such comet was observed twice with MIPS (once with the comet centered in the field and again later as a “shadow” observation) so that we could identify the comet by its motion. We used MIPS’s 24  $\mu\text{m}$  channel (monochromatic wavelength 23.68  $\mu\text{m}$  after color correction), which makes use of a 128-by-128 pixel Si:As array with a field of view of 5.4 arcmin (with 2.55-arcsec wide pixels). Observations with MIPS used a 14-point dither pattern to improve image quality. Integration times of individual exposures were 10 seconds, so the total integration time on a particular comet was  $10 \times 14 \times n_{cyc}$  seconds, where  $n_{cyc}$  is the number of cycles requested, ranging from 1 to 18, depending on how bright we anticipated the nucleus would be in the passband. The telescope tracked the comet’s apparent motion during an AOR. In all, 36 of the 100 comets were targeted with MIPS.

Once the observations were taken, the individual exposures were processed by the Spitzer Science Center’s own pipeline. For IRS data, this was version S17.0.0, and for MIPS data,

---

<sup>1</sup> See <http://www.physics.ucf.edu/~yfernandez/cometlist.html> for a list.

this was version S17. We then used these data products to perform further processing, i.e. extra flat-fielding and stacking of all images into the comet’s reference frame. Our resulting images are shown in Figs. 1 and 2, for IRS and MIPS observations, respectively.

**Fig. 1**

Not all 100 comets in our sample were detected. Comets 43P, 54P, 120P, 141P, 240P/2002 X2, 243P/2003 S2, and P/2003 S1 were not detected by IRS, so in total 57 out of the 64 targets were seen. Comets 203P/1999 WJ<sub>7</sub>, 244P/2000 Y3, P/1998 VS<sub>24</sub>, and P/2004 T1 were not detected by MIPS, so in total 32 out of the 36 targets were seen. Thus, out of our original 100 targets, we have detections of 89 of them, a good success rate.

**Fig. 2**

Among the 11 other comets, there are a few reasons for their non-detection. Comet 141P was not seen because the comet was outside the field of view; Spitzer was using an incorrect ephemeris (possibly because the comet had split in the 1990s and the ephemeris was for the original comet, not one of its fragments). Comet 240P had not yet been recovered when the observations occurred, but by using the newer, two-apparition orbit, we see that the comet would not have been in the IRS field of view. Comets 203P, 243P, and 244P had likewise not been recovered, but the two-apparition orbit indicates that Spitzer was pointed in the correct directions. Presumably these nuclei were too faint to be seen, and so we obtained upper-limit photometry. Comets 43P, 54P, and 120P – already having multi-apparition orbits by the time of the Spitzer observations – are likewise simply too faint to be detected, so we obtained upper-limit photometry for them as well. That leaves the three single-apparition comets – P/1998 VS<sub>24</sub>, P/2003 S1, and P/2004 T1 – that (at time of writing) have yet to be recovered. The reason for the non-detection could be either faintness or incorrect ephemeris; we provide upper limits for these objects on the assumption that the former reason is correct.

### 3. Analysis

#### 3.1. Photometric Nucleus Extraction

A notable property of many of the comets in Figs. 1 and 2 is the extended emission due to dust despite the great heliocentric distance of the comets at the time. Of the 57 detected IRS comets, 34 were bare but 23 had discernible dust. Of the 32 detected MIPS comets, 20 were bare but 12 had discernible dust. The properties of the dust from these 35 comets with dust are discussed in the companion paper by Kelley et al. (2013). For this paper, where we focus on the properties of the nuclei, we performed image processing techniques to photometrically extract the point-source nucleus out of each image. We describe this procedure below.

One technique that we employed was a “coma-fitting technique”, which was developed by several of our team members and has been in successful use for many years with many images of comets (e.g. Lamy et al. 1996, 1998a, 2004, Lisse et al. 1999, Groussin et al. 2004, 2009, Stansberry et al. 2004). In particular, this technique allowed us to correctly predict the nuclear radii of comets 19P/Borrelly (Lamy et al. 1998b), 81P/Wild 2 (Fernández 1999), 9P/Tempel 1 (Fernández et al. 2003; Lisse et al. 2005), and 103P/Hartley 2 (Lisse et al. 2009) before their spacecraft flybys.

The technique uses the radial profiles of surface-brightness in the parts of the coma and/or tail away from the comet’s head to extrapolate the dust’s contribution to the flux in

the pixels that are within the head. The radial profiles are assumed to follow power-laws. Ideally, after accounting for the dust’s flux, a point-source remains, which is interpreted as having the flux from the nucleus. The technique is described in detail by (e.g.) Lamy et al. (2004) and Lisse et al. (2009).

This method does assume that the dust’s photometric behavior is consistent all the way in to the coma-nucleus boundary. This assumption is most easily confirmed when the spatial resolution is good, so that one can actually see what the dust is doing closer and closer to the nucleus. In this regard, the Spitzer data are not optimal since the pixels are large and the comets are far away. For example, for  $\Delta = 4$  AU, one IRS pixel covers 5200 km and one MIPS pixel covers 7400 km. However, the method also works well when there is high contrast between the point-source nucleus and the dust. Fortunately this is the case for many of our dusty images in Figs. 1 and 2 – there is often such a strong point-source within the dust that even the first Airy ring shows up clearly. This gives us confidence that our extractions yield realistic estimates of the nuclear flux. In later sections of this paper we will mention instances where our results are consistent with the assumption that our extractions have been successful.

The other processing technique that was applied is related to the coma-fitting technique, but attacks the problem by fitting and subtracting a range of scaled point-spread functions (PSFs) from the image. The criterion for quality is that the net image must still have a plausibly-shaped dust coma and tail; for example, the resulting dust cannot have a sharp drop in brightness near the photocenter. As before, the photometry of the subtracted PSF is interpreted as the nucleus’s flux. This approach has the advantage of not relying on a single power-law to describe the dust’s brightness as a function of cometocentric distance, which is useful when there are strong tails and/or comae whose grains have already deviated from radial motion due to radiation pressure.

Examples of this latter technique are shown in Figs. 3 and 4, which show the 23 IRS comets with extended emission and the 12 MIPS comets with extended emission, respectively. (For the other 54 comets – 34 IRS and 20 MIPS – the extraction of the point-source was trivial.) The six images in each row pertain to a single comet. The first and fourth columns show the comet itself; for IRS images, these are the “blue” and “red” PU images, whereas for MIPS images, these are the images from the two visits, though we note that in nearly all cases the sky-subtracted image is displayed, i.e. the “visit1” image is the image from the first visit minus the sidereally-aligned image from the second visit, and the “visit2” image is the image from the second visit minus the sidereally-aligned image from the first visit. This “shadow” subtraction technique does a great job of cleaning up the sky background near the comet.

The second and fifth columns of Fig. 3 show the best-fitting PSF, which has been scaled to the best overall flux, aligned to the best location, and pixelized to match the IRS or MIPS pixel scale. The third and sixth columns show the subtraction of the previous two images, i.e. the residuals. In other words this shows the comet with no nucleus, only dust. We note that for a few images it was also helpful to remove a planar sky-background. As mentioned, in many cases, the point-source nucleus is quite strong, and is easy to separate. For a few

**Fig. 3**

such cases, the amount of remaining dust has very low surface brightness and is hard to see in an image (e.g., 6P). However for other comets, the point-source is rather faint and/or the flux from dust dominates the total flux from the comet. In those cases, the fractional uncertainty on the nucleus’s flux is naturally higher since it was more difficult to determine a “best” fit.

**Fig. 4**

A more quantitative demonstration of the technique is shown in Fig. 5, where we have taken 10 comets from our sample to show the effects of removing the PSF. Each comet has two panels; the comet’s name and the particular band or visit is written in the panel. The first five pairs of panels show comets observed with IRS; the next five pairs of panels are from comets observed with MIPS. Each panel shows line cuts in the x-direction through the image, best-fitting PSF, and the residual. If the comet’s centroid was in pixel  $(x, y) = (x_c, y_c)$ , then the main plot shows (in grey) line cuts through the image at  $y = y_c$ ,  $y = y_c + 1$ , and  $y = y_c - 1$ . The main plot also shows (in dashed black) line cuts through the best-fitting PSF at those same pixels. The plots below and to the right of the main plot show the residuals. The plot below shows (in grey) line cuts through the residuals at those same  $y$  pixels; the plot to the right shows (in grey) line cuts through the residuals at  $x = x_c$ ,  $x = x_c + 1$ , and  $x = x_c - 1$ .

The first IRS comet and the first MIPS comet in Fig. 5 both have almost all their flux coming from the nucleus; hence the residuals straddle zero. The other eight comets have at least some dust in the residual images and correspond to comets shown in Figs. 3 and 4. The second IRS and second MIPS comets have faint comae and faint point-sources. The third IRS and third MIPS comets have bright comae but still faint point-sources. The fourth IRS and fourth MIPS comets have faint comae but bright point-sources. The fifth IRS and fifth MIPS comets have bright comae and bright point-sources. Thus this figure gives a flavor for our ability to extract point-sources from comets of various signal levels and nucleus-to-coma contrasts.

**Fig. 5**

As a summary of the various strengths of the point-sources within our comet sample, we list in Table 2 each nucleus’s fractional contribution to the overall comet flux (within a 3-pixel radius circular aperture). We note again that a very sizable majority of our sample showed all or nearly all nucleus (zero or almost zero dust). The 35 (out of the 89) nuclei with discernible dust are underlined in the table. We do note that a few of the comets with some dust (e.g. 121P) have nuclei that contribute about 100% of the flux within the aperture anyway; these comets either are (a) faint, so that the dust is visible but quite diffuse, or (b) only showing dust in tails rather than in comae. We also note that some comets without dust (e.g. 79P, 127P, 228P) appear to have fluxes that contribute less than 100% or even more than 100% of the flux. This is not a contradiction; these comets were faint and the flux is obtained from the equivalent best-fitting PSF rather than from the image itself.

**Table 2**

As a self-consistency check we performed the image processing twice, with two subsets of our survey team doing the analysis entirely independently, using completely different codes. In particular, one group predominantly used the coma-fitting technique, with the other using most often the point-source fitting-and-subtraction approach. The final nucleus photometry is reported in Table 3, and those numbers are derived from the combination of these analyses.



We note that each team used the same images for their work – mosaics created from the output of the Spitzer pipeline. In almost all cases, the two groups yielded consistent results. The two independent approaches agreed very well with a 6% mean difference in the IRS photometry and 2% mean difference in the MIPS photometry. Errors reported in Table 3 account for the differences in the results from the two techniques. In ten cases, one analysis yielded clearly spurious results (evident e.g. by a very unlikely color temperature) while the other did not, and so for those comets we used only the more physically plausible result. The reason for the spurious results was the fact that (a) some comets had unusually-shaped dust emission not conducive to characterization by power-laws, and (b) some comets had noisy sky and/or Galactic/extragalactic background sources near the head.

**Table 3**

Before leaving this topic, it is important to emphasize a universal problem that affects most studies of nuclei – not just the study presented here but those already in the literature as well. Jewitt (1991) gives a list of criteria for deciding when one is observing a bare nucleus, one of which is that the “the image should appear unresolved.” But as Jewitt (1991) goes on to discuss, while this is a necessary condition, it is not a sufficient one, and unresolved coma can hide within the seeing disk or PSF. Indeed there is good evidence that this phenomenon occurs frequently with comet 2P/Encke (Fernández et al. 2000, 2005b). Nonetheless, if there is a lack of evidence to the contrary, most workers assume that a point-source is identical to the nucleus even though there is often no way to tell for a given comet if this assumption is true or false. Many of our images presented here (Figs. 1 and 2) show point-sources, and one may hope that the assumption is true, but there is no telling what unexpected dust flux there is within the volume of space covered by the central pixel. Our other images show extractable point-sources embedded in extended dust emission, and while we can make more assumptions about the dust’s behavior, there is again no telling what is really going on within the hundreds or thousands of kilometers within the central pixel. So the general reliability of nucleus photometry will always be suspect at that level if there are no corroborating data that can independently establish the population of dust in the near-nucleus environment. On the other hand, our success at successfully predicting the effective radii of nuclei that are then confirmed with spacecraft flybys (as mentioned at the beginning of this section) gives us confidence that in many cases the point-source photometry is indeed identical to the nucleus’s photometry.

### 3.2. Thermal Modeling

The conversion of mid-infrared photometry to physical properties requires the use of a thermal model. For this work we used the Near-Earth Asteroid Thermal Model (NEATM), created by Harris (1998) and based on the Standard Thermal Model (STM; Lebofsky et al. 1986, Lebofsky and Spencer 1989). We have described our modeling technique in many other works (e.g. Lamy et al. 2004, Fernández et al. 2005a, 2006, 2009) and we only describe here the details that are particular to the present case. The basic premise of the thermal model is that the thermal inertia is very low and so the temperature map of an object’s sunlit surface mainly depends on the instantaneous local zenith angle of the Sun,  $\theta$ . The temperature is maximized at the subsolar point and falls to zero at the terminator as  $\sqrt[4]{\cos\theta}$ . In other words

the night-side retains little thermal memory and so does not normally contribute much to the thermal emission.

The thermal model requires some assumptions: we assumed that (a) the nucleus was spherical, (b) the emissivity was 0.95, (c) the visible-wavelength geometric albedo was 0.04, and (d) the infrared phase darkening follows the behavior described by Harris (1998), i.e. is proportional to the fraction of sunlit hemisphere that is on the Spitzer-facing side. Of these four items, the last three are not likely to influence our results significantly. Emissivity of rock is unlikely to be lower than 0.9. The thermal emission is proportional to one minus the Bond albedo, so as long as the geometric albedo is low the emission is hardly influenced by the actual value. Our observations occurred at low phase angles (9 to 17 degrees) and so our views of the nuclei are almost at “full” phase, requiring relatively small corrections. The sphericity assumption is the one most likely to skew our results, since for example Brown (1985), Lagerros (1996), and Howell et al. (2012) describe how radiometric diameters of asteroids can be miscalculated with spherical models due to shape effects. However currently there is no obvious way to correct for such an effect without better data on the specific objects, so our analysis remains for spherical bodies and their effective radii.

Usually the crucial parameter in the modeling is  $\eta$ , the beaming parameter. This parameter is a proxy for thermal inertia and surface roughness, and traditionally has described the amount of infrared ‘beaming’ that a body has. Objects with zero thermal inertia and no significant topography will have  $\eta = 1$ . Of course many real small bodies have some night-side emission and/or can have non-isotropic emission due to significant surface features such as deep and/or large craters. The former effect lowers the surface temperatures and raises  $\eta$  above 1. The latter effect can make more of their infrared emission ‘beam’ out at smaller opening angles and reduces  $\eta$  below 1. The STM originally assumed a constant value for  $\eta$  but the NEATM lets  $\eta$  float as a parameter to be derived. It is important to either measure  $\eta$  or have a solid assumption for it if one is to obtain radii that are close to reality (Delbo et al. 2007, Harris et al. 2011, Mainzer et al. 2011), as demonstrated from cases where spacecraft visits have tested the analyses of remote observations (e.g. Lisse et al. 2005, 2009).

Of the 100 comets in the survey, 57 were detected by IRS in both wavelengths, 32 comets were detected at just one wavelength by MIPS, and 11 were not detected at all. (None of the IRS comets were detected in just one IRS wavelength.) For the multi-wavelength objects, we performed a two-parameter fit that yielded both the effective radius  $R_N$  and the beaming parameter  $\eta$  (similar to what was done by Groussin et al. (2009) and Licandro et al. (2009)). In this case, since we formally have no degrees of freedom and could fit a two-parameter model perfectly to two data points, we could not use the usual  $\chi^2$  statistic to characterize a goodness-of-fit. To remedy this, we performed multiple model fits to a nucleus’s photometry, requiring that a ‘good’ fit be one where the model passes within  $1\sigma$  of both photometry points. The resulting ranges of parameters that yielded such ‘good’ fits are reported in Table 4.

**Table 4**

For the 32 MIPS comets, we have photometry at only one wavelength, but we have it at two epochs. We modeled each photometry point individually. We performed a one-parameter fit to find  $R_N$  by assuming  $\eta$ , and the value we assumed is  $\eta = 1.03 \pm 0.11$  (which

we explain in §4.1 below). As before, we have no degrees of freedom, so we used the same criterion as above to describe a ‘good’ fit. The resulting effective radii at each epoch are reported in Table 5.

Finally, we note that for the six comets that we did not detect but that were within the field of view, and for the three other undetected comets that could have been in the field of view, we used the  $3\sigma$  upper limits to photometry to derive an upper limit to their radii, using the same assumption for  $\eta$ . These numbers are also in Table 5.

**Table 5**

## 4. Discussion

### 4.1. Beaming Parameters

#### 4.1.1. Means and Distributions

The 57 beaming parameters in Table 4 are represented graphically in the top panel of Fig. 6. This represents the largest collection by far of measured cometary beaming parameters to date. Most of the values are near unity, suggesting that infrared beaming is not significant, that there is little night-side emission from the nuclei, and that the thermal inertia is low – e.g. comparable to the values measured by Groussin et al. (2007, 2013) for Tempel 1 and Hartley 2 from spacecraft data.

**Fig. 6**

We calculated the mean beaming parameter,  $\bar{\eta}$ , by using all 57 points and using  $\chi^2$  minimization – i.e. by making use of the error bars to the individual points. The best fit is  $\bar{\eta} = 1.00 \pm 0.12$ .<sup>2</sup> We note that the error is the error in the mean, not the standard deviation. The minimum  $\chi^2_\nu$  is 1.47 ( $\nu = 56$ ), 49% higher than the expected value. A closer look reveals that about 30% of the  $\chi^2$  comes from just two of the 57 comets, 89P and P/2005 JQ<sub>5</sub>. These two points have very low and very high values of  $\eta$ , respectively, as listed in Table 4. More importantly, they have relatively small error bars – so even though there are comets with even higher  $\eta$ , these two are the farthest outlying comets because of the apparent ostensible high-quality of each measurement. 89P’s  $\eta$  is over  $3\sigma$  below the mean, and P/2005 JQ<sub>5</sub>’s  $\eta$  is over  $3\sigma$  above the mean. With 57 data points, if the beaming parameters were in reality distributed normally about a mean, then we would not expect any points to be that many  $\sigma$  away; for example Chauvenet’s criterion is  $2.6\sigma$ . It is of course the case that  $\eta$  will not be perfectly normally distributed, since  $\eta$  can physically only be so low ( $\sim 0.7$ ) but can be quite high. However for the sample size here we can work on the assumption that the distribution would be approximately normal.

We will discuss comets 89P and P/2005 JQ<sub>5</sub> later, but for now, recalculating  $\bar{\eta}$  without those two outliers yields  $\bar{\eta} = 1.03 \pm 0.11$  with  $\chi^2_\nu = 1.13$ , very close to the expected value of 0.99 for  $\nu = 54$ . We adopt this value of  $\bar{\eta}$  as our final answer, rather than the 1.00 value mentioned above that includes the outliers.

On the top panel of Fig. 6, we have drawn a grey rectangle to represent  $\bar{\eta}$  and its error. Inspection of the points shows good clustering near the mean, but an alternate way to see this is to look at the bottom panel of Fig. 6, where we have plotted each point’s offset in

---

<sup>2</sup> All errors quoted in this paper are  $1\sigma$ .

units of its own  $\sigma$  from  $\bar{\eta}$ . The distribution here is close to what would be expected for a normal distribution. For 55 points, we would expect 37.5 points within  $\pm 1\sigma$  of the mean, and we have 36. We would expect 15 points between  $\pm 1$  and  $\pm 2\sigma$ , and we have 16. We would expect 2.4 points between  $\pm 2$  and  $\pm 3\sigma$  and we have 3. Furthermore, in this representation, 89P and P/2005 JQ<sub>5</sub> are clearly outliers, being more than  $3\sigma$  off.

We can roughly quantify the closeness of the  $\eta$  distribution to a normal distribution by calculating the skew and kurtosis. Since each data point  $\eta_i$  ( $i = 1, \dots, n$ ) has its own error bar  $\sigma_i$ , we calculate skew and kurtosis using  $(\eta_i - \bar{\eta})/\sigma_i$ , instead of  $(\eta_i - \bar{\eta})/\sigma$ , i.e. instead of the standard deviation  $\sigma$ . We also use the best-fitting  $\bar{\eta}$  described above instead of the raw mean (sum of the data divided by the number of entries). Using all 57 data points, we find that the skew is 1.12 and the kurtosis is 3.98. With only 55 data points (excluding 89P and P/2005 JQ<sub>5</sub>), we calculate a skew of 0.97 (little change) and a kurtosis of 0.17 (quite smaller). Press et al. (1992) state that estimates of the standard deviations of the skew and kurtosis are  $\sqrt{15/n}$  and  $\sqrt{96/n}$ , respectively. With  $n = 55$ , the numbers here suggest that our  $\eta$  distribution is perhaps somewhat skewed to the positive side but not radically so, and that the removal of the outliers has removed most of the kurtosis. This is consistent with the assumption stated above that the  $\eta$  distribution is approximately normal.

One may wonder if there is any difference between the beaming parameters among the comets that showed some dust and those that did not, perhaps indicating if there is any overall systematic problem with the nucleus extraction described in §3.1. The two kinds of comets are distinguished in Fig. 6 with filled and unfilled circles. Among the 23 IRS comets that showed dust (i.e., the underlined comets in Table 2 and the open circles in Fig. 6), we find that  $\bar{\eta} = 1.21 \pm 0.24$  with  $\chi^2_\nu = 1.08$  and  $\nu = 22$ . For the 32 IRS comets that did not show dust (excluding 89P and P/2005 JQ<sub>5</sub> from the group of 34, as justified earlier), we find that  $\bar{\eta} = 1.00 \pm 0.11$  with  $\chi^2_\nu = 1.05$  and  $\nu = 31$ . Both of these mean values are consistent with each other. Furthermore, a Student- $t$  test comparison of the two subgroups' means yields a  $t$ -statistic significance of 47%. For the Student- $t$  test, a lower significance implies a greater likelihood for the means to be significantly different. In this case, the significance suggests that the means of the two subgroups are not significantly different.

Since the error bars on  $\eta$  vary widely from comet to comet, we can instead perform this statistical test using the offsets shown in the bottom half of Fig. 6, rather than using the values themselves. In this case, the Student- $t$  test returns a significance for a difference in the means of 1.5%. We can also compare the entire distribution of values by using the Kolmogorov-Smirnov test. Again, a lower significance of the statistic suggests a higher likelihood that the groups are drawn from different distributions. We find that this test yields a significance of 3.7%. Thus both the Student- $t$  and Kolmogorov-Smirnov tests offer a hint that there may be some systematic difference in the  $\eta$  values from comets that showed dust versus those from comets that did not. Since this is unlikely to be a physical effect, it is probably tied to the general problem in extracting nuclei from dusty comets. However, since neither significance crosses the  $3\sigma$  threshold, and since the overall distribution of all  $\eta$  values together mimics a Gaussian, we proceed with an analysis that includes all the comets.

#### 4.1.2. Trends

To investigate whether  $\eta$  showed trends with any observational or orbital parameters, we compared our 57 beaming parameters to a variety of other comet-related quantities. The 16 parameters we tried are listed in Table 6. Using a variety of statistical tests, we found no significant correlations at better than the  $3\sigma$  level between  $\eta$  and any of these 16. We give more detail on the tests below. Scatter plots of four of these 16 quantities are shown in Fig. 7. The plots are of the four that were most likely to reveal a trend: heliocentric distance  $r$ , phase angle  $\alpha$ , perihelion distance  $q$ , and time before perihelion  $d_{peri}$ . With regard to  $r$  and  $d_{peri}$ , it is easier for a cooler object to retain thermal memory, with could be seen as higher  $\eta$ . With regard to  $\alpha$ , such a trend has been reported in near-Earth asteroids by Delbó et al. (2007). With regard to  $q$ , perhaps surface properties are affected by the maximal heating received (as coma gas daughter species appear to be; A’Hearn et al. 1995). Unfortunately, Fig. 7 and Table 6 show that there are no significant correlations.

**Table 6**

Our first test was to try a simple linear regression with  $\eta$  as the ordinate and each of the 16 parameters as the abscissa. The 16 values of the slopes to the fitted lines,  $m$ , are given in the second column of Table 6, and indeed for 13 of the 16 parameters the slopes are within  $1\sigma$  of zero. Two others have  $m$  within  $1.5\sigma$  of zero. The slope of the fit to Spitzer-centric distance,  $\Delta$ , is non-zero at the  $3\sigma$  level, but it is hard to explain why this would be significant if the fits to heliocentric distance and perihelion are not. Also, further tests (explained below) led us to reject any significance to this slope.

For a second test we calculated the Spearman “ $\rho$ ” (Press et al. 1992) to look for a correlation between  $\eta$  and another quantity. This test first makes two ranked lists of  $\eta$  and the independent quantity, and then calculates  $\rho$ , a sum-squared difference of the ranks. This  $\rho$  can be compared to the expected value if there were no correlation. Table 6 lists values of  $Z$ , the number of standard deviations that  $\rho$  is away from this expected value, and  $P_Z$ , the probability that one would by chance get this value of  $Z$  in uncorrelated data. Lower probabilities mean a higher likelihood of a real correlation. For all 16 quantities, there is no value of  $|Z|$  higher than  $3\sigma$  and only one quantity is better than  $2\sigma$ . In particular, there is no correlation of  $\eta$  with  $\Delta$  suggested by this test.

**Fig. 7**

The strongest correlation is with days from perihelion,  $d_{peri}$ , and indeed visual inspection of Fig. 7 suggests that pre-perihelion nuclei, on average, have a slightly lower  $\eta$  compared to post-perihelion nuclei. We calculate that the best-fitting mean (in the  $\chi^2$  sense) of the pre-perihelion  $\eta$  values is  $0.94 \pm 0.12$ ; and of the post-perihelion values,  $1.14 \pm 0.14$ . (These numbers exclude the two outliers 89P and P/2005 JQ<sub>5</sub>.) So the numbers are consistent with the plot, but the difference between the means is only  $0.20 \pm 0.19$ , i.e. not significant. Also, if the correlation were real, one might expect to see a similar correlation with heliocentric or perihelion distance, but there is no evidence for this. So while such a correlation would suggest a difference in a nucleus’s thermal memory post-perihelion vs. pre-perihelion, we conclude that the result is tantalizing but not yet statistically significant.

The Spearman  $\rho$  calculations make no use of the error bars to  $\eta$ , only the measured values themselves. Since for many  $\eta$  the error bars are large, it is possible that the  $\rho$  that we calculate is misleading and just happens to indicate a correlation (with e.g.  $d_{peri}$ ) because

of our luckiness (or unluckiness) in the values. To investigate this, we performed our third test, a modification of the second. We ran a Monte Carlo simulation of our 57 beaming parameters, generating 100,000 sets of 57 values of  $\eta$  based on the error bars assigned to each  $\eta$  (assuming a normal distribution with the error bar representing the sigma). For each set, we then reran the Spearman  $\rho$  calculations against the 16 quantities in Table 6, generating 100,000 values of  $Z$  for each quantity. We then determined what the average value of  $Z$  ( $\bar{Z}$ ) is out of those 100,000 so that we could tell if our particular 57 values of  $\eta$  were indeed fooling us. We also calculated  $\mathcal{N}$ , the fraction of the 100,000 runs that yielded values of  $Z$  that had better than  $3\sigma$  significance.  $\mathcal{N}$  is simply another estimate of our likelihood in being fooled, though a qualitative estimate, since we did not explore the expectation of  $\mathcal{N}$  in detail. These results are given in two columns of Table 6. For 15 of the 16 parameters,  $\bar{Z}$  is always within  $1.1\sigma$  and  $\mathcal{N}$  is under 1%. Only for the correlation with  $d_{peri}$  did this analysis return a more significant  $\bar{Z}$  than  $1\sigma$ , but the value is not beyond the  $3\sigma$  threshold.

For our fourth and final test, we attempted to pull out any correlation with the 16 quantities by dividing the  $\eta$  values into two groups – one group characterized by having low values of the independent variable, and one having high values – and then using a Student- $t$  test to compare the means. The division between “low” and “high” was made at the median value of the independent variable (except for  $d_{peri}$ , where we made the split at  $d_{peri} = 0$ ). A correlation might reveal itself with a significant difference in the means of the two groups. The results of these calculations are given in the last column of Table 6. The significances are high percentages, so there is no statistically significant difference found with this analysis.

In summary, from Table 6 we conclude that there is no statistically significant trend of  $\eta$  vs. any of the other quantities.

We also repeated this entire trend analysis using the subset of the comets that showed no emission from dust, i.e. the 34 comets mentioned earlier, just in case the dusty comets were influencing the results. No statistically significant correlations were found in this case between the 34  $\eta$  values and any of the 16 quantities.

All this implies that our results for  $\eta$  are not strongly dependent on the observational and geometric circumstances, although admittedly for some of the 16 parameters we do not have a wide range of values for the test to be strong. (For example, our range in  $r$  only covers a change in subsolar temperature of  $\sim 30$  K.) Nonetheless, at face value the results suggest that cometary nuclei have little infrared beaming and thermal memory. Indeed the results are consistent with the hypothesis that all JFC nuclei have about the same bulk thermal properties. This would be a very useful result because it means that future snapshot radiometry can be used to derive cometary radii and cross sections with good confidence without worrying about a large uncertainty from an otherwise-unmeasured beaming parameter.

#### 4.1.3. Outliers

While there are individual comets in our survey with ostensibly elevated or diminished values of  $\eta$  – such as 127P, 173P, 213P, etc. – for the most part they have sufficiently large error bars that we cannot claim that they are in reality unusual. As mentioned, the statistics suggest that perhaps only two of the 57 comets (3.4%) have  $\eta$  significantly outside a normal

distribution.

About those two comets, one can ask why 89P and P/2005 JQ<sub>5</sub> could have such unusual results. As shown in Fig. 1, 89P does not appear to have dust, so we might expect the nucleus photometry to be robust. The very low beaming parameter (0.48) could be explained if the red IRS photometry was measured too low, or the blue IRS photometry was measured too high. The bright pixels near the comet in the blue image were not included in the photometry, so that cannot explain it. There was a latent image problem in the red image; if that had been incorrectly removed so that too much background behind the comet was removed, then we might obtain an artificially depressed flux. We would need to inflate the red flux by about 30% to bring 89P’s  $\eta$  to the ensemble average of 1.03, however, and that is more than we would expect to be able to correct the flux by based on any improper latency removal. A 10% error would raise 89P’s  $\eta$  only up to 0.65, still quite low. We currently have no other systemic explanation for why the  $\eta$  is so low. We know of no other published reports about this comet that would shed light on the issue.

As for P/2005 JQ<sub>5</sub>, Fig. 1 again shows that there was no discernible dust. In this case, the beaming parameter is very high (2.72), which could be explained if the red photometry was measured too high, or the blue photometry was measured too low. Another explanation however could be that the comet’s head is showing almost mostly dust and very little nucleus. At the comet’s heliocentric distance, we would expect grains to have a blackbody temperature of about 140 K, and the flux ratio between the red and blue photometry, converted into a Planck-function temperature, is in fact consistent with this –  $143 \pm 7$  K. So it is possible that this comet’s nucleus is even smaller than reported here and we are simply seeing grains of a near-nucleus coma that does not extend past the PSF. It should be pointed out though that this comet’s nucleus was detected at radar wavelengths by Harmon et al. (2006), one of the first to be so observed with delay-Doppler imaging. Their echoes indicate a nucleus of radius 0.7 km, about half the effective radius we report in Table 4. Such a size would provide roughly one-fourth the flux density of what we report in Table 3, consistent with the idea that our observations might be dominated by dust. Interestingly, Harmon et al. (2006) also say that the nucleus’s surface has “extremely rough surface texture at wavelength (decimeter) scales.” Such surface structure argues against a high value of  $\eta$  unless that roughness is smoothed out at  $\sim 10\text{-}\mu\text{m}$  scales.

#### 4.2. Radii and Trends

To analyze our 89 (IRS plus MIPS) new radii, we could just use the values reported in Tables 4 and 5. However, we prefer to make all the radii self-consistent by first recalculating the radii of the 57 IRS comets using an assumed beaming parameter of  $\bar{\eta} = 1.03 \pm 0.11$ , i.e. the same value we used for the MIPS comets.

There are good reasons for this. First, we showed in §4.1 that 55 of the 57 beaming parameters are statistically consistent with  $\eta = 1.03 \pm 0.11$ , i.e. a single value with small error bar, and in fact we also showed that the distribution is quite similar to a Gaussian.

Second, at face value, the range of  $\eta$  among the 57 comets covers more than 1 dex, from about 0.5 to 6. The low end is very low and the high end is very high; indeed there

are virtually no small bodies known with such measured values. If the distribution were telling us something real about comet parameters, it would suggest that cometary surfaces in general are very different from what we have come to believe from spacecraft flybys. Furthermore such radical differences in infrared beaming, conductivity, and thermal inertia for such a small range of radii – about 1.5 dex – seem implausible. We should point out that a Spearman rank correlation calculation does show that nominally there is a trend between the 57 values of  $R_N$  and of  $\eta$  that is significant at the  $3.8\sigma$  level. But, for the two reasons just described, we do not attribute this to a real trend in the surface properties. Using a mean value for all comets is the safer conclusion.

For these reasons we will continue on the assumption that all nuclei can be studied using  $\eta = 1.03 \pm 0.11$ . An example of the benefit of this can be seen by considering comet 173P’s result in Table 4. It is certainly not impossible that this comet really has radius 16 km and large thermal inertia. But it seems much more likely that its  $\eta$  is high because of random error; dropping the  $\eta$  to 1.03 drops the radius (since a lower beaming parameter means the object is hotter overall and so requires a smaller radius to explain a given flux density) and so this in a sense debiases 173P’s ostensible radius to make its entry into a size distribution more appropriate.

The recalculated radii that all use  $\bar{\eta}$  – for MIPS comets and IRS comets alike – are listed in Table 7. The table gives the values that we use to look for trends with other quantities and to create the size distribution. We note that for the multi-epoch MIPS radii, we have combined the two results into one value. If the standard deviation of the two radii was higher than the error bars on the individual measurements, then we assigned the error to be the standard deviation. Otherwise, we assigned the error to be the average of the errors of the individual measurements.

**Table 7**

We first look at some trends in the radii. Figure 8 shows how the radii compare with perihelion distance  $q$ . This is important to understand since it is presumably on average easier to discover the smaller JFCs that happen to approach closer to the Sun and Earth. Therefore we may expect that there would be a trend of greater  $R_N$  with greater  $q$ . From the Spearman  $\rho$  value, we find however that the trend is not significant, yielding a significance at only the  $2.6\sigma$  level. In fact any apparent trend is enhanced perhaps more than it should be by the one comet at the highest perihelion (5.5 AU); without it, the significance is  $2.4\sigma$ . It is also enhanced by our exclusion of some previously-studied, relatively-large, small- $q$  JFCs from the survey (see below).

**Fig. 8**

Figure 8 also shows that there is little difference in the radii among comets for which there was no discernible dust versus those that had discernible dust. The only appreciable difference is in the 3.75- and 4.25-AU bins, where there are not very many comets anyway. A Kolmogorov-Smirnov test of these two subgroups of radii – 54 with no dust and 35 with dust – returns a statistic with significance 51.6%, suggesting that the two subgroups are indeed drawn from the same distribution and that there is no significant difference in the radius distributions. This is an important point since it gives us more confidence about the the quality of the nucleus extraction procedure on the 35 comets that showed dust.

Figures 7 and 8 make it clear that many comets in our sample lie in a restricted range



of perihelia. Fortunately, our sample is not much different from the entire *known* JFC population. This is shown in Fig. 9, which shows the cumulative fractional distribution of perihelia among the 89 detected SEPPCoN comets and all 450 JFCs that were known at time of writing. The curves match quite closely, and a Kolmogorov-Smirnov test yields a statistic with significance of 81%. So while there is certainly a bias in the discovery rate of JFCs, the biases in SEPPCoN are no different.

**Fig. 9**

Fig. 8 also shows graphically the relative number of large, medium, and small nuclei. In particular, the upper left part of the plot is fairly blank. Why are there so few nuclei larger than about 3.0 km with perihelia below 2 AU? This is partly a result of our excluding from the survey several comets that have already been characterized. In particular, there are nine nuclei we excluded whose effective radii have been measured by spacecraft flybys or by earlier mid-IR photometry. Those nine radii are: 2.4 km for 2P/Encke (Fernández et al. 1999, Harmon and Nolan 2005), 3.0 km for 9P/Tempel 1 (A’Hearn et al. 2005), 5.2 km for 10P/Tempel 2 (A’Hearn et al. 1989), 2.2 km for 19P/Borrelly (Soderblom et al. 2002), 10.7 km for 28P/Neujmin 1 (Campins et al. 1987), 4.6 km for 49P/Arend-Rigaux (Campins et al. 1995, Millis et al. 1988), 2.0 km for 67P/Churyumov-Gerasimenko (Lamy et al. 2008), 2.1 km for 81P/Wild 2 (Brownlee et al. 2004, Duxbury et al. 2004), and 1.0 km for 103P/Hartley 2 (A’Hearn et al. 2011, Lisse et al. 2009). All of these comets have  $q < 2$  AU, and all but one of them have radii above our SEPPCoN sample median of 1.4 km. So they would fill in some of the sparser area in Fig. 8.

Yet another interesting feature of Fig. 8 is apparent if one checks the discovery date of the largest nuclei in the plot. Of the 12 nuclei with  $R_N > 3$  km, six (50%) were discovered in just the four years before the survey. And of the 17 nuclei with  $R_N$  between 2 and 3 km, five (29%) were discovered as recently. In other words, had our survey been done, for example, in the 1990s, many large nuclei would not have been discovered or available for study.

This point is illustrated in Fig. 10, where we have plotted perihelion distance and discovery year and used the symbol size to represent radius. This plot includes not only our SEPPCoN detections but also those comets among the nine discussed above that were discovered after 1970. Many large nuclei in our sample were discovered in the 2000s. This indicates that the census of the JFC population is likely incomplete at most radii, certainly even up to 2 or 3 km. Furthermore, we are probably incomplete even for comets with low perihelion. Among those 11 recent comets with nuclei greater than 2 km are comets 162P, 169P, P/2005 XA<sub>54</sub> – three comets with perihelia of only 1.2, 0.6, and 1.8 AU, respectively. If we divide the 98 nuclei here (89 SEPPCoN plus nine from the literature) into a pre-2000 and post-2000 group, there are 61 comets in the former and 37 in the latter. A Kolmogorov-Smirnov test of the radii in those two groups indicates that they are likely drawn from the same distribution, since the statistic yields a significance of 68%.

**Fig. 10**

### 4.3. Notes about Radii

#### 4.3.1. Previous Studies of Radii

To make a broad comparison with our radii, we checked for comets that were both in our sample and in several recent compilations of radii created by Lamy et al. (2004, hereafter

L04; using the “ $r_{n,v}$ ” column in their Table 1), Tancredi et al. (2006; hereafter T06), Weiler et al. (2011; hereafter W11), and Snodgrass et al. (2011; hereafter S11). The compilations represent a combination of radii from original data and from reviews of the literature, and so are not entirely independent from each other, but it is useful to make comparisons across a wide range of published results. The compiled radii themselves are derived mostly from photometry of apparently-bare nuclei, measurements of point-sources embedded in faint comae, and extrapolations of activity to high  $r$  — i.e., from a range of methods. Among the radii that we are comparing to SEPPCoN, they are almost entirely derived from visible-wavelength data, and so our SEPPCoN results are independent snapshots.

We found 59 SEPPCoN comets that overlap with at least one of those four works. The comparisons are shown in Fig. 11, where we show the ratios of our radii to the radii from each older work. Some statistics about the ratios (excluding the upper-limits) are listed in Table 8. We note that the ratios do tend to straddle unity. We also note that there is no significant difference in the means between the ratios from comets showing dust in the SEPPCoN data, and the ratios from comets that do not. This is reflected in the significance of the Student- $t$  statistic for such a comparison, given in the last column of Table 8. One possible interpretation of this is that the nuclei that we had to extract from dust comae are unlikely to be significantly larger than those that were bare. This is reassuring since it would mean the dust removal process was successful. Admittedly a more conservative interpretation might be that it is equally hard to extract robust nucleus photometry from comets with dust comae in both the infrared and visible wavelengths.

**Table 8**

Another representation of the ratios is shown in the top four panels of Fig. 12, which has the histograms of the data in Fig. 11, divided into 0.25-unit wide bins. The white histograms include all the detected SEPPCoN comets, and the grey histograms include only comets that showed no discernible dust. Such comets have only slightly lower ratios on average.

All this perhaps suggests that there is broad consistency between the SEPPCoN and the visible-wavelength measurements — and in particular that (a) the dust accounting we (and others) have had to employ is mostly being used consistently, and (b) a geometric albedo of 0.04 is a reasonable assumption for visible-wavelength studies.

**Fig. 11**

However a little more digging reveals an interesting effect. To demonstrate this, we start by postulating what the expected scatter of the points in Fig. 11 around unity should be. Suppose all nuclei were prolate-ellipsoids with semiaxes  $a > b = c$ , and that they all spin around one of their short axes. If a spin axis were perpendicular to the observer’s line of sight, a nucleus would show a variable effective radius that oscillates between  $b$  and  $\sqrt{ab}$  as it spins. For a rotation axis that is not perpendicular, the bounds will be different, but the effective radius will still vary (as long as the view is not pole-on). Let  $S$  be the cross section of the nucleus; both L04 and S11 discuss how  $S$  varies for a nucleus viewed with aspect angle  $\varepsilon$  (i.e. the angle between the line-of-sight and the spin axis):

$$S = \pi ab^2 \sqrt{\frac{\cos^2 \varepsilon + \sin^2 \varepsilon \cos^2 \phi}{b^2} + \frac{\sin^2 \varepsilon \sin^2 \phi}{a^2}}, \quad (1)$$

where  $\phi$  is the sub-observer longitude, varying uniformly from 0 to 360° over the course of a

rotation period. If we let  $\mathcal{R}$  be the axial ratio,  $a/b$ , then Eq. 1 simplifies to

$$S = \pi b^2 \sqrt{\mathcal{R}^2 + (1 - \mathcal{R}^2) \sin^2 \varepsilon \sin^2 \phi}. \quad (2)$$

The effective radius,  $R_{ss}$ , one would measure from taking a snapshot of such a rotating nucleus at some time would be  $R_{ss} \equiv \sqrt{S/\pi}$ , so

$$R_{ss} = b \sqrt[4]{\mathcal{R}^2 + (1 - \mathcal{R}^2) \sin^2 \varepsilon \sin^2 \phi}. \quad (3)$$

If we were to take two snapshots of such a nucleus and get two radii,  $R_1$  and  $R_2$ , the ratio of those snapshot radii would be

$$\frac{R_1}{R_2} = \sqrt[4]{\frac{\mathcal{R}^2 + (1 - \mathcal{R}^2) \sin^2 \varepsilon \sin^2 \phi_1}{\mathcal{R}^2 + (1 - \mathcal{R}^2) \sin^2 \varepsilon \sin^2 \phi_2}} \quad (4)$$

and would only depend on  $\mathcal{R}$ ,  $\varepsilon$ , and the specific longitudes – i.e., not on the individual dimensions themselves. Thus, an analysis of snapshot radii ratios can be done without having to worry about what the true radii actually are, and so it is easy to determine if the widths of the histograms in the top half of Fig. 12 are simply manifestations of looking at non-spherical nuclei.

**Fig. 12**

Unfortunately, it seems the easy answer is not the correct one. This is shown in the bottom half of Fig. 12, showing histograms of expected radii ratios from an ensemble of 100,000 virtual nuclei. Each nucleus was given a value of  $\cos \varepsilon$  between  $-1$  and  $1$ , uniformly distributed, and two values of  $\phi$  between  $0$  and  $360^\circ$ , also uniformly distributed. We then assumed a common axial ratio for all 100,000, just for ease; the value of the axial ratio is given in the upper right corner of each panel in the bottom half of Fig. 12. The application of Eq. 4 yields 100,000 radii ratios, which we plotted with bins 0.01-units wide. While larger axial ratios result in wider distributions, the radii ratios are always strongly peaked near unity regardless, and look nothing like the observed histograms in the top of Fig. 12.

We note that this is not the first time that snapshot radii have been shown to be (in principle) excellent estimates of “true” effective radii. Weissman and Lowry (2003), L04, and S11 all discuss how snapshot radii are related to the true effective radii, and show that on average a snapshot radius is usually close (within a few percent) to the nucleus’s true effective radius. What we show in the bottom of Fig. 12 is simply a different manifestation of the same conclusion.

The widths of the observed histograms at the top of Fig. 12 remain to be explained. There are several possible explanations for this; perhaps the radii (ours and/or the earlier ones) are simply wrong. There are certainly systematic effects that could be influencing the radii: perhaps the statistics are fooling us and  $\eta$  in actuality really does vary greatly across nuclei; perhaps incorrect phase laws in the mid-IR and/or in the visible are being applied; perhaps dust in the visible and mid-IR has not been properly accounted for, and the photometry includes lingering dust or an overzealous subtraction of dust; perhaps cometary

albedos have a greater range than is thought; perhaps nuclei that appear bare have significant, variable amounts of dust within the seeing disk. It is possible that a combination of these effects is at work.

The last point bears elaboration; as mentioned earlier this phenomenon appears to be at work in the case of comet 2P/Encke (Fernández et al. 2000, 2005b). Perhaps our dataset is suggesting that dust hiding within the seeing disk is a more common phenomenon than previously thought, and not limited to 2P. This would indeed make studies of nuclei much more difficult since it would require significantly more photometry at multiple epochs and over a range of heliocentric distances.

One important clue however is the fact that each of the four mean ratios between our radii and the four compilations (mentioned earlier this section) is close to unity, as seen in Table 8. Furthermore the standard deviations are comparable. This suggests that there is no single effect that is systematically biasing the radii of any of the compilations (theirs and ours) in one direction. This is important because in general it is easier to overestimate radii than to underestimate them. Yet that does not seem to be happening; the disparate estimates of radii must have some other explanation. In any case, the relationship between SEPPCoN radii and visible-wavelength photometry will be addressed in future work.

We now discuss some individual comets whose SEPPCoN radii are noticeably different from values reported in the four compilations, L04, T06, S11, and W11. We note that these four works did not necessarily use the same basic assumptions to convert visible photometry to radii, so the same magnitude report can result in slightly different answers for the radius.

#### 4.3.2. *31P/Schwassmann-Wachmann 2*

We obtained a snapshot radius of 1.65 km, and this comet did not have discernible dust (see Fig. 1). In contrast to this radius, T06, L04, and S11 all compiled a radius of 3.0 to 3.3 km, all based on near-aphelion CCD photometry reported by Luu and Jewitt (1992). Luu and Jewitt did report a faint detection of coma in a sum of images, but otherwise saw only a star-like point-source in individual images. Perhaps this is a case of 31P having dust in the seeing disk near aphelion.

#### 4.3.3. *37P/Forbes*

We obtained a snapshot radius of 1.23 km. The accounting for the dust was somewhat more complicated than usual due to the tail (see Fig. 1). This radius is in contrast to the 0.78 km compiled by S11 and 0.81 km compiled by W11. Both reports derive from the analysis presented by Lamy et al. (2009) of their HST snapshots. Coma subtraction was applied to these images as well and the nucleus was “detected with good contrast.” It is of course possible that we have underestimated the dust contribution.

#### 4.3.4. *43P/Wolf-Harrington*

We obtained an upper limit of 1.01 km, though we point out that there was a bright star whose first Airy ring was close to the expected position of 43P in our IRS data (see Fig. 1), complicating the estimate of an upper limit. Nonetheless, our radius is smaller than earlier results: L04 list 1.8 km, T06 list 2.1 km, and W11 list 3.4 km. S11 give an upper limit of 2.4 km, and in fact Snodgrass et al. (2006) discuss the case of 43P in detail, arguing that it has unresolved coma in the known visible-wavelength observations out to almost  $r = 4.9$

AU. Thus, all previously-published radii should be treated as upper limits. Our observations occurred when the comet was over 5.3 AU, so our small radius upper-limit is consistent with the hypothesis of unresolved coma affecting the earlier results.

#### 4.3.5. *50P/Arend*

We obtained a snapshot radius of 1.49 km, with not much dust to remove and a high-contrast point-source. Our four comparison works all compile about 0.95 km, all based on the work of Lamy et al. (2004) using HST data when the comet was at  $r = 2.4$  AU. The nucleus there was reported to have “moderate contrast” but the coma subtraction fits are excellent. Our observations of course have lower resolution so perhaps there is dust residing in the seeing disk closer to aphelion.

#### 4.3.6. *69P/Taylor*

Our snapshot radius is 0.87 km. Dust removal in the IRS blue image was straightforward, but was somewhat more complicated in the red image (see Fig. 1). Nonetheless the comet appeared fainter than expected in our imaging. The radius is much smaller than previously reported: W11 list 3.60 km and S11 list 3.88 km, both based on the work of Lowry et al. (1999), who reported an unresolved point-source when observed at  $r = 4.9$  AU. T06 list 2.1 km, and they and L04 remark that the trend of photometry with  $r$  suggests the comet is still active out to 4 to 5 AU. (And indeed our observations showing dust occurred at  $r = 4.2$  AU.) Perhaps this is another case of a comet showing dust in the seeing disk near aphelion.

#### 4.3.7. *79P/du Toit-Hartley*

This comet appeared fainter than expected also, and was not a comet with discernible dust. Our snapshot radius is 0.70 km, compared to 1.4 to 1.5 km compiled by all four of our comparison works, all based on the work of Lowry et al. (1999), who found an unresolved point-source comet when observing it at 4.74 AU, near aphelion. However they do also mention that “the dominant flux source” – i.e. nucleus vs. dust – “is uncertain.” Admittedly, the same could certainly be said for the IRS imaging at 4.37 AU.

#### 4.3.8. *118P/Shoemaker-Levy 4*

Here is yet another case where our snapshot radius is smaller than expected. Some dust was detected in our IRS imaging (see Fig. 1) and in particular it was difficult to remove the dust from the blue image. The point source in the head of both images was definitely fainter than predicted, however. We obtained a radius of 1.30 km. L04, W11, and S11 all list radii of 2.4 to 2.6 km based on the work of Lowry et al. (2003), whose snapshots showed an unresolved point-source when observed at  $r = 4.7$  AU. Our observations occurred at  $r = 4.9$  AU, only slightly farther but essentially at aphelion. Perhaps that was enough for the comet to actually have turned off.

#### 4.3.9. *120P/Mueller 1*

We obtained an upper limit of 0.48 km for the radius. This is smaller than other reported values, suggesting that we should have seen the comet in our IRS imaging. L04 and W04 compiled 1.5 km, based on work by Lowry et al. (1999) observing the comet at  $r = 3.1$  AU. S11 compiled 0.77 km based on more recent observations by Snodgrass et al. (2008) at higher  $r$ , 3.9 AU, suggesting that the comet might have still been active at 3.1 AU. Our SEPPCoN observations occurred at higher  $r$  still, 4.8 AU, so perhaps this comet has dust in

the seeing disk until very close to aphelion.

#### 4.3.10. 121P/Shoemaker-Holt 2

This comet was brighter than expected, with our finding of a snapshot radius of 3.87 km. The comet showed dust in our IRS imaging (see Fig. 1), but the point-source had high contrast against it (with the Airy rings visible), and so the dust removal was relatively straightforward. In comparison, L04 compiled 1.6 km, T06 compiled 2.0 km, and W11 compiled 1.6 km, based on the work by Lowry et al. (2003) that indicated a point-source comet when observed near  $r = 5$  AU. S11 lists 3.34 km however, much closer to our value, and is based on more recent data from Snodgrass et al. (2008) that also show a point-source in the head of the comet but with a faint tail next to it. These data were taken when  $r \approx 4$  AU, near the value for the IRS data (4.3 AU). Perhaps the comet keeps dust in the seeing-disk but fades rapidly once it turns off close to 5 AU.

#### 4.3.11. 243P/2003 S2 (NEAT)

We obtained an upper limit of 0.55 km, which is smaller than the 1.5 km compiled by S11 from observations by Mazzotta Epifani et al. (2008). However, Mazzotta Epifani et al. (2008) do state that an estimate of coma contamination in their (albeit very deep and stellar-looking) comet image could yield a radius as small as 0.8 km.

#### 4.3.12. Sky Survey Comets from W11

Among the 32 comets that overlap between our survey and the compilation by W11, there are 15 comets for which W11 derived radii using photometry of archival sky survey observations. These points are on the right half of W11's panel in Fig. 11, and most of them are very clearly offset from the other 17 comets and from the unity line. For 10 of those 15, the ratios are below 0.5, i.e. W11's radius is more than twice as large as ours. For seven of those the W11 is radius is more than four times as large. This suggests perhaps a systematic effect is in play. For example maybe the sky survey observations are not as clean of coma as would be indicated from the radial profiles, although W11 did try to account for such an effect. As mentioned in §4.3.1, future work will try to understand the large differences in radii of these comets.

### 4.4. Radii and Size Distribution

The size distribution of the JFCs depends on the properties of the source region and the evolutionary processes that have changed the radii of the nuclei from their initial values. We can use our 89 new radii to estimate this distribution. To augment these 89, we now add in the nine other radii we mentioned in §4.2. Thus we are extracting a size distribution from 98 JFC nuclei. The cumulative size distribution (CSD) for these 98 comets is shown with the solid line in Fig. 13. The CSD is moderately steep in the larger sizes, trending almost as the inverse-square of radius, but it has a break in slope at smaller radii. The turnover is primarily due to our relatively poor sampling of that size regime. However, Meech et al. (2004) modeled the expected sampling bias one would expect from the discovery of comets and found that such a turnover in the CSD could be explained by an actual dearth of sub-kilometer JFCs. According to Meech et al., many more sub-kilometer JFCs should have been discovered by now. In other words, while the slope of the CSD in Fig. 13 gets shallower at

smaller sizes partly because of sampling, it apparently would also do the same thing if there were not as many small JFCs out there to be discovered in the first place. We will discuss this further in the next section.

**Fig. 13**

We have also plotted on Fig. 13 a curve that only includes the 54 SEPPCoN comets that had no discernible dust. We added the nine literature comets to make the total 63. The figure shows that there is no significant difference between the 63- and 98-comet CSDs. This is gratifying since (as we have mentioned in other contexts earlier in this paper) it suggests that the radii from SEPPCoN comets that did appear with discernible dust should not be wildly off, and thus their inclusion in the CSD is not biasing our conclusions about the CSD.

The CSD approximates a power-law, and as is common we will characterize the distribution with a power-law slope  $\beta$ , defined as  $N(> R_N) \propto R_N^\beta$ , where  $N$  is the cumulative number of comets. Best fitting  $\beta$  values to the 98-comet CSD are given in Table 9, where we present the slopes using a variety of radius-ranges to do the fitting. Choosing an appropriate range over which to fit the observed CSD is an uncertain process; on the small end, it is difficult to quantify just where the CSD starts to turnover, and on the large end, the small-number statistics are problematic and one does not want to give too much weight to the few largest comets. These realities motivated us to try different choices for the range of radii. A better way to approach the problem is to follow the procedures of Meech et al. (2004) or of Snodgrass et al. (2011) and account for some of observational uncertainties and biases explicitly. We address these issues in future work, so here we report for completeness slopes fitted to many ranges. The median  $\beta$  among the 20 ranges we tried is  $-1.92$ , with a standard deviation of 0.23.

**Table 9**

We note that if we had *not* converted the IRS radii to a common value of  $\eta$  (as described in §4.2), but instead just used the radii in Table 4, we would have found that the resulting 98-comet CSD would be shallower. Using the same radii bounds as given in Table 9, we find that the median  $\beta$  of such a CSD would be  $-1.72$  with a standard deviation of 0.17. This is largely due to the fact that (a) there are more high- $\eta$  IRS comets than low- $\eta$  IRS comets, and (b) the range of fitted  $\eta$  values seems to extend farther above the mean than it does below it (so since higher  $\eta$  means higher  $R_N$ , we have more of a boost to the CSD at the large-radius end than at the small-radius end). The validity of this CSD over the one shown in Fig. 13 would rest on whether or not one assumes that JFCs have a common beaming parameter. Even though nearly all of our IRS comets have  $\eta$  values consistent with a single value near unity, suggesting that this might be a common property (§4.1), it is of course possible that this is the wrong conclusion, and that there is more variety to the beaming parameter. A more detailed analysis of this aspect of the CSD will be addressed in a future paper.

Figure 13 also shows the observed CSD if we restrict the sample by perihelion distance. One can argue that we are more likely to have a complete census of the JFC population at the smaller radii if we only consider JFCs that approach to within 1.5 or 2.0 AU of the Sun, since such comets are more likely to be discovered. Perhaps such a perihelion-restricted CSD is less likely to suffer from discovery biases. However Fig. 13 shows that the shapes of the CSDs are not radically different, at least away from the very largest end of the CSDs where

there are only one or two comets. This is confirmed quantitatively with Kolmogorov-Smirnov tests. The test returns a statistic with significance near 100% for a comparison of the 98-comet distribution and the  $q < 3$  AU distribution, a significance of 99% for the  $q < 2.5$  AU distribution, a significance of 70% for the  $q < 2.0$  AU distribution, and a significance of 22% for the  $q < 1.5$  AU distribution. Tests using other limiting values of  $q$  and tests that use a limiting  $q$  as a lower limit yield similarly high probabilities. Thus there is good confirmation that a  $q$ -limited subset of the radii are no different than the entire 98-comet CSD.

This result is also evident from the  $\beta$  values for these  $q$ -limited CSDs listed in Table 9. The typical slopes of each CSD are similar regardless of where we cut off the perihelion. For the CSD restricted to  $q < 3$  AU, the median  $\beta$  is  $-1.96$ ; for  $q < 2.5$  AU, it is  $-1.85$ ; and for  $q < 2$  AU, it is  $-1.84$ . (We did not fit  $\beta$  for the  $q < 1.5$  AU CSD since there are too few comets left.) There are some outliers among the slopes in Table 9, but the similarity of the medians suggests that there is not a significant perihelion bias in the overall, 98-comet CSD, at least among the sample of comets we selected to study here.

Closer inspection of Fig. 13 reveals an interesting feature in the 98-comet CSD: it has a small bump at radii from 3 to 6 km. Such waviness is seen in the CSD of main-belt asteroids, and is related to the asteroids' strength (e.g. Jedicke and Metcalfe 1998, O'Brien and Greenberg 2003). If the JFC bump is real and not an artifact, one exciting hypothesis is that it is a remnant feature of the primordial size distribution of the JFC's progenitor SDOs. If the SDOs are the source of today's JFCs and they originally had a peak in their CSD at 3-6 km radii, subsequent evolution (e.g., collisions, activity, fragmentation) would produce smaller objects that would fill out the CSD but also could have left a bump at the radii where we see one in Fig. 13. In this interpretation, the CSD is giving us clues about the original properties of the population. However corroborating this hypothesis will require surveying many more JFCs to gain confidence in the reality of the bump. In particular we will need to be sure that most of the large nuclei have been discovered (cf. §4.2), since we can only identify a bump in the context of the shape of the CSD that surrounds it. Furthermore, it would be useful to identify such a peak in the SDO CSD, which means finding SDOs with R-band magnitudes near  $\sim 28-29$ , a quite challenging task.

We also note that the perihelion-restricted CSDs in Fig. 13 appear to have more waviness than the all-comet CSD does. We surmise that this is due to the particular radii of recently-discovered comets, but a better census of nucleus sizes (among both JFCs that are known and those waiting to be discovered) could certainly address whether the waviness is real.

#### 4.5. Implications of the CSD

We show in Fig. 14 a comparison of our CSD to those of L04, T06, S11, W11, and also to that of Meech et al. (2004). For S11, we excluded upper limits in their Table 3 to make this plot. For L04, we only used values of  $r_{n,v}$  in their Table 1. For T06, we only used entries with quality code 3 or better from their Table 1. For W11, we only used the 46 comets in their Table 5 and excluded the sky-survey comets in their Table 4 (cf. §4.3.12). The top set of curves shows that our CSD is broadly similar to these others. This is somewhat easier to see in the bottom set of curves, where we have greyed out the individual points for clarity



and placed simple power-law fits over a restricted (but common to all) range of radii – 2 to 5 km – to aid the eye.

Fig. 14

Comparing our CSD slope to other *reported* slopes we find that our  $\beta$  is similar to that found by L04 ( $\beta = -1.9 \pm 0.3$  for  $R_N=1.6$  to 15 km), S11 ( $\beta = -1.92 \pm 0.20$ , for  $R_N \geq 1.25$  km), and W11 ( $\beta = -1.76 \pm 0.45$ , for  $R_N \geq 2.0$  km), as well as that reported by Weissman et al. (2009;  $\beta = -1.86 \pm 0.15$ ). In contrast, T06 reported a steeper result,  $\beta = -2.7 \pm 0.3$  ( $R_N=1.7$  to 4.5 km). We note the differing ranges of radii that were applied by these workers to derive these slopes. In some cases, slopes over multiple ranges were published (cf. our Table 9); W11 did this, as did Meech et al. (2004), who report  $\beta = -1.45 \pm 0.05$  for  $R_N=1$  to 10 km but  $\beta = -1.91 \pm 0.06$  for  $R_N=2$  to 5 km.

We also used Kolmogorov-Smirnov tests to compare our radii with those five other compilations and quantify how well they match. The likelihoods are quite high that all radius distributions are drawn from the same distribution. For our radii and those of Meech et al. (2004), the statistic has a significance of 41%; for our radii and those of S11, it is 79%; for our radii and those of W11, it is 73%; for our radii and those of L04, it is 67%; and for our radii and those of T06, it is 22%.

We note that all these other works for the most part make use of visible-wavelength data. Thus our CSD is almost entirely independent of these earlier results. The similarity in power-law slope does indicate that there is likely no strong albedo trend with radius among the JFCs. In other words, the assumption of a common geometric albedo to all JFCs that is so frequently invoked when interpreting visible-wavelength photometry appears to be valid. This is consistent with the arguments presented by Lamy et al. (2004), though it remains to be seen what the measured spread of albedos across JFCs actually is.

Also shown in Fig. 14 is model ‘Pb’ from Meech et al. (2004), the predicted CSD that one would measure given an intrinsic CSD that is subject to discovery biases. This model has a base *differential* size distribution (not CSD) with power-law slope of  $-3.5$ , but multiplied by a three-piece continuous function that was valued at 0 for  $R_N \leq 0.3$  km, was valued at unity for  $R_N \geq 2.0$  km, and was a line in between. Hence the intrinsic size distribution is truncated entirely below 0.3 km and suppressed to varying degrees below 2.0 km. By forcing the JFCs to have no very small members and relatively fewer small (kilometer-scale) members than would otherwise be expected, and by convolving the intrinsic distribution with a model of activity and of discovery biases, Meech et al. (2004) were able to reproduce their observed CSD. As Fig. 14 demonstrates, our CSD has a similar shape to that of Meech et al. (2004), suggesting that a similar model with truncation at small radii (perhaps just with different truncation parameters) could potentially reproduce the overall shape of our CSD (excluding the bump mentioned in §4.4). However it is important to once again note that our sample criteria tended to remove relatively small nuclei from our observations, and it is unclear if this bias is the same in mid-IR observations as it could be at visible wavelengths.

If the Meech et al. (2004) intrinsic distribution is correct, it suggests that the JFC population is collisionally relaxed (Dohnanyi 1969) but also suffers from some processes that remove the smaller members and flatten the true and observed distributions. These could be, for example, regular cometary activity and fragmentation. The effects of these processes

on the CSD have been discussed previously by, e.g., Lowry et al. (2003) and Weissman and Lowry (2003). In particular, fragmentation is a promising phenomenon since it has been directly observed in many JFCs (Boehnhardt 2004, Chen and Jewitt 1994, Fernández 2009), and once in a Centaur (Bauer et al. 2008). Given the observed rates of fragmentation (Chen and Jewitt 1994), an individual JFC likely suffers tens or hundreds of fragmentation events over its active lifetime.

Interestingly, studies of fragment populations in individual comets suggest that the fragmentation process itself leads to shallow size distributions. For example, Fuse et al. (2007) took a visible-wavelength snapshot of Fragment B of comet 73P/Schwassmann-Wachmann 3 and found many tiny (meter-scale) subfragments that had come off of Fragment B in the previous few days. The CSD of the fragments had a power-law slope of around  $-1.1$ . Reach et al. (2007) studied several of 73P’s fragments in a wider-field Spitzer mosaic, fragments that had probably been released  $\sim 10$  years in the past. The “large” fragments (roughly  $>150$  m in radius) had a CSD slope of  $-1.6$ , while the “small” fragments (roughly  $<150$  m) had a slope of around  $-0.8$ . This is an especially interesting result since it suggests that perhaps the effects of fragmentation itself are size-dependent. Fernández (2009) derived a power-law slope of  $-1.3$  for the CSD of the fragments released by comet 57P/du Toit-Neujmin-Delporte over the course of (apparently) several months in 2002. These fragments had diameters of roughly hectometer-scale. We note that all these  $\beta$  are even shallower than what has been derived here for the JFC nuclei as an ensemble, suggesting that fragmentation could play a significant role in controlling the cometary size distribution. If fragmentation events supply a shallow distribution of smaller JFCs into the inner Solar System (as the fragments get perturbed onto different orbits, as happened for 42P and 53P [Kresák et al. 1984]), then the overall JFC CSD should reflect that.

We should note that if the bump mentioned in §4.4 is real, then perhaps the input population’s CSD is not a perfect collisionally-relaxed power-law. In that case, the overall JFC CSD upon which the fragmentation process operates would not be a collisionally-relaxed power-law either. Evidently this would complicate finding a model for the intrinsic CSD that would uniquely match the observed CSD.

Traditionally the trans-Neptunian region – and in particular, the scattered disk – has been thought to be the primary, original source region for the JFCs we see today (e.g. Duncan et al. 2004). A comparison of the size distributions among these populations would thus be worthwhile. One significant issue however is the fact that there is minimal size matching between JFCs and known TNOs; few known TNOs, and no known SDOs, are small enough. Therefore estimates of the TNO size distribution at the kilometer scale – which would be necessary if one is to make a direct comparison – are still uncertain. Centaurs are closer in size to the JFCs (cf. P/2004 A1 in Table 5) but the number with known sizes matching the JFCs’ sizes is still too limited.

One deep survey of the trans-Neptunian region sensitive to TNOs with somewhat JFC-like sizes is that of Bernstein et al. (2004), which used the Hubble Space Telescope (HST) and would have been able to find TNOs at about  $\sim 29$ th magnitude in R band. For reference, an object at opposition that is 34 AU from the Sun and has 4.0% geometric albedo would

have an R band magnitude of 29.0 if the radius were 5.0 km. Thus the Bernstein et al. survey was looking for objects similar but still mostly larger than the bulk of the JFCs. The survey detected about 1.5 orders of magnitude fewer objects than they would expect based on the measured luminosity function of TNOs at larger ( $\sim 100$  km) sizes. In other words the survey implies there is a break in the TNO luminosity function and so a distinct underabundance of JFC-sized objects currently in the trans-Neptunian region. While there is still some uncertainty in the large-TNO luminosity function and size distribution (as addressed in detail by e.g. Petit et al. (2008)), the Bernstein et al. survey would suggest that there are too few objects to explain the current size of the JFC population, as Bernstein et al. (2004) themselves note as do Volk and Malhotra (2008) in a more detailed analysis. Essentially, the size distribution function of  $\sim 1$ -km TNOs, as extrapolated from the Bernstein et al. detections of larger objects, is too flat.

More recently, Schlichting et al. (2012) have reported an analysis of small TNOs that were found via a survey of stars observed by the Fine Guidance Sensors aboard HST. The stars' photometry was searched for signs of occultations by intervening TNOs. Their two detected objects have sub-kilometer radii and so are objects that really do overlap the size of many JFCs. The distribution at these sub-kilometer scales, as implied by this survey and its detections, is still shallower than that implied by the size distribution of larger TNOs – so they confirm the break in the size distribution – but it is not as shallow as implied by the Bernstein et al. (2004) survey. As a result, Schlichting et al. (2012) conclude that there are in fact sufficient number of objects to explain the JFC population as estimated by Volk and Malhotra (2008).

Furthermore, Schlichting et al. (2012) report that the exponent of the differential size distribution's power-law is around  $-3.4$  to  $-4.0$ , depending on the ecliptic latitude distribution. If true, it means there would be significant flattening of the size distribution (likely as a result of physical evolution) as these small TNOs become JFCs. Interestingly, Shankman et al. (2013) have recently argued for a “divot” in the TNO size distribution, where the number of objects in a size bin suddenly drops but then rises again with a different power-law. This would explain the observational results and likewise provide for enough objects to explain the JFC population.

In any case, since the observational biases for JFCs are so different from those for Centaurs and TNOs (as mentioned by Meech et al. (2004)), direct comparisons of CSDs can be problematic. But certainly more discoveries of TNOs closer in size to the JFCs are necessary. Petit et al. (2008) point out that understanding the apparent break in the TNO size distribution is going to at least require a survey covering several square-degrees of sky that can reliably discover objects of 28th magnitude, an ambitious project to be sure.

## 5. Summary

SEPPCoN has detected 89 nuclei of JFCs with the Spitzer Space Telescope, making SEPPCoN the largest photometric survey so far of JFCs in the mid-infrared. Of the sample, 54 of the comets appeared bare, and 35 appeared with discernible dust. For comets in the latter group, a photometric extraction technique was used to measure the nucleus's brightness

alone. We assumed that the point-source was identical to the nucleus. We conclude the following:

1. Of our 57 nuclei detected at two wavelengths, 55 are consistent with the hypothesis that the nuclei all have the same beaming parameter. We find that the mean beaming parameter is  $1.03 \pm 0.11$ . Only two of the 57 comets (3.4%), 89P and P/2005 JQ<sub>5</sub>, have beaming parameters inconsistent with this value, and the latter is consistent with having a dust-dominated head with minimal nucleus.

2. By virtue of this beaming parameter's value, we conclude that nearly all JFC nuclei have low thermal inertia with little night-side emission, and little anisotropy in their day-side thermal emission. This conclusion is even more robust considering that virtually all observations occurred when the comets were 4 to 5 AU from the Sun, i.e., when the nuclei should be relatively cold and it should be easier for any thermal memory to be retained onto the night side.

3. The beaming parameter is uncorrelated with any observational or orbital parameter in our sample, indicating that it is probably intrinsic to the nuclei.

4. The census of the JFC population is apparently incomplete even in the inner part of the Solar System and even up to fairly large radii,  $\sim 3$  km. Many of the recently-discovered comets in our sample (i.e. in the four years before the survey was conducted) have radii of 2 km and larger and so contribute to the large end of the size distribution. While it is not surprising that this is true for comets with perihelia out beyond 2.5-3 AU, we conclude that there must still be large, undiscovered JFCs that approach to 1.5-2 AU from the Sun.

5. Combining our 89 new radii with nine radii from the literature yields a total sample of 98 JFCs. The resulting CSD follows a power-law with slope of about  $\beta = -1.9$ . Varying the range in radius over which the CSD is fit yields a standard deviation in  $\beta$  of about  $\pm 0.2$ .

6. The CSD slope is similar even if we restrict our sample to those comets with perihelia under 2, 2.5, or 3 AU. This indicates that even though many large nuclei in the JFC population may be missing, our sample currently shows no extra bias with respect to perihelion distance.

7. Our CSD appears to show a bump near radii of 3 to 6 km, suggesting an excess of JFCs with those sizes. A more complete sampling of JFC radii will be required to establish the reality of this bump, which could have interesting implications for the origin and/or evolution of the nuclei.

8. The best fit power-law slope is consistent with results taken in the visible-wavelengths, and suggests that there is no broad dependence of albedo on radius among the JFC population; i.e., that the assumption of a single geometric albedo for all nuclei is reasonable.

9. In particular, the power-law slope is reasonably close to the best fitting model of Meech et al. (2004), suggesting that our observed CSD is consistent with an intrinsic population that is truncated at sub-kilometer scales.

## Acknowledgements

We are grateful for the recommendations and suggestions to this manuscript made by Olivier Hainaut and one anonymous referee. This work is based on observations made with

the Spitzer Space Telescope, which is operated by the Jet Propulsion Laboratory, California Institute of Technology under a contract with NASA. Support for this work was provided by NASA through an award issued by JPL/Caltech, RSA #1289123, to YRF and HC. Support for this work also came from NASA through grant NNX-09AB44G to YRF, SCL, KJM, and JMB; from the National Science Foundation through grant AST-0808004 to YRF, SCL, and KJM; and from the European Union Seventh Framework Programme (FP7/2007-2013) under grant agreement no. 268421 to CS.

## References

- A'Hearn, M.F., Campins, H., Schleicher, D.G., Millis, R.L., 1989. The nucleus of comet P/Tempel 2. *Astrophys. J.* 347, 1155–1166.
- A'Hearn, M.F., Millis, R.L., Schleicher, D.G., Osip, D.J., Birch, P.V., 1995. The ensemble properties of comets: Results from narrowband photometry of 85 comets, 1976-1992. *Icarus* 118, 223–270.
- A'Hearn, M.F., et al., 2005. Deep Impact: Excavating comet Tempel 1. *Science*, 310, 258–264.
- A'Hearn, M.F., et al. 2011. EPOXI at comet Hartley 2. *Science* 332, 1396–1400.
- A'Hearn, M.F., et al. 2012. Cometary volatiles and the origin of comets. *Astrophys. J.* 758, 29.
- Alvarez-Candal, A., Licandro, J., 2006. The size distribution of asteroids in cometary orbits and related populations. *Astron. & Astrophys.* 458, 1007–1011.
- Bauer, J.M., et al., 2008. The large-grained dust coma of 174P/Echeclus. *Publ. Astron. Soc. Pacific* 120, 393–404.
- Bernstein, G.M., et al., 2004. The size distribution of trans-Neptunian bodies. *Astron. J.* 128, 1364–1390.
- Boehnhardt, H., 2004. Split comets. In: Festou, M.C., Keller, H.U., Weaver, H.A. (Eds.), *Comets II*. Univ. of Arizona Press, Tucson, pp. 301–316.
- Brown, R. H., 1985. Ellipsoidal geometry in asteroid thermal models – The standard radiometric model. *Icarus* 64, 53–63.
- Brownlee, D.E., et al., 2004. Surface of young Jupiter family comet 81 P/Wild 2: View from the Stardust spacecraft. *Science* 304, 1764–1769.
- Campins, H., A'Hearn, M.F., McFadden, L.A., 1987. The bare nucleus of comet Neujmin 1. *Astrophys. J.* 316, 847–857.
- Campins, H., Osip, D.J., Rieke, G.H., Rieke, M.J., 1995. Estimates of the radius and albedo of comet-asteroid transition object 4015 Wilson-Harrington based on infrared observations. *Planet. & Space Sci.* 43, 733–736.
- Chen, J., Jewitt, D., 1994. On the rate at which comets split. *Icarus* 108, 265–271.
- Delbó, M., Dell'oro, A., Harris, A.W., Mottola, S., Mueller, M., 2007. Thermal inertia of near-Earth asteroids and implications for the magnitude of the Yarkovsky effect. *Icarus* 190, 236–249.
- Dohnanyi, J.S., 1969. Collisional models of asteroids and their debris. *J. Geophys. Res.* 74, 2531–2554.

- Duncan, M., Levison, H., Dones, L. 2004. Dynamical evolution of ecliptic comets. In: Festou, M.C., Keller, H.U., Weaver, H.A. (Eds.), *Comets II*. Univ. of Arizona Press, Tucson, pp 193–204.
- Duxbury, T.C., Newburn, R.L., Brownlee, D.E. 2004. Comet 81P/Wild 2 size, shape, and orientation. *J. Geophys. Res.* 109, E1202.
- Ernst, C.M., Schultz, P.H., 2007. Evolution of the Deep Impact flash: Implications for the nucleus surface based on laboratory experiments. *Icarus* 190, 334344 (2007)
- Farinella, P., Davis, D. R., 1996. Short-period comets: Primordial bodies or collisional fragments? *Science* 273, 938–941.
- Fernández, J.A., Morbidelli, A., 2006. The population of faint Jupiter family comets near the Earth. *Icarus* 185, 211–222.
- Fernández, J.A., Sosa, A., 2012. Magnitude and size distribution of long-period comets in Earth-crossing or approaching orbits. *Mon. Not. R. Astron. Soc.* 423, 1674–1690.
- Fernández, Y.R., 1999. Physical properties of cometary nuclei. Thesis, University of Maryland, College Park.
- Fernández, Y.R., 2009. That’s the way the comet crumbles: Splitting Jupiter-family comets. *Planet. & Space Sci.*, 57, 1218–1227.
- Fernández, Y.R., et al., 2000. Physical properties of the nucleus of comet 2P/Encke. *Icarus* 147, 145–160.
- Fernández, Y.R., Meech, K. J., Lisse, C. M., A’Hearn, M. F., Pittichová, J., Belton, M. J. S. 2003. The nucleus of Deep Impact target comet 9P/Tempel 1. *Icarus* 164, 481–491.
- Fernández, Y.R., Jewitt, D.C., Sheppard, S.S., 2005a. Albedos of asteroids in comet-like orbits. *Astron. J.* 130, 308–318.
- Fernández, Y.R., Lowry, S.C., Weissman, P.R., Mueller, B.E.A., Samarasinha, N.H., Belton, M.J.S., Meech, K.J. 2005b. New near-aphelion light curves of comet 2P/Encke. *Icarus* 175, 194–214.
- Fernández, Y.R., et al., 2006. Comet 162P/Siding Spring: A surprisingly large nucleus. *Astron. J.* 132, 1354–1360.
- Fernández, Y.R., Jewitt, D., Ziffer, J.E., 2009. Albedos of small Jovian Trojans. *Astron. J.* 138, 240–250.
- Fuentes, C.I., George, M.W., Holman, M.J., 2009. A Subaru pencil-beam search for  $m_R \sim 27$  trans-Neptunian bodies. *Astrophys. J.* 696, 91–95.
- Fuse, T., Yamamoto, N., Kinoshita, D., Furusawa, H., Watanabe, J., 2007. Observations of fragments split from nucleus B of comet 73P/Schwassmann-Wachmann 3 with Subaru Telescope. *Publ. Astron. Soc. Japan* 59, 381–386.
- Groussin, O., Lamy, P., Jorda, L., Toth, I., 2004. The nuclei of comets 126P/IRAS and 103P/Hartley 2. *Astron. & Astrophys.* 419, 375–383.
- Groussin, O., et al., 2007. Surface temperature of the nucleus of comet 9P/Tempel 1. *Icarus* 187, 16–25.
- Groussin, O., et al., 2009. The size and thermal properties of the nucleus of comet 22P/Kopff. *Icarus* 199, 568–570.

- Groussin, O., et al. 2013. The temperature, thermal inertia, roughness and color of the nuclei of comet 103P/Hartley 2 and 9P/Tempel 1. *Icarus* 222, 580–594.
- Harmon, J.K., Nolan, M.C., 2005. Radar observations of comet 2P/Encke during the 2003 apparition. *Icarus* 176, 175–183.
- Harmon, J.K., Nolan, M.C., Margot, J.L., Campbell, D.B., Benner, L.A.M., Giorgini, J.D. 2006. Radar observations of comet P/2005 JQ5 (Catalina). *Icarus* 184, 285–288.
- Harris, A.W., 1998. A thermal model for near-Earth asteroids. *Icarus* 131, 291–301.
- Harris, A.W., et al., 2011. ExploreNEOs. II. The accuracy of the warm Spitzer near-Earth object survey. *Astron. J.* 141, 75.
- Houck, J.R., et al., 2004. The Infrared Spectrograph (IRS) on the Spitzer Space Telescope. *Astrophys. J. Suppl. Ser.* 154, 18–24.
- Howell, E.S., Vervack, R.J., Nolan, M.C., Magri, C., Fernández, Y.R., Taylor, P.A., Rivkin, A.S. 2012. Combining thermal and radar observations of near-Earth asteroids. In: *Asteroids, Comets, Meteors 2012, Proceedings of the conference held May 16-20, 2012, in Niigata, Japan.* LPI Contribution No. 1667. LPI, Houston, id. 6273 [abstract].
- Jedicke, R., Metcalfe, T.S., 1998. The orbital and absolute magnitude distributions of main-belt asteroids. *Icarus* 131, 245–260.
- Jewitt, D. 1991. Cometary photometry. In: Newburn, R. L., Neugebauer, M., Rahe, J. (Eds.), *Comets in the Post-Halley Era.* Kluwer, Dordrecht, pp. 19–65.
- Kelley, M.S., et al., 2013. The persistent activity of Jupiter-family comets at 3-7 AU. *Icarus* 225, 475–494.
- Kenyon, S.J., Bromley, B.C., O’Brien, D.P., Davis, D.R., 2008. Formation and collisional evolution of Kuiper Belt objects. In: Barucci, M.A., Boehnhardt, H., Cruikshank, D.P., Morbidelli, A. (Eds.), *The Solar System Beyond Neptune.* Univ. of Arizona Press, Tucson, pp. 293–313.
- Kresák, L., Carusi, A., Perozzi, E., Valsecchi, G. 1984. Periodic comets Neujmin 3 and van Biesbroeck. *Intl. Astron. Union Circ.* 3940.
- Lagerros, J.S.V., 1996. Thermal physics of asteroids. I. Effects of shape, heat conduction and beaming. *Astron. & Astrophys.* 310, 1011–1020.
- Lamy, P.L., et al., 1996. Observations of comet P/Faye 1991 XXI with the Planetary Camera of the Hubble Space Telescope. *Icarus* 119, 370–384.
- Lamy, P.L., Toth, I., Jorda, L., Weaver, H.A., A’Hearn, M., 1998a. The nucleus and inner coma of comet 46P/Wirtanen. *Astron. & Astrophys.* 335, L25–L29.
- Lamy, P.L., Toth, I., Weaver, H. A., 1998b. Hubble Space Telescope observations of the nucleus and inner coma of comet 19P/1904 Y2 (Borrelly). *Astron. & Astrophys.* 337, 945–954.
- Lamy, P.L., Toth, I., Fernández, Y.R., Weaver, H.A., 2004. The sizes, shapes, albedos, and colors of cometary nuclei. In: Festou, M.C., Keller, H.U., Weaver, H.A. (Eds.), *Comets II.* Univ. of Arizona Press, Tucson, pp 223–264.
- Lamy, P.L., et al., 2008. Spitzer Space Telescope observations of the nucleus of comet 67P/Churyumov-Gerasimenko. *Astron. & Astrophys.* 489, 777–785.

- Lamy, P.L., Toth, I., Weaver, H.A., A'Hearn, M.F., Jorda, L., 2009. Properties of the nuclei and comae of 13 ecliptic comets from Hubble Space Telescope snapshot observations. *Astron. & Astrophys.* 508, 1045–1056.
- Lebofsky, L.A., et al., 1986. A refined ‘standard’ thermal model for asteroids based on observations of 1 Ceres and 2 Pallas. *Icarus* 68, 239–251.
- Lebofsky, L.A., Spencer, J.R., 1989. Radiometry and a thermal modeling of asteroids. In: Binzel, R.P., Gehrels, T., Shapley Matthews, M. (Eds.), *Asteroids II*. U. Ariz. Press, Tucson, pp. 128–147.
- Levison, H.F., 1996. Comet taxonomy. In: Rettig, T., Hahn, J.M. (Eds.), *Completing the Inventory of the Solar System*. Astronomical Society of the Pacific, San Francisco, pp. 173–191.
- Licandro, J., et al., 2009. Spitzer observations of the asteroid-comet transition object and potential spacecraft target 107P (4015) Wilson-Harrington. *Astron. & Astrophys.* 507, 1667–1670.
- Lisse, C.M., et al., 1999. The nucleus of comet Hyakutake (C/1996 B2). *Icarus* 140, 189–204.
- Lisse, C.M., et al., 2005. Rotationally resolved 8–35 micron Spitzer Space Telescope observations of the nucleus of comet 9P/Tempel 1. *Astrophys. J.* 625, L139–L142.
- Lisse, C.M., et al., 2009. Spitzer Space Telescope observations of the nucleus of comet 103P/Hartley 2. *Publ. Astron. Soc. Pacific* 121, 968–975.
- Lowry, S.C., Fitzsimmons, A., Cartwright, I.M., Williams, I.P., 1999. CCD photometry of distant comets. *Astron. & Astrophys.* 349, 649–659.
- Lowry, S.C., Fitzsimmons, A., Collander-Brown, S., 2003. CCD photometry of distant comets. III. Ensemble properties of Jupiter-family comets. *Astron. & Astrophys.* 397, 329–343.
- Lowry, S.C., Fitzsimmons, A., Lamy, P., Weissman, P., 2008. Kuiper Belt Objects in the planetary region: The Jupiter-family comets. In: Barucci, M.A., Boehnhardt, H., Cruikshank, D.P., Morbidelli, A. (Eds.), *The Solar System Beyond Neptune*. Univ. of Arizona Press, Tucson, pp. 397–410.
- Luu, J.X., Jewitt, D.C., 1992. Near-aphelion CCD photometry of comet P/Schwassmann-Wachmann 2. *Astron. J.* 104, 2243–2249.
- Mainzer, A., et al., 2011. Thermal model calibration for minor planets observed with WISE/NEOWISE. *Astrophys. J.* 736, 100.
- Mazzotta Epifani, E., et al., 2008. The distant activity of short period comets II. *Mon. Not. R. Astron. Soc.* 390 265–280.
- Meech, K.J., Hainaut, O.R., Marsden, B.G., 2004. Comet nucleus size distribution from HST and Keck telescopes. *Icarus* 170, 463–491.
- Meech, K.J., and Svoreň, J., 2004. Using cometary activity to trace the physical and chemical evolution of cometary nuclei. In: Festou, M.C., Keller, H.U., Weaver, H.A. (Eds.), *Comets II*. Univ. of Arizona Press, Tucson, pp. 317–335.
- Millis, R. L., A'Hearn M. F., Campins H., 1988. An investigation of the nucleus and coma of comet P/Arend-Rigaux. *Astrophys. J.*, 324, 11941209.



- O'Brien, D.P., Greenberg, R., 2003. Steady-state size distributions for collisional populations: Analytical solution with size-dependent strength. *Icarus* 164, 334–345.
- Petit, J.M., Kavelars, J.J., Gladman, B., Loredó, T., 2008. Size distribution of multikilometer transneptunian objects. In: Barucci, M.A., Boehnhardt, H., Cruikshank, D.P., Morbidelli, A. (Eds.), *The Solar System Beyond Neptune*. Univ. of Arizona Press, Tucson, pp. 71–87.
- Press, W.H., Teukolsky, S.A., Vetterling, W.T., Flannery, B.P., 1992. *Numerical recipes in FORTRAN: The art of scientific computing*, 2nd Ed. Cambridge Univ. Press, Cambridge.
- Reach, W.T., Kelley, M.S., Sykes, M.V., 2007. A survey of debris trails from short-period comets. *Icarus* 191, 298–322.
- Richardson, J.E., Melosh, H.J., Lisse, C.M., Carcich, B., 2007. A ballistics analysis of the Deep Impact ejecta plume: Determining comet Tempel 1's gravity, mass, and density. *Icarus* 190, 357–390.
- Rieke, G.H., et al., 2004. The Multiband Imaging Photometry for Spitzer (MIPS). *Astrophys. J. Suppl. Ser.* 154, 25–29.
- Schlichting, H.E., et al., 2012. Measuring the abundance of sub-kilometer-sized Kuiper Belt objects using stellar occultations. *Astrophys. J.* 761, 150.
- Shankman, C., Gladman, B. J., Kaib, N., Kavelars, J. J., Petit, J. M., 2013. A possible divot in the size distribution of the Kuiper Belt's scattering objects. *Astrophys. J.* 764, L2.
- Snodgrass, C., Fitzsimmons, A., Lowry, S.C., Weissman, P.R., 2011. The size distribution of Jupiter family comet nuclei. *Mon. Not. R. Astron. Soc.* 414, 458–469.
- Snodgrass, C., Lowry, S.C., Fitzsimmons, A., 2006. Photometry of cometary nuclei: Rotation rates, colours, and a comparison with Kuiper Belt Objects. *Mon. Not. R. Astron. Soc.* 373, 1590–1602.
- Snodgrass, C., Lowry, S.C., Fitzsimmons, A., 2008. Optical observations of 23 distant Jupiter family comets, including 36P/Whipple at multiple phase angles. *Mon. Not. R. Astron. Soc.* 385, 737–756.
- Soderblom L.A., et al., 2002. Observations of comet 19P/Borrelly by the Miniature Integrated Camera and Spectrometer aboard Deep Space 1. *Science* 296, 1087–1091.
- Sunshine, J.M., et al., 2006. Exposed water ice deposits on the surface of comet 9P/Tempel 1. *Science* 311, 1453–1455.
- Stansberry, J.A., et al., 2004. Spitzer observations of the dust coma and nucleus of 29P/Schwassmann-Wachmann 1. *Astrophys. J. Suppl. Ser.* 154, 463–468.
- Tancredi, G., Fernández, J.A., Rickman, H., Licandro, J., 2006. Nuclear magnitudes and the size distribution of Jupiter family comets. *Icarus* 182, 527–549.
- Volk, K., Malhotra, R., 2008. The scattered disk as the source of the Jupiter Family comets. *Astrophys. J.* 687, 714–725.
- Weiler, M., Rauer, H., Sterken, C., 2011. Cometary nuclear magnitudes from sky survey observations. *Icarus* 212, 351–366.

- Weissman, P.R., Lowry, S.C., 2003. The size distribution of Jupiter-family cometary nuclei. *Lunar Planet. Sci. XXXIV*, #2003 (abstract).
- Werner, M., et al., 2004. The Spitzer Space Telescope Mission. *Astrophys. J. Suppl. Ser.* 154, 1–9.
- Whitman, K., Morbidelli, A., Jedicke, R., 2006. The size frequency distribution of dormant Jupiter family comets. *Icarus* 183, 101–114.

**Table 1**

Observations and Target Geometry. Table columns are: “Comet Desig.” = comet’s designation, giving permanent number, temporary designation (if the comet was known by that at the time of observation), or both (if a single-apparition comet has been recovered since the observations); “I.&C.” = instrument and Spitzer campaign number; “UT at start” = UT in YYYY-MM-DD HH:MM:SS.S format at the start of the AOR; “Dur.” = duration of AOR in minutes; “ $r \pm$ ” = heliocentric distance in AU with  $+$ ( $-$ ) signifying post(pre)-perihelion; “ $\Delta$ ” = Spitzer-centric distance in AU; and “ $\alpha$ ” = Spitzer-centric phase angle in degrees.

Comet Desig.	I.&C.	UT at start	Dur.	$r \pm$	$\Delta$	$\alpha$
6P	IRS 38	2007-02-13 22:24:59.9	31.82	4.386-	3.849	11.9
7P	IRS 40	2007-04-19 14:39:10.3	11.63	4.340-	4.032	13.1
11P	MIPS 34	2006-09-01 14:44:54.3	41.99	4.400-	4.042	13.1
11P	MIPS 34	2006-09-02 01:01:44.6	41.99	4.398-	4.048	13.1
14P	IRS 39	2007-03-20 17:49:43.7	13.47	4.515-	4.527	12.7
15P	MIPS 39	2007-02-28 02:54:36.8	36.86	4.397-	4.315	13.1
15P	MIPS 39	2007-02-28 07:59:25.9	36.86	4.396-	4.311	13.1
16P	MIPS 40	2007-04-10 08:57:13.0	49.34	3.398-	3.367	17.0
16P	MIPS 40	2007-04-10 13:23:37.5	49.34	3.397-	3.363	17.0
22P	IRS 40	2007-04-19 13:32:00.2	63.00	4.866-	4.381	10.9
31P	IRS 36	2006-11-09 10:29:14.1	11.63	5.016-	4.594	11.1
32P	IRS 33	2006-08-01 03:05:00.7	90.50	4.141+	3.763	13.8
33P	IRS 36	2006-11-09 16:53:26.9	46.48	4.395-	4.172	13.4
37P	IRS 39	2007-03-11 23:11:26.8	123.52	4.313+	4.193	13.4
43P	IRS 40	2007-05-02 20:10:34.4	74.00	5.353+	4.984	10.4
47P	IRS 39	2007-03-21 10:55:23.7	9.80	4.319-	4.317	13.3
48P	IRS 36	2006-11-11 18:40:39.7	9.80	4.412+	4.323	13.4
50P	IRS 35	2006-10-23 17:28:50.4	110.68	3.478-	3.307	17.1
51P-A	MIPS 40	2007-04-06 18:07:47.5	45.67	3.768-	3.353	14.7
51P-A	MIPS 40	2007-04-06 22:46:33.7	45.67	3.767-	3.349	14.7
54P	IRS 39	2007-03-11 02:07:46.0	107.02	5.130-	4.684	10.5
56P	IRS 37	2006-12-23 13:43:59.8	130.93	5.075+	5.034	11.5
57P-A	IRS 41	2007-06-15 08:32:14.3	127.18	4.110-	3.919	14.2
62P	MIPS 35	2006-10-02 12:10:15.2	53.37	4.715+	4.646	12.5
62P	MIPS 35	2006-10-03 01:31:59.0	53.37	4.717+	4.656	12.5
68P	IRS 38	2007-02-12 09:40:34.4	28.15	5.469-	5.277	10.5
69P	IRS 33	2006-07-29 04:01:52.9	134.60	4.251+	3.663	12.2
74P	IRS 38	2007-01-28 16:56:47.0	13.47	4.420-	4.009	12.5
77P	IRS 38	2007-02-10 07:06:19.6	61.17	4.589-	4.178	12.0
78P	IRS 39	2007-03-10 01:56:45.4	40.99	4.983+	4.456	10.3
79P	IRS 34	2006-09-17 23:07:46.3	44.65	4.374-	4.082	13.4

Table 1 (cont'd)

Comet Desig.	I.&C.	UT at start	Dur.	$r \pm$	$\Delta$	$\alpha$
89P	IRS 40	2007-05-01 09:13:59.3	81.34	4.758-	4.176	10.5
93P	MIPS 35	2006-10-04 00:11:29.4	20.34	4.005-	3.559	14.0
93P	MIPS 35	2006-10-04 02:03:46.7	20.34	4.005-	3.560	14.0
94P	IRS 36	2006-11-14 19:05:48.3	77.67	4.789+	4.199	10.6
101P	IRS 40	2007-04-22 13:19:07.9	37.32	4.339+	3.760	11.6
107P	IRS 38	2007-02-12 07:36:55.2	17.14	4.078+	3.519	12.7
113P	IRS 35	2006-10-22 14:35:11.4	108.85	3.855-	3.547	15.2
118P	IRS 34	2006-09-17 11:37:10.0	18.97	4.946+	4.578	11.5
119P	IRS 38	2007-02-12 07:56:34.9	13.47	4.212+	3.672	12.4
120P	IRS 38	2007-02-12 06:05:17.9	88.67	4.798+	4.246	10.7
121P	IRS 33	2006-08-01 02:33:15.2	28.15	4.351+	3.966	13.1
123P	IRS 35	2006-10-21 21:32:12.6	136.43	5.344+	4.905	10.4
124P	IRS 34	2006-09-16 18:45:13.8	121.68	4.233-	3.762	13.1
127P	IRS 39	2007-03-08 16:24:16.4	42.82	4.588-	4.429	12.6
129P	IRS 40	2007-04-19 00:37:44.8	11.63	4.013+	3.671	14.1
130P	IRS 36	2006-11-14 10:12:40.0	50.15	4.452+	4.198	13.1
131P	IRS 38	2007-02-12 08:51:35.1	44.65	4.417+	3.964	12.3
132P	IRS 41	2007-06-07 18:44:05.3	129.02	3.987+	3.797	14.7
137P	IRS 39	2007-03-16 13:09:35.1	26.30	5.474-	5.450	10.5
138P	MIPS 38	2007-01-22 08:46:03.1	36.86	4.207+	4.214	13.7
138P	MIPS 38	2007-01-22 19:38:38.0	36.86	4.209+	4.209	13.7
139P	MIPS 36	2006-11-02 07:16:15.2	7.51	4.097-	3.572	13.2
139P	MIPS 36	2006-11-02 11:00:52.0	7.51	4.097-	3.574	13.2
141P	IRS 39	2007-03-25 03:18:48.5	136.45	5.112+	4.539	9.8
143P	IRS 39	2007-03-09 16:14:09.4	9.80	4.988-	4.740	11.4
144P	MIPS 42	2007-07-09 21:58:01.2	49.34	4.606-	4.162	12.0
144P	MIPS 42	2007-07-10 01:32:37.3	49.34	4.605-	4.158	12.0
146P	IRS 33	2006-08-06 18:12:08.5	132.68	5.084-	4.856	11.5
148P	MIPS 36	2006-11-02 10:10:13.2	36.86	4.307-	3.890	13.1
148P	MIPS 36	2006-11-02 15:24:37.7	36.86	4.306-	3.892	13.1
149P	IRS 38	2007-02-09 02:19:40.4	118.02	5.552-	5.460	10.4
152P	IRS 34	2006-09-17 18:38:21.7	129.12	5.698+	5.580	10.4
159P	IRS 38	2007-02-13 08:41:54.7	114.35	6.121+	5.737	9.0
160P	IRS 37	2006-12-19 16:03:31.7	132.77	4.990+	4.828	11.7
162P	IRS 39	2007-03-17 21:48:23.8	134.62	4.820+	4.269	10.6
163P	IRS 33	2006-08-06 16:36:16.4	92.33	4.089+	3.947	14.5
168P	MIPS 41	2007-05-23 02:01:22.8	41.99	4.486+	4.090	12.4
168P	MIPS 41	2007-05-23 14:05:18.3	41.99	4.488+	4.099	12.4

Table 1 (cont'd)

Comet Desig.	I.&C.	UT at start	Dur.	$r \pm$	$\Delta$	$\alpha$
169P	MIPS 39	2007-03-01 14:03:41.1	36.86	4.293+	4.013	13.3
169P	MIPS 39	2007-03-01 18:31:54.1	36.86	4.294+	4.011	13.3
171P	IRS 39	2007-03-16 10:45:15.5	140.12	4.158+	4.087	13.9
172P	IRS 35	2006-10-18 20:31:32.1	28.13	4.250-	4.055	13.9
173P	IRS 35	2006-10-24 09:11:36.4	31.82	4.817-	4.317	11.2
197P/2003 KV <sub>2</sub>	MIPS 36	2006-11-04 17:12:43.1	22.91	4.208-	4.019	14.0
197P/2003 KV <sub>2</sub>	MIPS 36	2006-11-05 00:07:12.3	22.91	4.207-	4.014	14.0
203P/1999 WJ <sub>7</sub>	MIPS 35	2006-10-05 15:10:54.9	12.65	5.646-	5.097	9.2
203P/1999 WJ <sub>7</sub>	MIPS 35	2006-10-06 01:44:01.5	12.65	5.645-	5.103	9.3
213P/2005 R2	IRS 36	2006-11-13 12:48:10.4	24.47	4.051+	3.706	14.2
215P/2002 O8	MIPS 38	2007-01-08 17:44:29.1	7.51	4.765-	4.235	11.0
215P/2002 O8	MIPS 38	2007-01-09 03:53:22.0	7.51	4.765-	4.229	10.9
216P/2001 CV <sub>8</sub>	MIPS 38	2007-01-01 12:48:02.7	12.65	4.411-	3.948	12.4
216P/2001 CV <sub>8</sub>	MIPS 38	2007-01-01 15:21:43.6	12.65	4.411-	3.949	12.4
219P/2002 LZ <sub>11</sub>	MIPS 41	2007-06-07 04:33:40.8	17.78	4.781-	4.223	10.8
219P/2002 LZ <sub>11</sub>	MIPS 41	2007-06-07 07:06:24.3	17.78	4.781-	4.224	10.8
221P/2002 JN <sub>16</sub>	MIPS 40	2007-04-09 23:45:17.8	36.86	4.404-	3.829	11.4
221P/2002 JN <sub>16</sub>	MIPS 40	2007-04-10 02:18:57.8	36.86	4.403-	3.830	11.5
223P/2002 S1	MIPS 40	2007-04-05 23:50:51.1	36.86	5.695-	5.144	8.8
223P/2002 S1	MIPS 40	2007-04-06 08:15:30.1	36.86	5.694-	5.139	8.8
228P/2001 YX <sub>127</sub>	IRS 35	2006-10-22 11:13:26.9	31.82	4.844+	4.439	11.6
240P/2002 X2	IRS 40	2007-04-21 22:48:14.9	88.67	5.540-	5.265	10.2
243P/2003 S2	IRS 38	2007-02-13 23:24:41.7	132.77	5.178+	4.846	10.9
244P/2000 Y3	MIPS 35	2006-10-03 02:28:12.6	26.59	5.976-	5.895	9.9
244P/2000 Y3	MIPS 35	2006-10-03 10:30:13.7	26.59	5.975-	5.900	9.9
246P/2004 F3	IRS 37	2006-12-17 23:18:30.2	11.63	4.280+	3.707	12.1
256P/2003 HT <sub>15</sub>	MIPS 37	2006-12-06 12:30:12.3	31.72	6.212+	5.660	8.2
256P/2003 HT <sub>15</sub>	MIPS 37	2006-12-06 19:57:46.7	31.72	6.213+	5.664	8.3
260P/2005 K3	MIPS 38	2007-01-01 03:29:24.1	31.72	4.202+	3.946	13.8
260P/2005 K3	MIPS 38	2007-01-01 07:24:09.7	31.72	4.203+	3.944	13.8
P/1998 VS <sub>24</sub>	MIPS 36	2006-11-02 07:27:01.2	7.51	4.173-	3.781	13.6
P/1998 VS <sub>24</sub>	MIPS 36	2006-11-02 10:50:05.4	7.51	4.173-	3.783	13.6
P/2001 R6	MIPS 40	2007-04-05 10:50:32.6	45.67	5.743-	5.178	8.7
P/2001 R6	MIPS 40	2007-04-05 13:56:06.1	45.67	5.743-	5.176	8.7
P/2003 O3	MIPS 42	2007-07-09 11:40:04.5	36.86	4.282-	4.100	13.7
P/2003 O3	MIPS 42	2007-07-09 17:09:50.8	36.86	4.281-	4.103	13.7
P/2003 S1	IRS 39	2007-03-08 10:42:49.4	48.32	5.772+	5.371	9.4
P/2004 A1 <sup>a</sup>	MIPS 39	2007-03-04 20:37:18.6	36.86	6.517+	6.418	8.8
P/2004 A1 <sup>a</sup>	MIPS 39	2007-03-05 01:00:51.0	36.86	6.517+	6.418	8.8

Table 1 (cont'd)

Comet Desig.	I.&C.	UT at start	Dur.	$r \pm$	$\Delta$	$\alpha$
P/2004 DO <sub>29</sub>	IRS 34	2006-09-18 03:38:42.4	99.68	5.550+	5.207	10.3
P/2004 H2	MIPS 38	2007-01-01 20:34:16.9	12.65	5.457+	5.070	10.2
P/2004 H2	MIPS 38	2007-01-02 00:06:03.0	12.65	5.457+	5.072	10.2
P/2004 T1	MIPS 39	2007-02-28 04:21:38.2	31.72	4.914+	4.419	10.7
P/2004 T1	MIPS 39	2007-02-28 09:33:17.3	31.72	4.915+	4.417	10.7
P/2004 V3	IRS 34	2006-09-18 05:29:58.8	83.17	5.358+	4.895	10.3
P/2004 V5-A	IRS 39	2007-03-10 00:42:43.1	48.32	5.811+	5.565	9.8
P/2004 VR <sub>8</sub>	IRS 33	2006-08-07 18:02:45.4	66.67	3.443+	3.350	17.2
P/2005 GF <sub>8</sub>	IRS 36	2006-11-12 23:26:43.4	11.63	4.164+	3.793	13.7
P/2005 JD <sub>108</sub>	MIPS 38	2007-01-01 20:08:55.7	7.51	4.772+	4.318	11.4
P/2005 JD <sub>108</sub>	MIPS 38	2007-01-01 21:19:22.2	7.51	4.772+	4.319	11.4
P/2005 JQ <sub>5</sub>	IRS 36	2006-11-21 13:10:28.5	108.85	4.022+	3.996	14.6
P/2005 L4	IRS 39	2007-03-11 22:46:06.3	22.63	4.145+	4.075	13.9
P/2005 Q4	MIPS 39	2007-02-28 03:36:18.6	41.99	4.409+	3.933	12.1
P/2005 Q4	MIPS 39	2007-02-28 08:47:57.7	41.99	4.411+	3.931	12.1
P/2005 R1	IRS 37	2006-12-19 12:35:13.0	29.98	4.116+	3.719	13.7
P/2005 S3	MIPS 41	2007-05-23 02:47:40.2	7.51	4.117+	3.876	14.0
P/2005 S3	MIPS 41	2007-05-23 14:51:35.7	7.51	4.119+	3.885	14.0
P/2005 T5	MIPS 35	2006-10-09 13:43:37.7	7.51	3.995+	3.705	14.7
P/2005 T5	MIPS 35	2006-10-09 15:53:20.8	7.51	3.995+	3.704	14.7
C/2005 W2 <sup>b</sup>	MIPS 38	2007-01-01 02:59:55.5	7.51	4.071+	3.764	14.1
C/2005 W2 <sup>b</sup>	MIPS 38	2007-01-01 04:26:05.0	7.51	4.071+	3.764	14.1
P/2005 W3	MIPS 37	2006-12-08 02:37:58.4	7.51	4.359+	4.349	13.4
P/2005 W3	MIPS 37	2006-12-08 04:33:05.3	7.51	4.360+	4.348	13.4
P/2005 XA <sub>54</sub>	MIPS 41	2007-06-04 15:57:41.9	41.99	4.423+	3.858	11.7
P/2005 XA <sub>54</sub>	MIPS 41	2007-06-04 23:09:21.8	41.99	4.425+	3.856	11.6
P/2005 Y2	MIPS 38	2007-01-19 22:46:26.2	10.08	5.410+	5.060	10.4
P/2005 Y2	MIPS 38	2007-01-20 05:00:15.2	10.08	5.411+	5.065	10.4

<sup>a</sup> P/2004 A1 is also a Centaur but has  $2 < T_J < 3$ .

<sup>b</sup> C/2005 W2 is possibly a Halley-family comet but has  $2 < T_J < 3$ .

**Table 2**

Nucleus contribution to comet flux within a radius 3-pixel circular aperture. Comets observed with IRS are listed first, followed by comets observed with MIPS. Table columns are: “Comet Desig.” = comet’s designation, as in Table 1; “ $f_A$ ” = fraction of comet’s flux from the nucleus at blue PU wavelength (for IRS observations) or at first epoch (for MIPS observations); “ $f_B$ ” = fraction at red PU wavelength (for IRS observations) or at second epoch (for MIPS observations). The 35 comets that showed discernible dust emission are indicated with underscored ratios (see §3.1).

Comet Desig.	$f_A$	$f_B$	Comet Desig.	$f_A$	$f_B$
<i>IRS</i>					
6P	<u><math>0.99 \pm 0.01</math></u>	<u><math>0.98 \pm 0.01</math></u>	127P	$1.14 \pm 0.10$	$1.11 \pm 0.10$
7P	$1.01 \pm 0.02$	$1.00 \pm 0.02$	129P	<u><math>0.35 \pm 0.04</math></u>	<u><math>0.26 \pm 0.03</math></u>
14P	$1.01 \pm 0.02$	$1.00 \pm 0.01$	130P	$0.99 \pm 0.01$	$0.95 \pm 0.01$
22P	<u><math>0.71 \pm 0.03</math></u>	<u><math>0.63 \pm 0.05</math></u>	131P	$1.11 \pm 0.04$	$1.01 \pm 0.04$
31P	$1.07 \pm 0.09$	$1.11 \pm 0.09$	132P	$0.94 \pm 0.03$	$1.00 \pm 0.04$
32P	<u><math>0.18 \pm 0.03</math></u>	<u><math>0.25 \pm 0.02</math></u>	137P	$1.03 \pm 0.02$	$0.99 \pm 0.01$
33P	$0.95 \pm 0.05$	$1.06 \pm 0.04$	143P	$1.00 \pm 0.01$	$1.01 \pm 0.01$
37P	<u><math>0.61 \pm 0.10</math></u>	<u><math>0.48 \pm 0.04</math></u>	146P	$1.08 \pm 0.11$	$1.00 \pm 0.08$
47P	$1.00 \pm 0.01$	$0.98 \pm 0.01$	149P	$0.91 \pm 0.04$	$0.99 \pm 0.04$
48P	<u><math>0.78 \pm 0.08</math></u>	<u><math>0.89 \pm 0.08</math></u>	152P	<u><math>0.33 \pm 0.07</math></u>	<u><math>0.34 \pm 0.11</math></u>
50P	<u><math>0.97 \pm 0.01</math></u>	<u><math>0.91 \pm 0.02</math></u>	159P	<u><math>0.35 \pm 0.12</math></u>	<u><math>0.55 \pm 0.10</math></u>
56P	<u><math>0.90 \pm 0.14</math></u>	<u><math>0.99 \pm 0.03</math></u>	160P	$1.16 \pm 0.09$	$0.89 \pm 0.05$
57P	$1.00 \pm 0.03$	$1.02 \pm 0.03$	162P	$1.00 \pm 0.01$	$1.00 \pm 0.01$
68P	$0.99 \pm 0.03$	$1.03 \pm 0.02$	163P	$1.01 \pm 0.02$	$1.00 \pm 0.02$
69P	<u><math>0.82 \pm 0.02</math></u>	<u><math>0.47 \pm 0.06</math></u>	171P	<u><math>0.68 \pm 0.04</math></u>	<u><math>0.68 \pm 0.07</math></u>
74P	<u><math>0.33 \pm 0.04</math></u>	<u><math>0.41 \pm 0.03</math></u>	172P	$1.01 \pm 0.01$	$1.01 \pm 0.01$
77P	$0.96 \pm 0.02$	$0.96 \pm 0.01$	173P	<u><math>0.39 \pm 0.08</math></u>	<u><math>0.51 \pm 0.08</math></u>
78P	<u><math>0.51 \pm 0.10</math></u>	<u><math>0.46 \pm 0.09</math></u>	213P/2005 R2	<u><math>0.10 \pm 0.01</math></u>	<u><math>0.12 \pm 0.02</math></u>
79P	$0.87 \pm 0.09$	$0.94 \pm 0.10$	228P/2001 YX127	$0.77 \pm 0.11$	$0.88 \pm 0.06$
89P	$1.00 \pm 0.02$	$0.88 \pm 0.03$	246P/2004 F3	<u><math>0.27 \pm 0.03</math></u>	<u><math>0.25 \pm 0.03</math></u>
94P	$1.01 \pm 0.01$	$0.97 \pm 0.01$	P/2004 DO29	$1.02 \pm 0.10$	$0.99 \pm 0.08$
101P	<u><math>0.28 \pm 0.06</math></u>	<u><math>0.26 \pm 0.05</math></u>	P/2004 V3	$1.07 \pm 0.09$	$1.17 \pm 0.08$
107P	$1.04 \pm 0.02$	$1.02 \pm 0.02$	P/2004 V5-A	<u><math>0.13 \pm 0.05</math></u>	<u><math>0.15 \pm 0.05</math></u>
113P	$1.02 \pm 0.01$	$1.01 \pm 0.01$	P/2004 VR8	<u><math>0.83 \pm 0.11</math></u>	<u><math>0.84 \pm 0.02</math></u>
118P	<u><math>0.23 \pm 0.06</math></u>	<u><math>0.63 \pm 0.05</math></u>	P/2005 GF8	$0.96 \pm 0.01$	$0.98 \pm 0.01$
119P	<u><math>0.26 \pm 0.04</math></u>	<u><math>0.24 \pm 0.08</math></u>	P/2005 JQ5	$0.88 \pm 0.07$	$0.90 \pm 0.05$
121P	<u><math>0.99 \pm 0.01</math></u>	<u><math>1.02 \pm 0.01</math></u>	P/2005 L4	$1.02 \pm 0.02$	$1.06 \pm 0.02$
123P	$0.97 \pm 0.01$	$1.00 \pm 0.01$	P/2005 R1	$1.00 \pm 0.02$	$1.00 \pm 0.02$
124P	$1.02 \pm 0.01$	$0.99 \pm 0.01$			

**Table 2 (cont'd)**

Comet Desig.	$f_A$	$f_B$	Comet Desig.	$f_A$	$f_B$
<i>MIPS</i>					
11P	$1.03 \pm 0.11$	$1.31 \pm 0.13$	221P/2002 JN16	$0.96 \pm 0.03$	$0.92 \pm 0.02$
15P	$0.93 \pm 0.05$	$0.94 \pm 0.06$	223P/2002 S1	$1.01 \pm 0.01$	$1.01 \pm 0.01$
16P	<u><math>0.61 \pm 0.09</math></u>	<u><math>0.47 \pm 0.06</math></u>	256P/2003 HT15	$0.95 \pm 0.19$	$0.76 \pm 0.18$
51P	$0.79 \pm 0.09$	$0.94 \pm 0.09$	260P/2005 K3	<u><math>0.98 \pm 0.01</math></u>	<u><math>0.97 \pm 0.02</math></u>
62P	<u><math>0.62 \pm 0.19</math></u>	<u><math>0.33 \pm 0.10</math></u>	P/2001 R6	$1.07 \pm 0.18$	$1.32 \pm 0.18$
93P	$1.01 \pm 0.01$	$0.98 \pm 0.01$	P/2003 O3	$0.95 \pm 0.10$	$1.07 \pm 0.15$
138P	$1.33 \pm 0.13$	$1.05 \pm 0.09$	P/2004 A1	<u><math>0.23 \pm 0.02</math></u>	<u><math>0.22 \pm 0.03</math></u>
139P	$0.89 \pm 0.05$	$0.91 \pm 0.06$	P/2004 H2	<u><math>0.45 \pm 0.05</math></u>	<u><math>0.46 \pm 0.15</math></u>
144P	<u><math>1.19 \pm 0.06</math></u>	<u><math>1.09 \pm 0.05</math></u>	P/2005 JD108	<u><math>0.34 \pm 0.04</math></u>	<u><math>0.30 \pm 0.03</math></u>
148P	$1.14 \pm 0.02$	$1.12 \pm 0.02$	P/2005 Q4	$1.11 \pm 0.01$	$1.08 \pm 0.01$
168P	$0.76 \pm 0.12$	$0.97 \pm 0.16$	P/2005 S3	$0.96 \pm 0.05$	$0.96 \pm 0.13$
169P	$1.00 \pm 0.01$	$1.03 \pm 0.01$	P/2005 T5	<u><math>0.76 \pm 0.08</math></u>	<u><math>0.77 \pm 0.07</math></u>
197P/2003 KV2	$0.90 \pm 0.07$	$0.89 \pm 0.06$	P/2005 W2	<u><math>0.18 \pm 0.06</math></u>	<u><math>1.24 \pm 0.44</math></u>
215P/2002 O8	$0.86 \pm 0.07$	$0.83 \pm 0.08$	P/2005 W3	<u><math>0.25 \pm 0.10</math></u>	<u><math>0.27 \pm 0.11</math></u>
216P/2001 CV8	$1.85 \pm 0.31$	$0.94 \pm 0.14$	P/2005 XA54	$1.01 \pm 0.01$	$0.97 \pm 0.01$
219P/2001 LZ11	<u><math>1.01 \pm 0.07</math></u>	<u><math>0.94 \pm 0.05</math></u>	P/2005 Y2	<u><math>0.39 \pm 0.04</math></u>	<u><math>0.35 \pm 0.04</math></u>



**Table 3.** Nucleus photometry. Entries with “<” indicate  $3\sigma$  upper limits. Comets observed with IRS are listed first, followed by comets observed with MIPS. Table columns are: “Comet Desig.” = comet’s designation, as in Table 1; “ $F_A$ ” = flux density in mJy at blue PU wavelength (for IRS observations) or at first epoch (for MIPS observations); “ $F_B$ ” = flux density in mJy at red PU wavelength (for IRS observations) or at second epoch (for MIPS observations). The 35 comets that showed discernible dust emission are indicated with underscored flux densities (see §3.1).

Comet Desig.	$F_A$ (mJy)	$F_B$ (mJy)	Comet Desig.	$F_A$ (mJy)	$F_B$ (mJy)
<i>IRS</i>					
6P	<u><math>2.22 \pm 0.11</math></u>	<u><math>3.47 \pm 0.17</math></u>	127P	$0.25 \pm 0.02$	$0.35 \pm 0.05$
7P	$2.96 \pm 0.15$	$4.50 \pm 0.22$	129P	<u><math>0.82 \pm 0.08</math></u>	<u><math>1.56 \pm 0.16</math></u>
14P	$2.55 \pm 0.13$	$4.27 \pm 0.21$	130P	$1.64 \pm 0.08$	$3.13 \pm 0.16$
22P	<u><math>1.28 \pm 0.10</math></u>	<u><math>1.93 \pm 0.18</math></u>	131P	$0.54 \pm 0.04$	$0.78 \pm 0.06$
31P	$0.59 \pm 0.04$	$1.03 \pm 0.08$	132P	$0.36 \pm 0.03$	$0.58 \pm 0.04$
32P	<u><math>3.03 \pm 0.61</math></u>	<u><math>4.64 \pm 0.93</math></u>	137P	$2.07 \pm 0.10$	$3.56 \pm 0.18$
33P	$0.46 \pm 0.02$	$0.86 \pm 0.04$	141P	— <sup>a</sup>	— <sup>a</sup>
37P	<u><math>0.57 \pm 0.07</math></u>	<u><math>0.96 \pm 0.10</math></u>	143P	$4.73 \pm 0.24$	$8.34 \pm 0.42$
43P	< 0.27	< 0.30	146P	$0.17 \pm 0.02$	$0.31 \pm 0.03$
47P	$3.41 \pm 0.17$	$5.77 \pm 0.29$	149P	$0.25 \pm 0.02$	$0.44 \pm 0.02$
48P	<u><math>2.96 \pm 0.20</math></u>	<u><math>5.02 \pm 0.32</math></u>	152P	<u><math>0.10 \pm 0.02</math></u>	<u><math>0.26 \pm 0.08</math></u>
50P	<u><math>2.07 \pm 0.10</math></u>	<u><math>3.73 \pm 0.19</math></u>	159P	<u><math>0.12 \pm 0.04</math></u>	<u><math>0.43 \pm 0.08</math></u>
54P	< 0.08	< 0.12	160P	$0.17 \pm 0.02$	$0.38 \pm 0.03$
56P	<u><math>0.58 \pm 0.07</math></u>	<u><math>1.22 \pm 0.10</math></u>	162P	$13.28 \pm 0.66$	$24.89 \pm 1.25$
57P-A	$0.46 \pm 0.03$	$0.65 \pm 0.09$	163P	$0.84 \pm 0.04$	$1.38 \pm 0.07$
68P	$1.02 \pm 0.05$	$1.88 \pm 0.09$	171P	<u><math>0.71 \pm 0.06</math></u>	<u><math>1.05 \pm 0.11</math></u>
69P	<u><math>0.39 \pm 0.02</math></u>	<u><math>0.62 \pm 0.08</math></u>	172P	$13.67 \pm 0.68$	$22.21 \pm 1.11$
74P	<u><math>3.09 \pm 0.39</math></u>	<u><math>9.98 \pm 0.77</math></u>	173P	<u><math>3.70 \pm 0.74</math></u>	<u><math>15.17 \pm 2.28</math></u>
77P	$0.82 \pm 0.06$	$1.63 \pm 0.08$	213P/2005 R2	<u><math>1.16 \pm 0.16</math></u>	<u><math>3.62 \pm 0.62</math></u>
78P	<u><math>0.41 \pm 0.08</math></u>	<u><math>0.78 \pm 0.16</math></u>	228P/2001 YX <sub>127</sub>	$0.28 \pm 0.04$	$0.80 \pm 0.06$
79P	$0.20 \pm 0.02$	$0.30 \pm 0.03$	240P/2002 X2	— <sup>a</sup>	— <sup>a</sup>
89P	$0.69 \pm 0.03$	$0.95 \pm 0.05$	243P/2003 S2	< 0.05	< 0.12
94P	$1.52 \pm 0.12$	$2.62 \pm 0.13$	246P/2004 F3	<u><math>8.08 \pm 0.81</math></u>	<u><math>17.86 \pm 2.33</math></u>
101P	<u><math>0.41 \pm 0.08</math></u>	<u><math>0.85 \pm 0.16</math></u>	P/2003 S1	< $0.12^b$	< $0.22^b$
107P	$1.25 \pm 0.06$	$2.20 \pm 0.11$	P/2004 DO <sub>29</sub>	$0.15 \pm 0.01$	$0.27 \pm 0.02$
113P	$2.00 \pm 0.10$	$3.12 \pm 0.16$	P/2004 V3	$0.14 \pm 0.01$	$0.24 \pm 0.02$
118P	<u><math>0.32 \pm 0.06</math></u>	<u><math>1.03 \pm 0.21</math></u>	P/2004 V5-A	<u><math>0.21 \pm 0.16</math></u>	<u><math>0.57 \pm 0.16</math></u>
119P	<u><math>0.48 \pm 0.08</math></u>	<u><math>1.16 \pm 0.39</math></u>	P/2004 VR <sub>8</sub>	<u><math>29.48 \pm 2.41</math></u>	<u><math>42.73 \pm 2.14</math></u>
120P	< 0.06	< 0.14	P/2005 GF <sub>8</sub>	$3.49 \pm 0.17$	$6.46 \pm 0.32$
121P	<u><math>5.92 \pm 0.30</math></u>	<u><math>10.85 \pm 0.54</math></u>	P/2005 JQ <sub>5</sub>	$0.19 \pm 0.01$	$0.44 \pm 0.02$
123P	$0.68 \pm 0.03$	$1.75 \pm 0.09$	P/2005 L4	$1.71 \pm 0.09$	$2.36 \pm 0.12$
124P	$3.37 \pm 0.17$	$5.65 \pm 0.28$	P/2005 R1	$1.50 \pm 0.08$	$2.35 \pm 0.12$

Table 3 (cont'd)

Comet Desig.	$F_A$ (mJy)	$F_B$ (mJy)	Comet Desig.	$F_A$ (mJy)	$F_B$ (mJy)
<i>MIPS</i>					
11P	$0.22 \pm 0.02$	$0.23 \pm 0.02$	223P/2002 S1	$2.37 \pm 0.02$	$2.10 \pm 0.02$
15P	$0.52 \pm 0.03$	$0.49 \pm 0.03$	244P/2000 Y3	< 0.30	< 0.30
16P	<u><math>0.91 \pm 0.13</math></u>	<u><math>0.64 \pm 0.08</math></u>	256P/2003 HT <sub>15</sub>	$0.11 \pm 0.02$	$0.09 \pm 0.02$
51P-A	$0.21 \pm 0.02$	$0.23 \pm 0.02$	260P/2005 K3	<u><math>1.86 \pm 0.03</math></u>	<u><math>1.81 \pm 0.03</math></u>
62P	<u><math>0.16 \pm 0.05</math></u>	<u><math>0.16 \pm 0.05</math></u>	P/1998 VS <sub>24</sub>	< $1.02^b$	< $1.02^b$
93P	$5.94 \pm 0.03$	$7.90 \pm 0.04$	P/2001 R6	$0.12 \pm 0.02$	$0.15 \pm 0.02$
138P	$0.43 \pm 0.04$	$0.35 \pm 0.03$	P/2003 O3	$0.25 \pm 0.03$	$0.20 \pm 0.03$
139P	$1.70 \pm 0.09$	$2.01 \pm 0.12$	P/2004 A1	<u><math>1.61 \pm 0.16</math></u>	<u><math>1.45 \pm 0.16</math></u>
144P	<u><math>0.39 \pm 0.02</math></u>	<u><math>0.44 \pm 0.02</math></u>	P/2004 H2	<u><math>0.43 \pm 0.05</math></u>	<u><math>0.48 \pm 0.16</math></u>
148P	$1.00 \pm 0.02$	$0.99 \pm 0.02$	P/2004 T1	< $0.30^b$	< $0.30^b$
168P	$0.15 \pm 0.02$	$0.15 \pm 0.02$	P/2005 JD <sub>108</sub>	<u><math>4.33 \pm 0.48</math></u>	<u><math>4.01 \pm 0.40</math></u>
169P	$4.20 \pm 0.02$	$4.72 \pm 0.02$	P/2005 Q4	$1.49 \pm 0.02$	$1.68 \pm 0.02$
197P/2003 KV <sub>2</sub>	$0.58 \pm 0.05$	$0.66 \pm 0.04$	P/2005 S3	$1.84 \pm 0.10$	$1.49 \pm 0.20$
203P/1999 WJ <sub>7</sub>	< 0.28	< 0.28	P/2005 T5	<u><math>1.60 \pm 0.16</math></u>	<u><math>1.76 \pm 0.16</math></u>
215P/2002 O8	$0.97 \pm 0.08$	$0.81 \pm 0.07$	C/2005 W2	<u><math>0.24 \pm 0.08</math></u>	<u><math>0.24 \pm 0.08</math></u>
216P/2001 CV <sub>8</sub>	$0.25 \pm 0.04$	$0.25 \pm 0.04$	P/2005 W3	<u><math>0.80 \pm 0.32</math></u>	<u><math>0.80 \pm 0.32</math></u>
219P/2002 LZ <sub>11</sub>	<u><math>0.49 \pm 0.03</math></u>	<u><math>0.58 \pm 0.03</math></u>	P/2005 XA <sub>54</sub>	$5.96 \pm 0.02$	$4.97 \pm 0.02$
221P/2002 JN <sub>16</sub>	$0.77 \pm 0.02$	$0.83 \pm 0.02$	P/2005 Y2	<u><math>8.04 \pm 0.80</math></u>	<u><math>7.24 \pm 0.80</math></u>

<sup>a</sup> Neither 141P nor 240P were in the field of view, hence no upper limit.

<sup>b</sup> P/1998 VS<sub>24</sub>, P/2003 S1, and P/2004 T1 may or may not have been in the field of view, the upper limits given here assume they were.

**Table 4**

Radius and beaming parameter for each of the 57 comets with two IRS detections. Table columns are: “Comet Desig.” = comet’s designation, as in Table 1; “ $R_N$ ” = effective radius in kilometers; “ $\eta$ ” = beaming parameter.

Comet Desig.	$R_N$ (km)	$\eta$	Comet Desig.	$R_N$ (km)	$\eta$
6P	$1.99^{+0.33}_{-0.27}$	$0.84^{+0.26}_{-0.21}$	127P	$0.62^{+0.25}_{-0.20}$	$0.52^{+0.45}_{-0.27}$
7P	$2.30^{+0.37}_{-0.33}$	$0.80^{+0.25}_{-0.21}$	129P	$1.65^{+0.59}_{-0.43}$	$1.71^{+1.04}_{-0.69}$
14P	$2.87^{+0.46}_{-0.39}$	$0.98^{+0.28}_{-0.23}$	130P	$2.67^{+0.45}_{-0.35}$	$1.39^{+0.40}_{-0.29}$
22P	$1.59^{+0.46}_{-0.36}$	$0.60^{+0.35}_{-0.24}$	131P	$0.88^{+0.22}_{-0.18}$	$0.65^{+0.34}_{-0.24}$
31P	$1.47^{+0.37}_{-0.28}$	$0.79^{+0.39}_{-0.27}$	132P	$0.89^{+0.24}_{-0.19}$	$1.24^{+0.32}_{-0.30}$
32P	$2.20^{+1.87}_{-1.06}$	$0.89^{+1.62}_{-0.67}$	137P	$3.22^{+0.51}_{-0.44}$	$0.71^{+0.20}_{-0.16}$
33P	$1.36^{+0.22}_{-0.18}$	$1.36^{+0.38}_{-0.29}$	143P	$4.45^{+0.72}_{-0.62}$	$0.91^{+0.26}_{-0.21}$
37P	$1.45^{+0.57}_{-0.42}$	$1.36^{+0.98}_{-0.62}$	146P	$0.93^{+0.34}_{-0.25}$	$0.98^{+0.64}_{-0.21}$
47P	$3.21^{+0.51}_{-0.46}$	$1.09^{+0.31}_{-0.27}$	149P	$1.25^{+0.24}_{-0.20}$	$0.82^{+0.28}_{-0.22}$
48P	$3.09^{+0.75}_{-0.60}$	$1.14^{+0.51}_{-0.37}$	152P	$1.36^{+1.53}_{-0.77}$	$1.19^{+2.40}_{-0.92}$
50P	$2.17^{+0.36}_{-0.31}$	$2.00^{+0.56}_{-0.46}$	159P	$2.90^{+4.53}_{-1.72}$	$2.46^{+5.19}_{-1.63}$
56P	$2.51^{+0.86}_{-0.63}$	$1.60^{+0.88}_{-0.60}$	160P	$1.21^{+0.42}_{-0.28}$	$1.41^{+0.83}_{-0.49}$
57P-A	$0.78^{+0.21}_{-0.21}$	$0.73^{+0.21}_{-0.21}$	162P	$7.53^{+1.23}_{-1.10}$	$1.15^{+0.31}_{-0.27}$
68P	$2.50^{+0.40}_{-0.34}$	$0.86^{+0.23}_{-0.19}$	163P	$1.39^{+0.23}_{-0.20}$	$1.13^{+0.34}_{-0.27}$
69P	$0.83^{+0.26}_{-0.22}$	$0.96^{+0.54}_{-0.40}$	171P	$1.06^{+0.34}_{-0.26}$	$0.74^{+0.48}_{-0.32}$
74P	$9.03^{+3.16}_{-2.28}$	$4.51^{+2.05}_{-1.46}$	172P	$5.60^{+0.92}_{-0.81}$	$1.00^{+0.31}_{-0.25}$
77P	$2.01^{+0.41}_{-0.31}$	$1.43^{+0.49}_{-0.35}$	173P	$16.18^{+11.14}_{-6.51}$	$5.81^{+4.47}_{-2.71}$
78P	$1.41^{+1.20}_{-0.67}$	$1.11^{+1.66}_{-0.77}$	213P/2005 R2	$4.84^{+2.86}_{-1.89}$	$5.04^{+3.66}_{-2.42}$
79P	$0.56^{+0.21}_{-0.15}$	$0.65^{+0.55}_{-0.33}$	228P/2001 YX <sub>127</sub>	$2.41^{+0.91}_{-0.63}$	$2.95^{+1.57}_{-1.05}$
89P	$0.95^{+0.15}_{-0.11}$	$0.48^{+0.16}_{-0.11}$	246P/2004 F3	$6.87^{+2.89}_{-2.11}$	$2.18^{+1.38}_{-0.95}$
94P	$2.05^{+0.40}_{-0.33}$	$0.85^{+0.32}_{-0.23}$	P/2004 DO <sub>29</sub>	$0.90^{+0.22}_{-0.16}$	$0.77^{+0.33}_{-0.22}$
101P	$1.40^{+1.10}_{-0.63}$	$1.83^{+2.36}_{-1.18}$	P/2004 V3	$0.75^{+0.20}_{-0.15}$	$0.73^{+0.35}_{-0.24}$
107P	$1.70^{+0.26}_{-0.24}$	$1.35^{+0.37}_{-0.31}$	P/2004 V5-A	$2.28^{+2.57}_{-1.20}$	$1.82^{+3.17}_{-1.28}$
113P	$1.77^{+0.27}_{-0.27}$	$1.11^{+0.32}_{-0.30}$	P/2004 VR <sub>8</sub>	$6.02^{+1.48}_{-1.12}$	$1.31^{+0.68}_{-0.45}$
118P	$3.29^{+2.71}_{-1.53}$	$3.57^{+3.61}_{-2.04}$	P/2005 GF <sub>8</sub>	$3.35^{+0.57}_{-0.46}$	$1.49^{+0.43}_{-0.33}$
119P	$1.96^{+2.13}_{-1.19}$	$2.78^{+4.11}_{-2.14}$	P/2005 JQ <sub>5</sub>	$1.25^{+0.20}_{-0.17}$	$2.72^{+0.66}_{-0.54}$
121P	$4.49^{+0.72}_{-0.63}$	$1.33^{+0.37}_{-0.31}$	P/2005 L4	$1.50^{+0.23}_{-0.22}$	$0.65^{+0.22}_{-0.18}$
123P	$3.44^{+0.56}_{-0.45}$	$1.95^{+0.44}_{-0.36}$	P/2005 R1	$1.60^{+0.24}_{-0.24}$	$0.97^{+0.27}_{-0.26}$
124P	$2.73^{+0.44}_{-0.38}$	$1.11^{+0.32}_{-0.26}$			

**Table 5**

Radii or radii limits for the other 43 comets in our survey. Two radii are given for each of the 32 comets detected by MIPS at two epochs. Table columns are: ‘‘Comet Desig.’’ = comet’s designation, as in Table 1; ‘‘ $R_{N1}$ ’’ = effective radius in kilometers at first MIPS epoch or blue IRS wavelength; ‘‘ $R_{N2}$ ’’ = effective radius in kilometers at second MIPS epoch or red IRS wavelength.

Comet Desig.	$R_{N1}$ (km)	$R_{N2}$ (km)	Comet Desig.	$R_{N1}$ (km)	$R_{N2}$ (km)
<i>MIPS detections</i>					
11P	$0.57^{+0.04}_{-0.04}$	$0.58^{+0.04}_{-0.04}$	221P/2002 JN <sub>16</sub>	$1.01^{+0.05}_{-0.06}$	$1.04^{+0.07}_{-0.06}$
15P	$0.93^{+0.05}_{-0.04}$	$0.91^{+0.04}_{-0.04}$	223P/2002 S1	$3.02^{+0.18}_{-0.18}$	$2.84^{+0.17}_{-0.18}$
16P	$0.78^{+0.06}_{-0.06}$	$0.65^{+0.05}_{-0.06}$	256P/2003 HT <sub>15</sub>	$0.78^{+0.09}_{-0.08}$	$0.71^{+0.08}_{-0.09}$
51P-A	$0.40^{+0.03}_{-0.02}$	$0.42^{+0.03}_{-0.02}$	260P/2005 K3	$1.55^{+0.09}_{-0.09}$	$1.53^{+0.09}_{-0.09}$
62P	$0.59^{+0.09}_{-0.09}$	$0.59^{+0.09}_{-0.09}$	P/2001 R6	$0.69^{+0.06}_{-0.06}$	$0.77^{+0.07}_{-0.06}$
93P	$2.40^{+0.13}_{-0.13}$	$2.77^{+0.14}_{-0.13}$	P/2003 O3	$0.60^{+0.04}_{-0.04}$	$0.54^{+0.04}_{-0.04}$
138P	$0.80^{+0.05}_{-0.06}$	$0.72^{+0.04}_{-0.06}$	P/2004 A1	$3.59^{+0.27}_{-0.28}$	$3.40^{+0.27}_{-0.28}$
139P	$1.31^{+0.07}_{-0.07}$	$1.43^{+0.08}_{-0.07}$	P/2004 H2	$1.22^{+0.09}_{-0.10}$	$1.29^{+0.20}_{-0.10}$
144P	$0.81^{+0.04}_{-0.04}$	$0.86^{+0.05}_{-0.04}$	P/2005 JD <sub>108</sub>	$2.90^{+0.21}_{-0.23}$	$2.79^{+0.19}_{-0.23}$
148P	$1.15^{+0.05}_{-0.07}$	$1.14^{+0.06}_{-0.07}$	P/2005 Q4	$1.44^{+0.08}_{-0.08}$	$1.53^{+0.09}_{-0.08}$
168P	$0.48^{+0.04}_{-0.03}$	$0.48^{+0.04}_{-0.03}$	P/2005 S3	$1.49^{+0.08}_{-0.08}$	$1.34^{+0.11}_{-0.08}$
169P	$2.41^{+0.13}_{-0.13}$	$2.56^{+0.13}_{-0.13}$	P/2005 T5	$1.30^{+0.08}_{-0.10}$	$1.36^{+0.08}_{-0.10}$
197P/2003 KV <sub>2</sub>	$0.88^{+0.06}_{-0.05}$	$0.94^{+0.06}_{-0.05}$	C/2005 W2	$0.52^{+0.07}_{-0.09}$	$0.52^{+0.07}_{-0.09}$
215P/2002 O8	$1.34^{+0.09}_{-0.09}$	$1.23^{+0.07}_{-0.09}$	P/2005 W3	$1.16^{+0.22}_{-0.27}$	$1.16^{+0.22}_{-0.27}$
216P/2001 CV <sub>8</sub>	$0.59^{+0.05}_{-0.05}$	$0.59^{+0.05}_{-0.05}$	P/2005 XA <sub>54</sub>	$2.83^{+0.16}_{-0.15}$	$2.59^{+0.14}_{-0.15}$
219P/2002 LZ <sub>11</sub>	$0.95^{+0.06}_{-0.05}$	$1.04^{+0.05}_{-0.05}$	P/2005 Y2	$5.22^{+0.37}_{-0.40}$	$4.95^{+0.37}_{-0.40}$
<i>MIPS non-detections</i>					
203P/1999 WJ <sub>7</sub>	< 1.02	< 1.02	P/1998 VS <sub>24</sub>	< 1.09 <sup>b</sup>	< 1.10 <sup>b</sup>
244P/2000 Y3	< 1.30	< 1.30	P/2004 T1	< 0.80 <sup>b</sup>	< 0.80 <sup>b</sup>
<i>IRS non-detections</i>					
43P	< 1.34	< 1.01	240P/2002 X2	— <sup>a</sup>	— <sup>a</sup>
54P	< 0.64	< 0.58	243P/2003 S2	< 0.55	< 0.60
120P	< 0.48	< 0.53	P/2003 S1	< 1.08 <sup>b</sup>	< 1.01 <sup>b</sup>
141P	— <sup>a</sup>	— <sup>a</sup>			

<sup>a</sup> 141P and 240P were not in the field of view, hence no upper limit.

<sup>b</sup> P/1998 VS<sub>24</sub>, P/2003 S1, and P/2004 T1 may or may not have been in the field of view, the upper limits given here assume they were.

**Table 6**

Statistics from search for trends of  $\eta$  with various quantities. See §4.1 for details. Table columns are: “Quantity” = the independent variable that is compared to  $\eta$ , with \* indicating that the scatter plot is shown in Fig. 7; “ $m$ ” = best-fitting slope to the linear fit (with  $1\sigma$  error); “ $Z$ ” = after calculating the Spearman “ $\rho$ ,” the number of standard deviations by which  $\rho$  deviates from its null-hypothesis expected value; “ $P_Z$ ” = the probability that the value of  $Z$  would occur by chance in an uncorrelated sample; “ $\mathcal{N}$ ” = the percentage of Monte Carlo runs that resulted in  $|Z| \geq 3\sigma$ ; “ $\bar{Z}$ ” = expected value of  $Z$  based on the Monte Carlo runs;  $P_t$  = after calculating the Student- $t$  statistic for a comparison of means between a group of  $\eta$  values with low values of the independent quantity and a second group with high values of the independent quantity, the probability that that value of  $t$  would occur by chance in an uncorrelated sample. Regarding absolute magnitudes, we note that they were drawn from both the Minor Planet Center website and from JPL’s Horizons ephemeris system, hence the two entries.

Quantity	$m$	$Z$	$P_Z$	$\mathcal{N}$	$\bar{Z}$	$P_t$
heliocentric distance*	$-0.18 \pm 0.18$	0.92	0.359	0.4%	0.95	0.60
Spitzer-centric distance	$-0.218 \pm 0.074$	1.17	0.244	0.9%	1.05	0.66
phase angle*	$0.089 \pm 0.061$	-0.71	0.478	0.3%	-0.88	0.52
days from perihelion*	$0.00019 \pm 0.00014$	-2.93	0.003	3.4%	-1.67	0.37
days until aphelion	$(4.8 \pm 9.9) \times 10^{-5}$	-1.24	0.214	0.0%	-0.44	0.43
duration of AORs	$0.0007 \pm 0.0023$	0.67	0.506	0.0%	0.47	0.92
perihelion distance*	$-0.05 \pm 0.15$	-1.94	0.052	0.3%	-1.02	0.79
semimajor axis	$-0.03 \pm 0.11$	-0.98	0.325	0.0%	-0.32	0.90
eccentricity	$0.34 \pm 0.88$	1.74	0.082	0.2%	1.11	0.69
inclination	$0.000 \pm 0.011$	0.17	0.862	0.0%	0.21	0.88
argument of perihelion	$-0.0001 \pm 0.0010$	0.81	0.419	0.0%	0.62	0.99
longitude of asc. node	$0.00014 \pm 0.00095$	0.38	0.704	0.0%	0.25	0.69
Tisserand invariant	$0.05 \pm 0.57$	-1.20	0.231	0.3%	-1.07	0.92
true anomaly	$-0.0012 \pm 0.0023$	1.13	0.257	0.0%	0.35	0.56
MPC absolute magnitude	$-0.011 \pm 0.029$	0.93	0.355	0.0%	0.54	0.60
JPL absolute magnitude	$-0.003 \pm 0.036$	1.59	0.111	0.1%	0.89	0.85

**Table 7**

Radii used in the derivation of size distribution. All radii assume  $\bar{\eta} = 1.03 \pm 0.11$ . These include the 57 nuclei successfully observed by IRS and the 32 by MIPS, for a total of 89 nuclei. Table columns are: ‘‘Comet Desig.’’ = comet’s designation, as in Table 1; ‘‘ $R_N$ ’’ = effective radius in kilometers.

Comet Desig.	$R_N$ (km)	Comet Desig.	$R_N$ (km)	Comet Desig.	$R_N$ (km)
6P	$2.23^{+0.13}_{-0.15}$	118P	$1.30^{+0.19}_{-0.22}$	215P/2002 O8	$1.29^{+0.08}_{-0.08}$
7P	$2.64^{+0.17}_{-0.17}$	119P	$0.98^{+0.08}_{-0.11}$	216P/2001 CV <sub>8</sub>	$0.59^{+0.05}_{-0.05}$
11P	$0.58^{+0.04}_{-0.04}$	121P	$3.87^{+0.26}_{-0.27}$	219P/2002 LZ <sub>11</sub>	$1.00^{+0.06}_{-0.06}$
14P	$2.95^{+0.19}_{-0.19}$	123P	$2.18^{+0.23}_{-0.23}$	221P/2002 JN <sub>16</sub>	$1.03^{+0.06}_{-0.06}$
15P	$0.92^{+0.05}_{-0.05}$	124P	$2.62^{+0.16}_{-0.16}$	223P/2002 S1	$2.93^{+0.18}_{-0.18}$
16P	$0.72^{+0.09}_{-0.09}$	127P	$0.90^{+0.07}_{-0.07}$	228P/2001 YX <sub>127</sub>	$1.23^{+0.15}_{-0.17}$
22P	$2.15^{+0.17}_{-0.17}$	129P	$1.22^{+0.10}_{-0.10}$	246P/2004 F3	$4.20^{+0.42}_{-0.43}$
31P	$1.65^{+0.11}_{-0.12}$	130P	$2.23^{+0.15}_{-0.17}$	256P/2003 HT <sub>15</sub>	$0.75^{+0.08}_{-0.09}$
32P	$2.38^{+0.21}_{-0.23}$	131P	$1.11^{+0.09}_{-0.07}$	260P/2005 K3	$1.54^{+0.09}_{-0.08}$
33P	$1.15^{+0.08}_{-0.09}$	132P	$0.81^{+0.04}_{-0.05}$	P/2001 R6	$0.73^{+0.07}_{-0.06}$
37P	$1.23^{+0.08}_{-0.09}$	137P	$4.04^{+0.31}_{-0.32}$	P/2003 O3	$0.57^{+0.04}_{-0.04}$
47P	$3.11^{+0.20}_{-0.21}$	138P	$0.76^{+0.06}_{-0.06}$	P/2004 A1	$3.49^{+0.27}_{-0.28}$
48P	$2.97^{+0.19}_{-0.20}$	139P	$1.37^{+0.08}_{-0.08}$	P/2004 DO <sub>29</sub>	$1.07^{+0.09}_{-0.07}$
50P	$1.49^{+0.13}_{-0.13}$	143P	$4.79^{+0.32}_{-0.33}$	P/2004 H2	$1.23^{+0.15}_{-0.17}$
51P-A	$0.41^{+0.03}_{-0.02}$	144P	$0.84^{+0.05}_{-0.04}$	P/2004 V3	$0.92^{+0.08}_{-0.07}$
56P	$1.92^{+0.13}_{-0.14}$	146P	$0.96^{+0.07}_{-0.08}$	P/2004 V5-A	$1.66^{+0.22}_{-0.24}$
57P-A	$0.96^{+0.06}_{-0.07}$	148P	$1.14^{+0.06}_{-0.07}$	P/2004 VR <sub>8</sub>	$5.41^{+0.30}_{-0.31}$
62P	$0.59^{+0.09}_{-0.09}$	149P	$1.42^{+0.09}_{-0.10}$	P/2005 GF <sub>8</sub>	$2.70^{+0.19}_{-0.20}$
68P	$2.80^{+0.19}_{-0.21}$	152P	$1.03^{+0.10}_{-0.11}$	P/2005 JD <sub>108</sub>	$2.84^{+0.20}_{-0.22}$
69P	$0.87^{+0.05}_{-0.07}$	159P	$1.46^{+0.20}_{-0.23}$	P/2005 JQ <sub>5</sub>	$0.67^{+0.07}_{-0.08}$
74P	$3.31^{+0.60}_{-0.69}$	160P	$0.99^{+0.09}_{-0.07}$	P/2005 L4	$1.88^{+0.13}_{-0.14}$
77P	$1.66^{+0.11}_{-0.12}$	162P	$7.03^{+0.47}_{-0.48}$	P/2005 Q4	$1.48^{+0.08}_{-0.08}$
78P	$1.35^{+0.12}_{-0.14}$	163P	$1.32^{+0.08}_{-0.08}$	P/2005 R1	$1.65^{+0.10}_{-0.10}$
79P	$0.70^{+0.04}_{-0.04}$	168P	$0.48^{+0.04}_{-0.03}$	P/2005 S3	$1.41^{+0.11}_{-0.11}$
89P	$1.43^{+0.13}_{-0.13}$	169P	$2.48^{+0.13}_{-0.14}$	P/2005 T5	$1.33^{+0.08}_{-0.10}$
93P	$2.59^{+0.26}_{-0.26}$	171P	$1.25^{+0.09}_{-0.08}$	C/2005 W2	$0.52^{+0.07}_{-0.09}$
94P	$2.27^{+0.13}_{-0.15}$	172P	$5.70^{+0.36}_{-0.37}$	P/2005 W3	$1.16^{+0.22}_{-0.27}$
101P	$0.98^{+0.09}_{-0.08}$	173P	$4.28^{+0.95}_{-1.17}$	P/2005 XA <sub>54</sub>	$2.71^{+0.17}_{-0.17}$
107P	$1.45^{+0.09}_{-0.10}$	197P/2003 KV <sub>2</sub>	$0.92^{+0.06}_{-0.05}$	P/2005 Y2	$5.08^{+0.37}_{-0.40}$
113P	$1.70^{+0.10}_{-0.10}$	213P/2005 R2	$1.53^{+0.24}_{-0.29}$		

**Table 8**

Statistics associated with the radii ratios in Figure 11. “Compilation” indicates the paper mentioned in §4.3.1 and in Figure 11. The middle columns give the mean  $\mu_m$  and standard deviation  $\sigma$  among the  $N$  radii ratios; the three columns pertain to all detected SEPPCoN comets that appear in the comparison compilation, just the SEPPCoN comets that appeared without discernible dust, and just the SEPPCoN comets that appear with discernible dust, respectively. The last column gives the significance of a Student- $t$  statistic comparing the means of the comets with and without discernible dust.

Compilation	All comets ( $N; \mu_m \pm \sigma$ )	No dust ( $N; \mu_m \pm \sigma$ )	Yes dust ( $N; \mu_m \pm \sigma$ )	Student- $t$
S11	25; $0.93 \pm 0.42$	13; $0.81 \pm 0.35$	12; $1.06 \pm 0.46$	14.7%
W11	29; $0.82 \pm 0.55$	17; $0.73 \pm 0.41$	12; $0.95 \pm 0.70$	29.7%
T06	37; $1.08 \pm 0.41$	19; $1.19 \pm 0.34$	18; $0.95 \pm 0.44$	7.2%
L04	20; $1.18 \pm 0.43$	10; $1.04 \pm 0.35$	10; $1.32 \pm 0.48$	15.5%

**Table 9**

Power-Law Slopes to CSDs in Figure 13. Table columns: “Range” = range in radii (in km) that was used for the fitting; “all  $q$ ” = slopes calculated including all perihelia; “ $q < x$  AU” = slopes calculated using only comets with perihelia under  $x$  AU; “ $\beta$ ” = power-law slope in the function  $R_N^\beta$ ; “No.” = number of comets included in the fit.

Range	all $q$		$q < 3$ AU		$q < 2.5$ AU		$q < 2$ AU	
	$\beta$	No.	$\beta$	No.	$\beta$	No.	$\beta$	No.
1.4 – 4.0	-1.43	42	-1.52	36	-1.73	29	-1.57	18
1.4 – 5.0	-1.55	47	-1.60	40	-1.68	31	-1.59	20
1.4 – 7.0	-1.75	51	-1.74	43	-1.71	34	-1.63	21
1.4 – 9.0	-1.82	52	-1.80	44	-1.75	35	-1.63	22
1.6 – 4.0	-1.60	33	-1.80	28	-2.10	23	-2.98	14
1.6 – 5.0	-1.70	38	-1.80	32	-1.84	25	-2.01	16
1.6 – 7.0	-1.92	42	-1.93	35	-1.81	28	-1.94	17
1.6 – 9.0	-2.00	43	-1.99	36	-1.85	29	-1.82	18
1.8 – 4.0	-1.88	28	-2.06	25	-2.67	20	-2.98	14
1.8 – 5.0	-1.88	33	-1.91	29	-1.99	22	-2.01	16
1.8 – 7.0	-2.10	37	-2.03	32	-1.87	25	-1.94	17
1.8 – 9.0	-2.17	38	-2.08	33	-1.91	26	-1.82	18
2.0 – 4.0	-1.97	26	-2.15	23	-2.84	19	-2.98	14
2.0 – 5.0	-1.92	31	-1.94	27	-2.00	21	-2.01	16
2.0 – 7.0	-2.15	35	-2.06	30	-1.87	24	-1.94	17
2.0 – 9.0	-2.22	36	-2.11	31	-1.91	25	-1.82	18
2.2 – 4.0	-2.00	22	-2.13	19	-2.90	15	-3.32	11
2.2 – 5.0	-1.93	27	-1.89	23	-1.85	17	-1.88	13
2.2 – 7.0	-2.18	31	-2.04	26	-1.78	20	-1.84	14
2.2 – 9.0	-2.26	32	-2.11	27	-1.84	21	-1.74	15



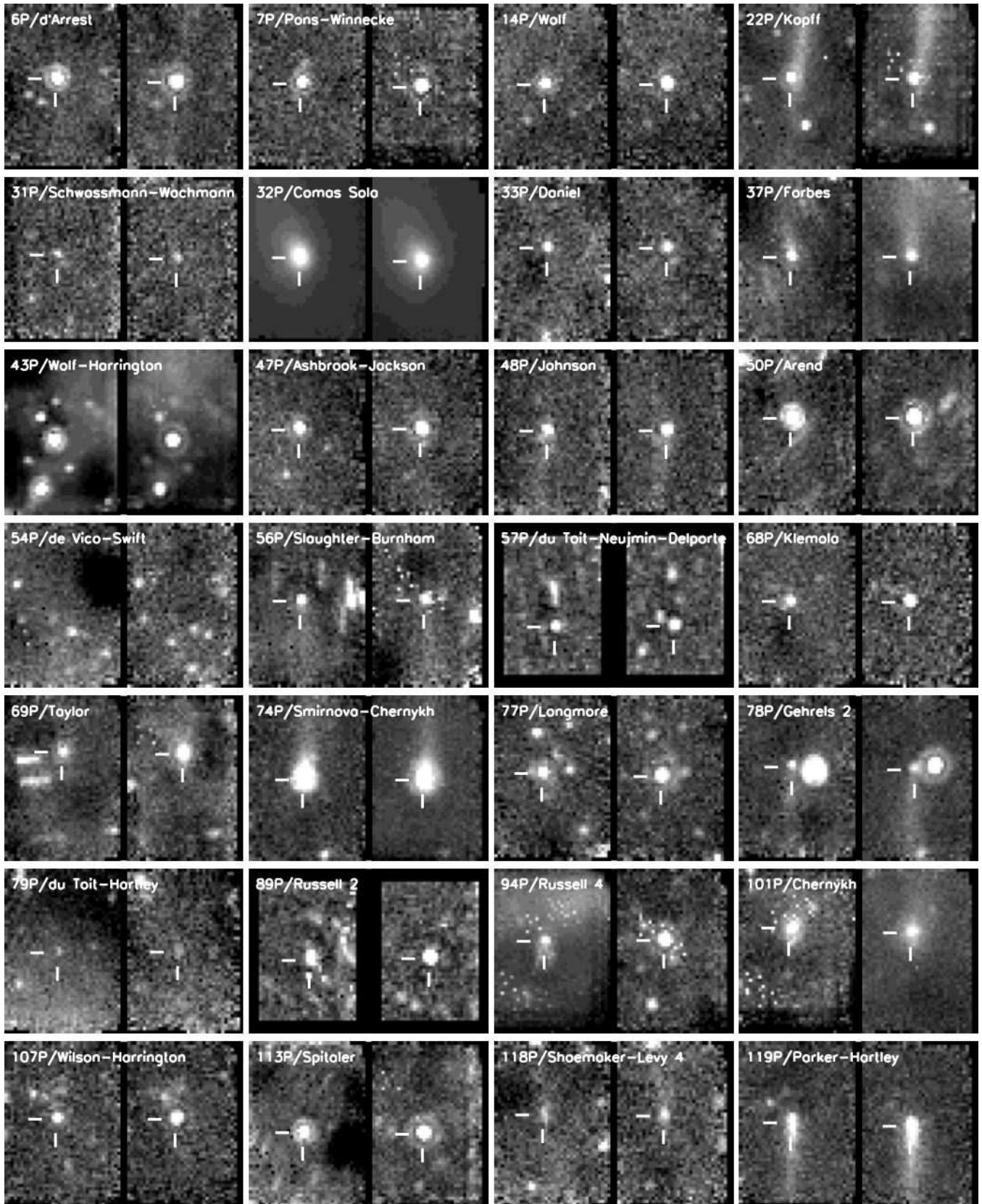


Figure 1, caption at end of figure.

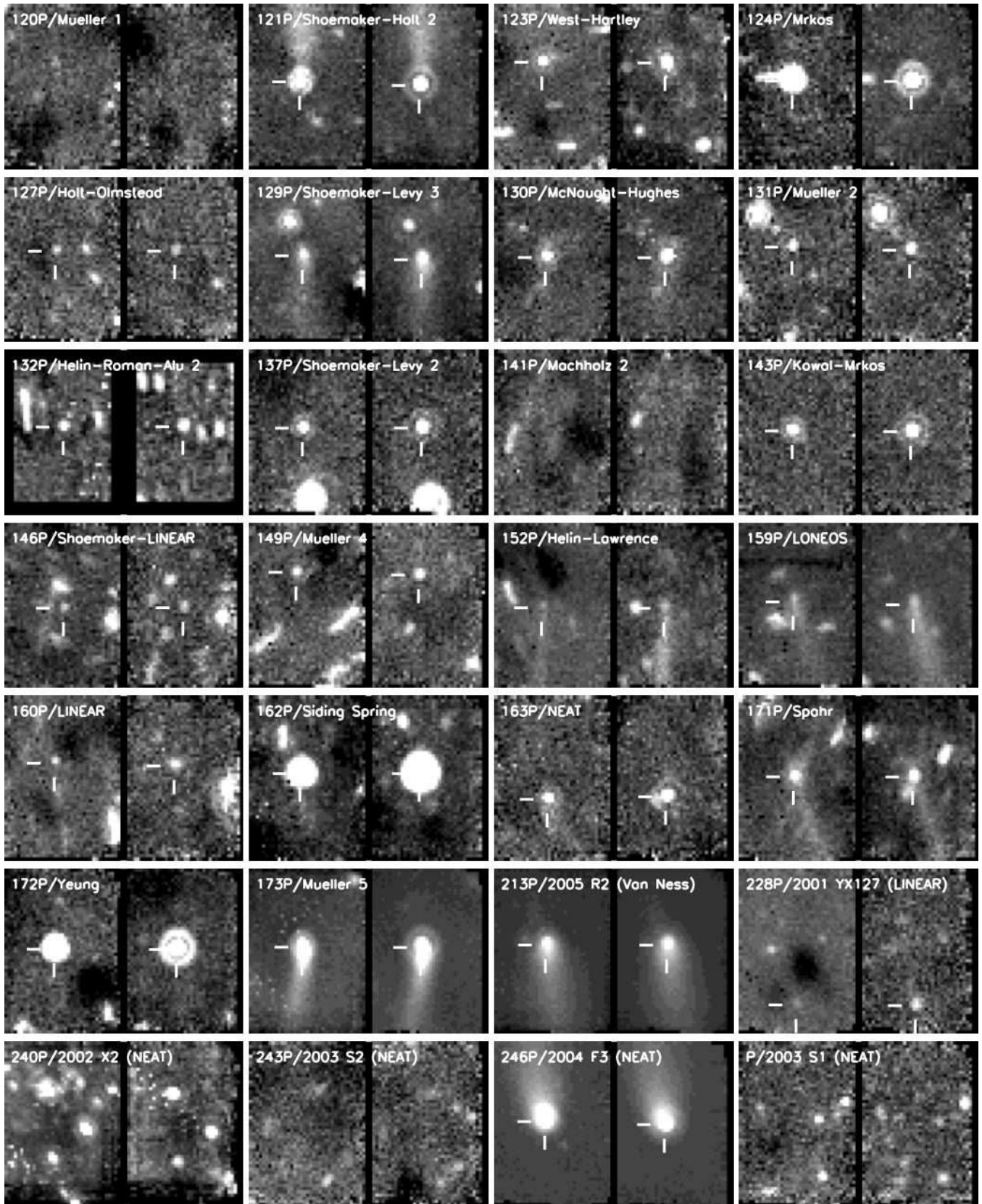


Figure 1 continued, caption at end of figure.

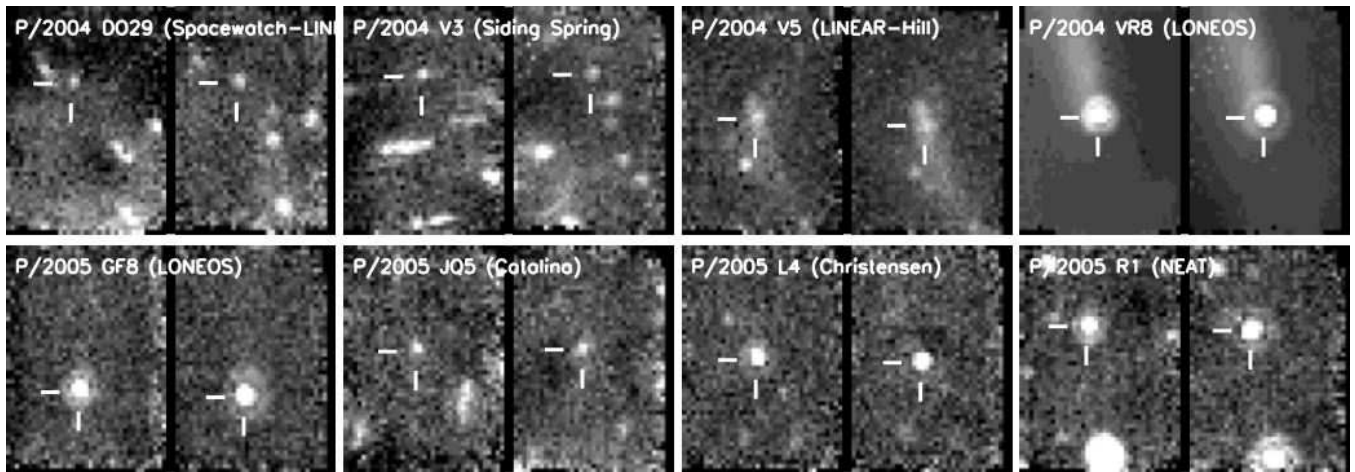


Figure 1 continued. Montage of the 64 comets in our survey observed by Spitzer’s IRS. For each comet, there are two panels: the left panel shows the “blue”  $16\ \mu\text{m}$  PU image; the right, the “red”  $22\ \mu\text{m}$  PU image. Tick marks indicate the location of the comet, except for the seven comets (see text) where we had no detection. Many comets appear as point-sources, evincing only emission from the nucleus; some however show extended emission from dust. Note that some images show bright background sources as well. Each panel is 67-by-92 arcsec.

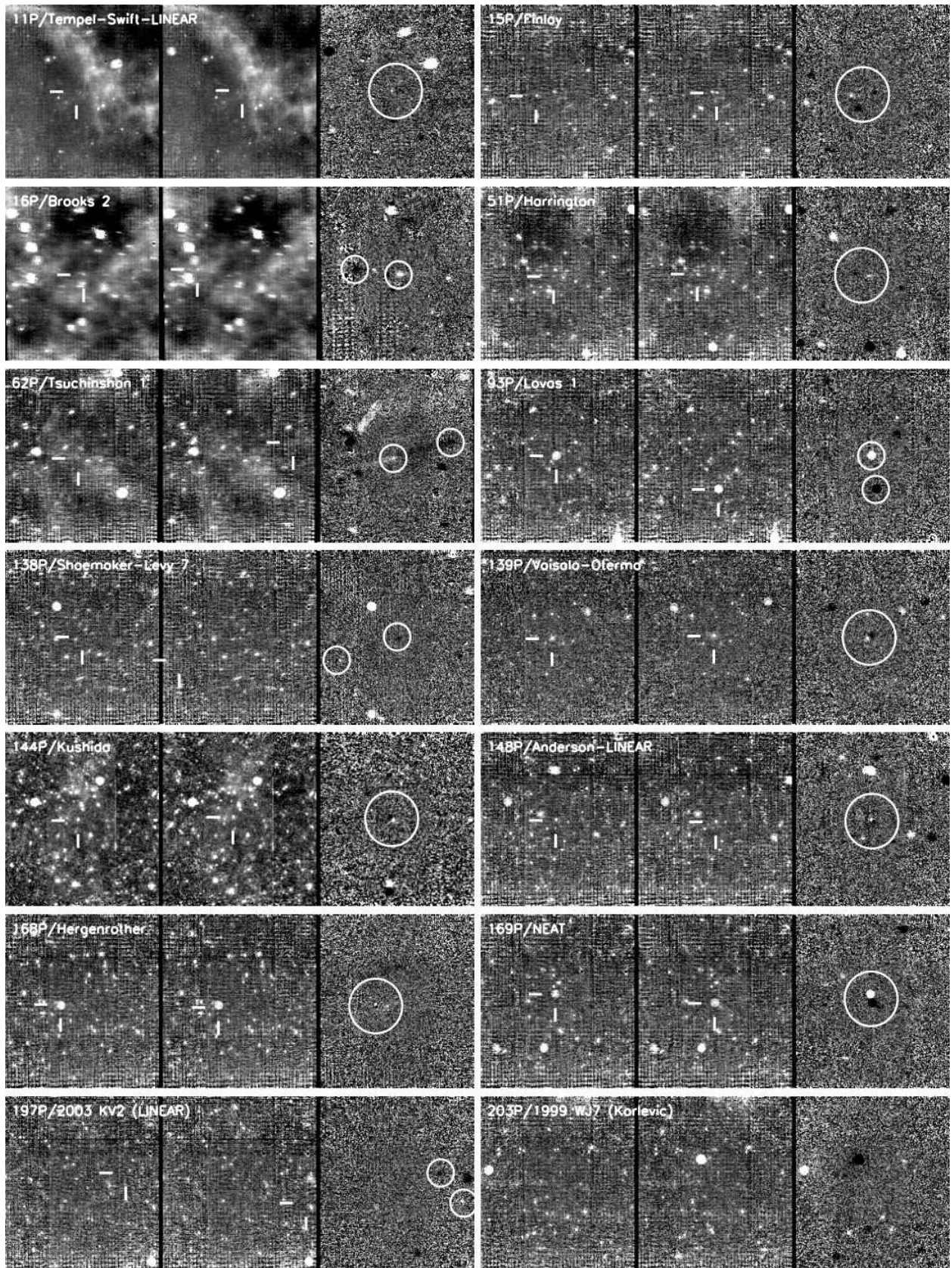


Figure 2, caption at end of figure.

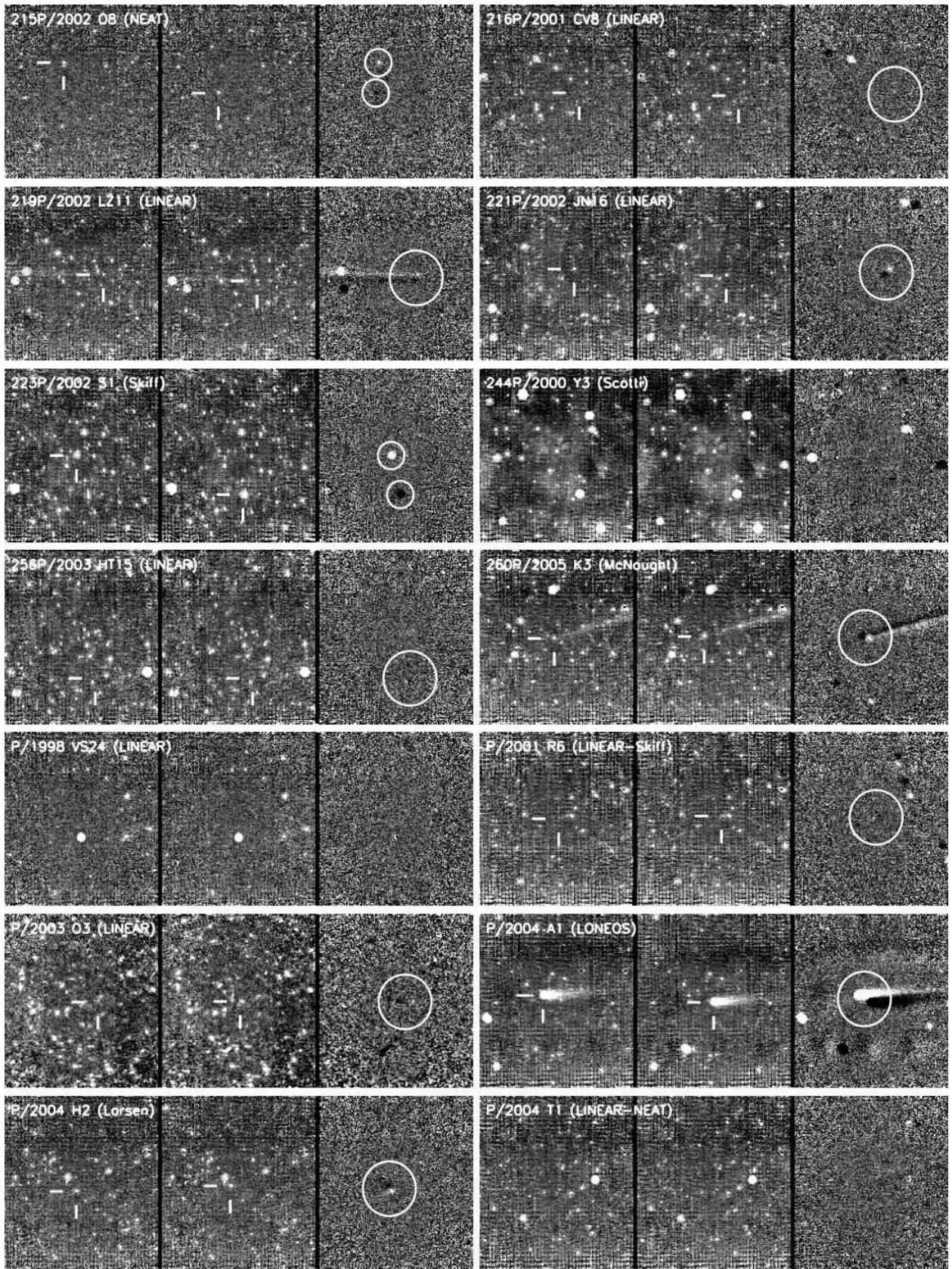


Figure 2 continued, caption at end of figure.

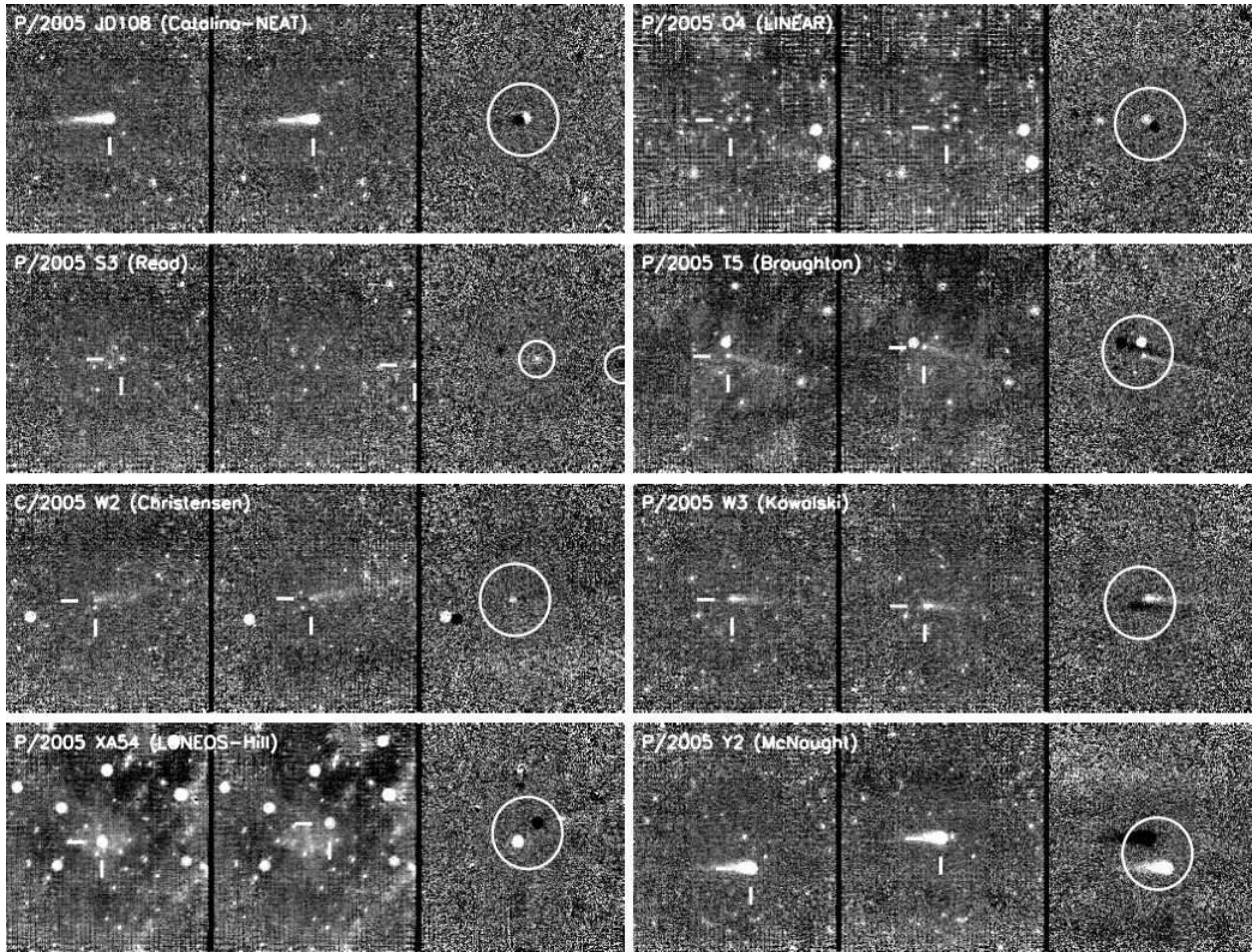


Figure 2 continued. Montage of the 36 comets in our survey observed by Spitzer’s MIPS at  $24\ \mu\text{m}$ . For each comet, there are three panels: the “on-source” image, the “shadow” image, and a difference image that is the subtraction of the two. Tick marks in the on-source and shadow images indicate the location of the comet, though the comets are most easily seen in the difference images. Circles in the difference images indicate the location of the comet’s positive and negative images (though if the two are close, then only one large circle is drawn around both). No ticks or circles are drawn for the 4 comets (see text) where we had no detection. As in Fig. 1, many comets appear as point-sources but several show extended emission from dust. Each panel is 7.3-by-7.9 arcmin. Several panels also have serendipitously-observed asteroids in the field.

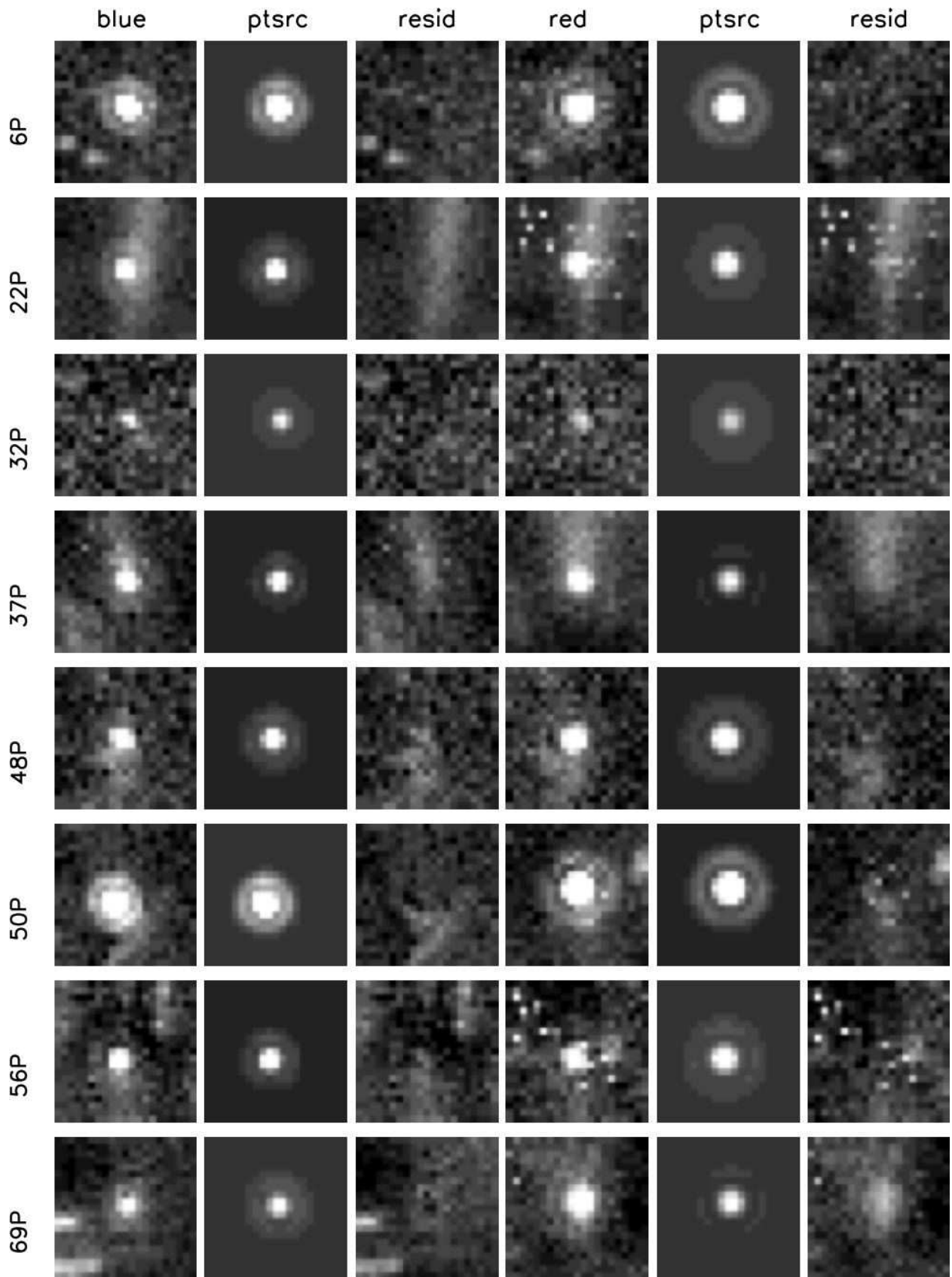


Figure 3, caption at end of figure.

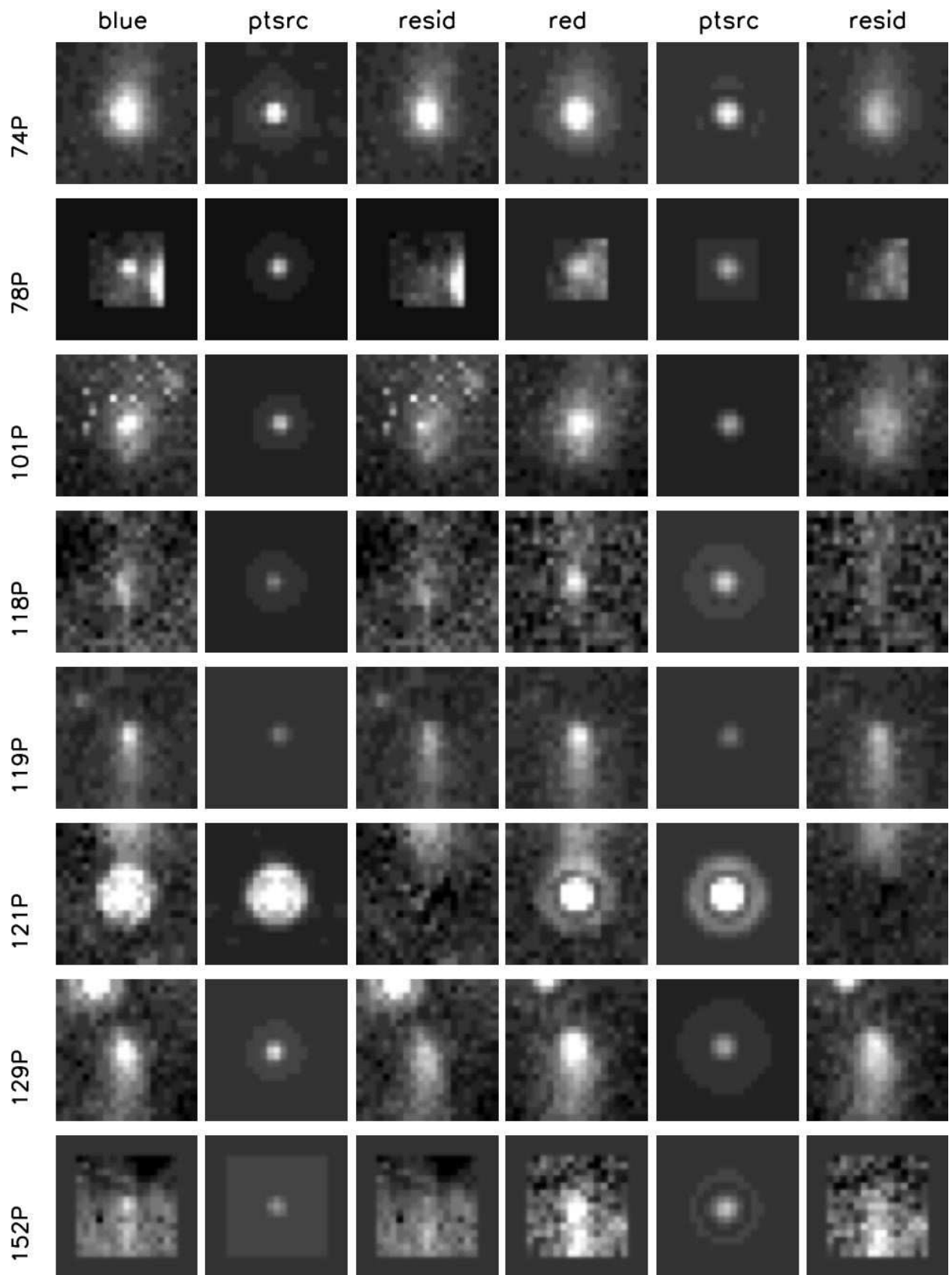


Figure 3 continued, caption at end of figure.



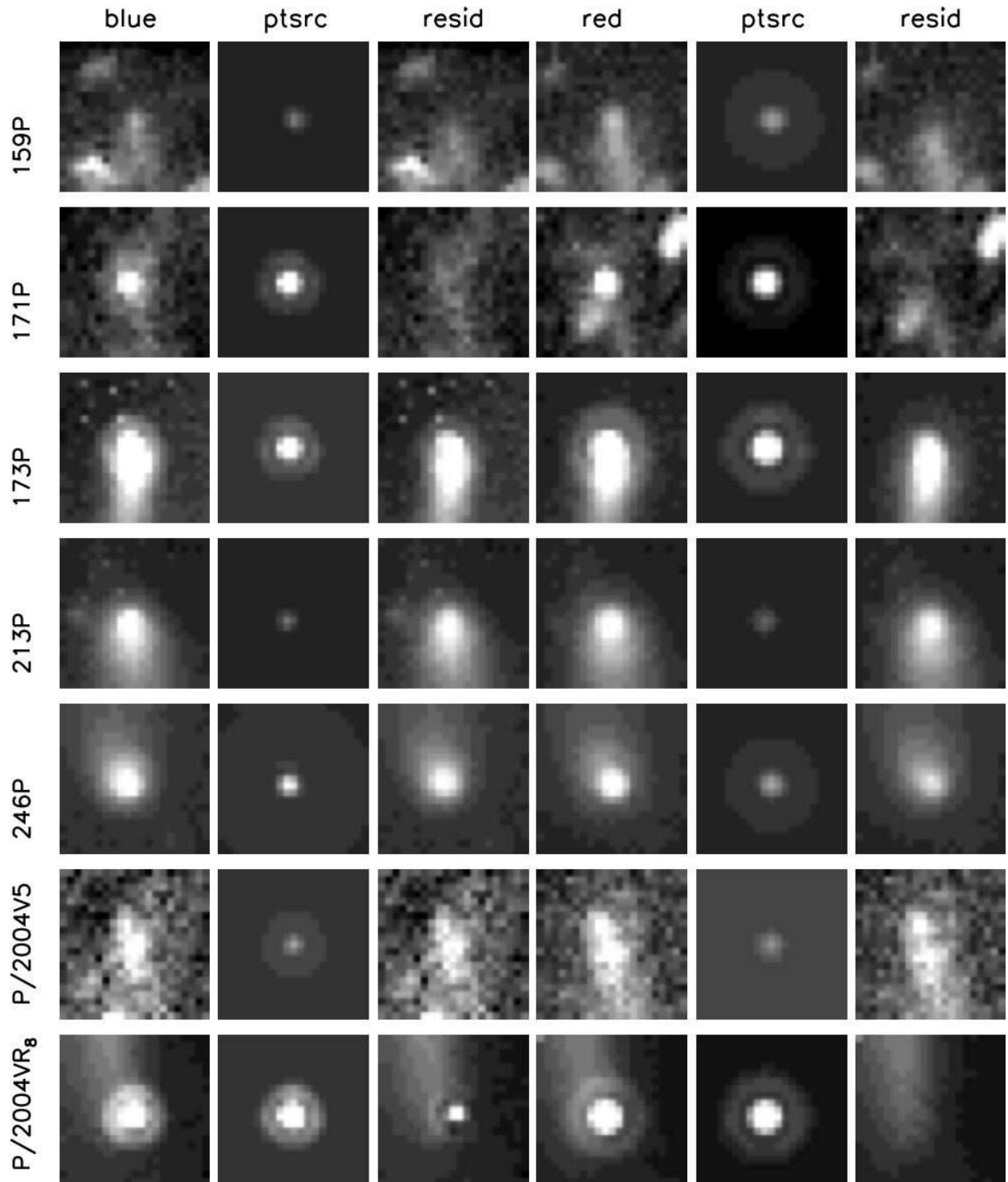


Figure 3 continued. Montage of the 23 comets observed by IRS with extended emission from dust. Each comet has a row of six images. Each image shows a 21-by-21 pixel region around the comet. The 6 images are, from left to right: “blue” PU image, best-fitting PSF for that image, residual after removing the PSF, “red” PU image, best-fitting PSF for that image, residual after removing the PSF. Note that for some comets (e.g. 6P, 32P) the dust is not obvious.

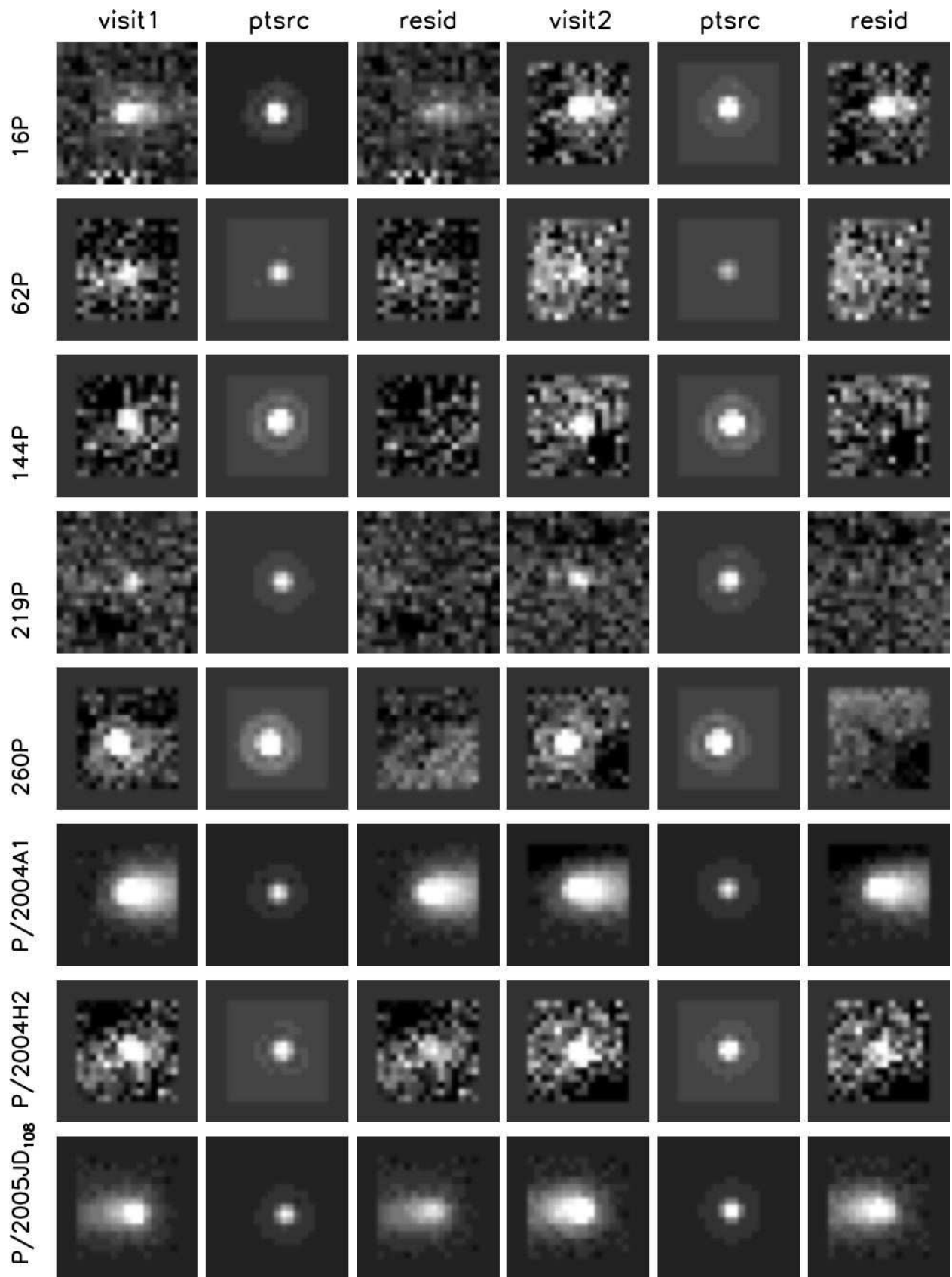


Figure 4, caption at end of figure.

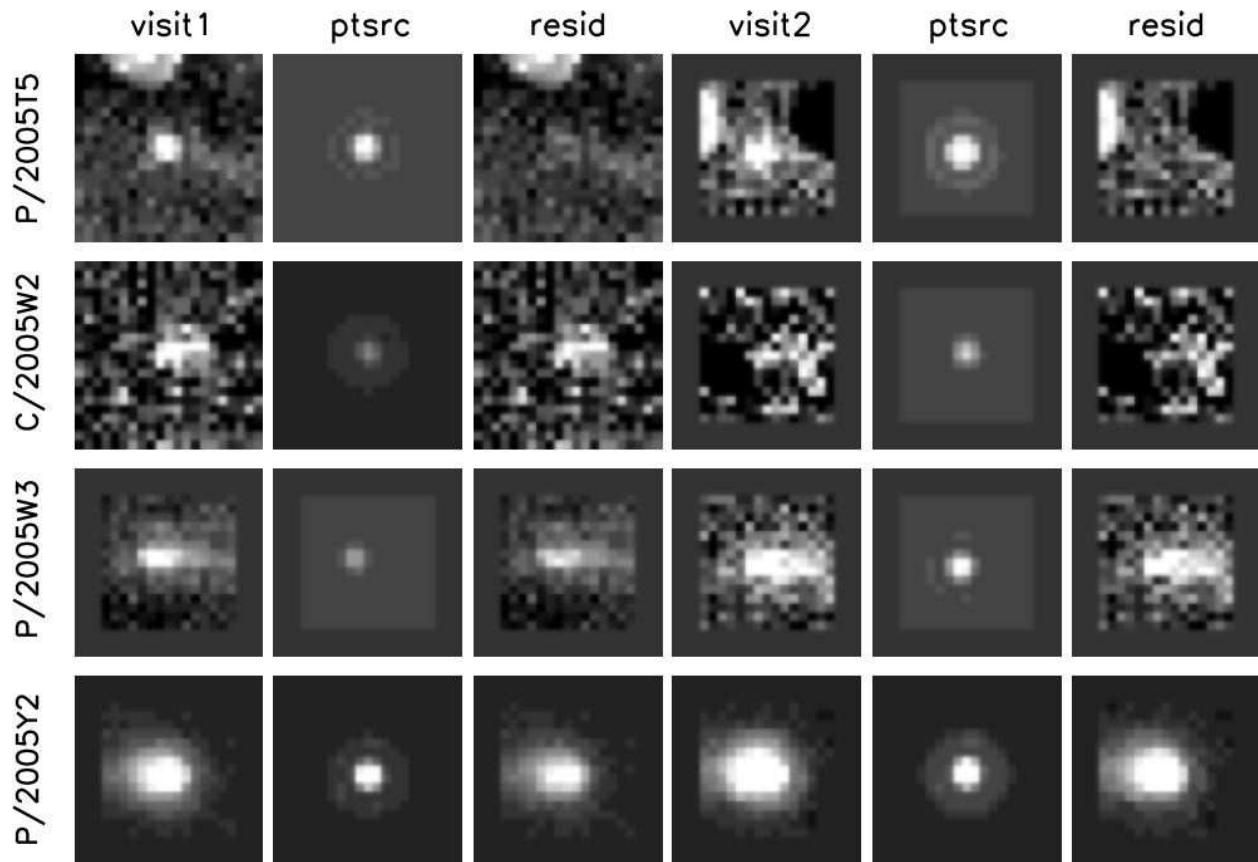


Figure 4 continued. Same as Fig. 3, except showing the 12 comets observed by MIPS with extended emission. The first and fourth images in each row display the comet at each visits after shadow-subtraction with the other visit. Note that for some comets (e.g. 144P, 219P) the dust is not obvious.

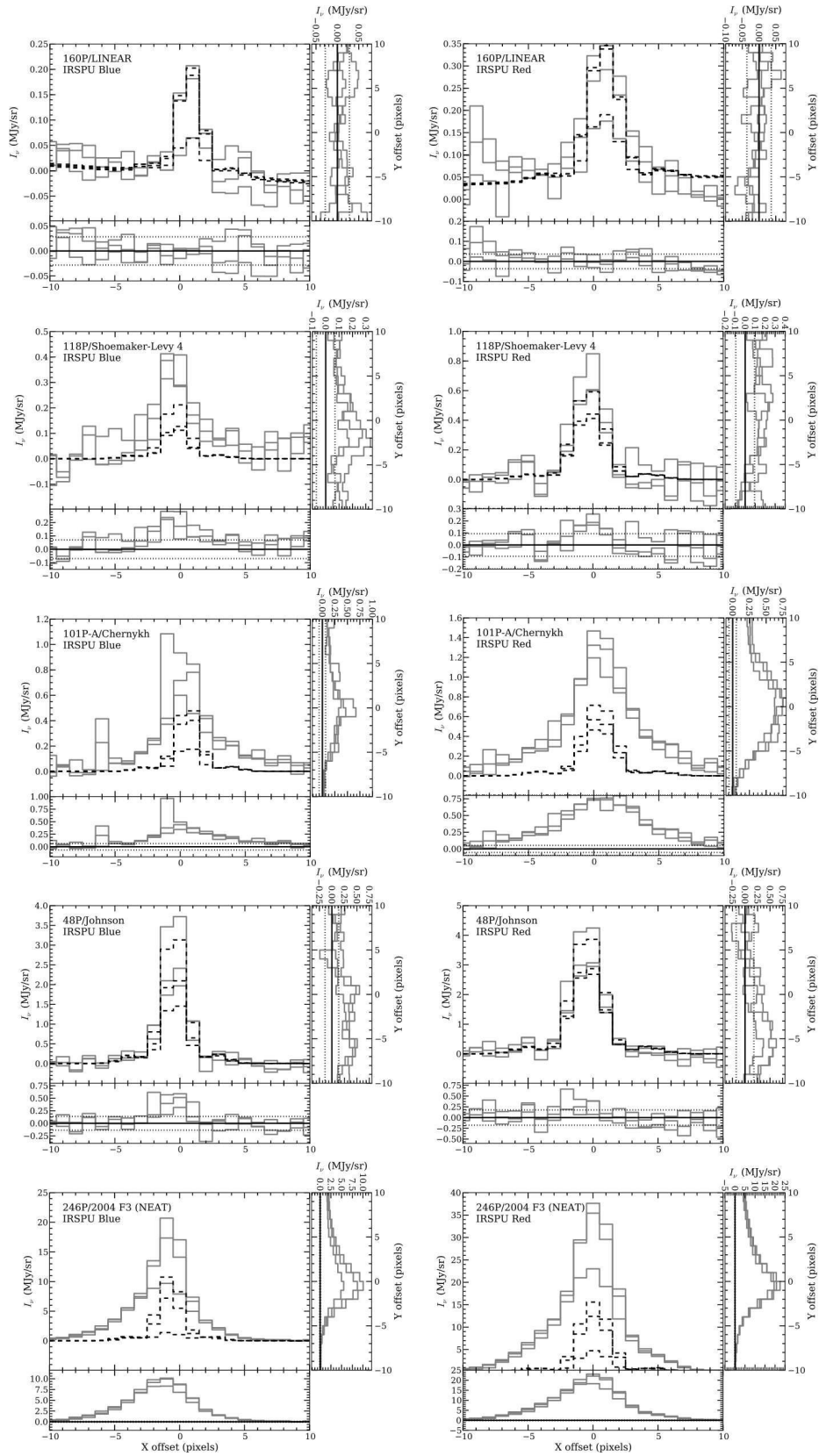


Figure 5, caption after end of figure.

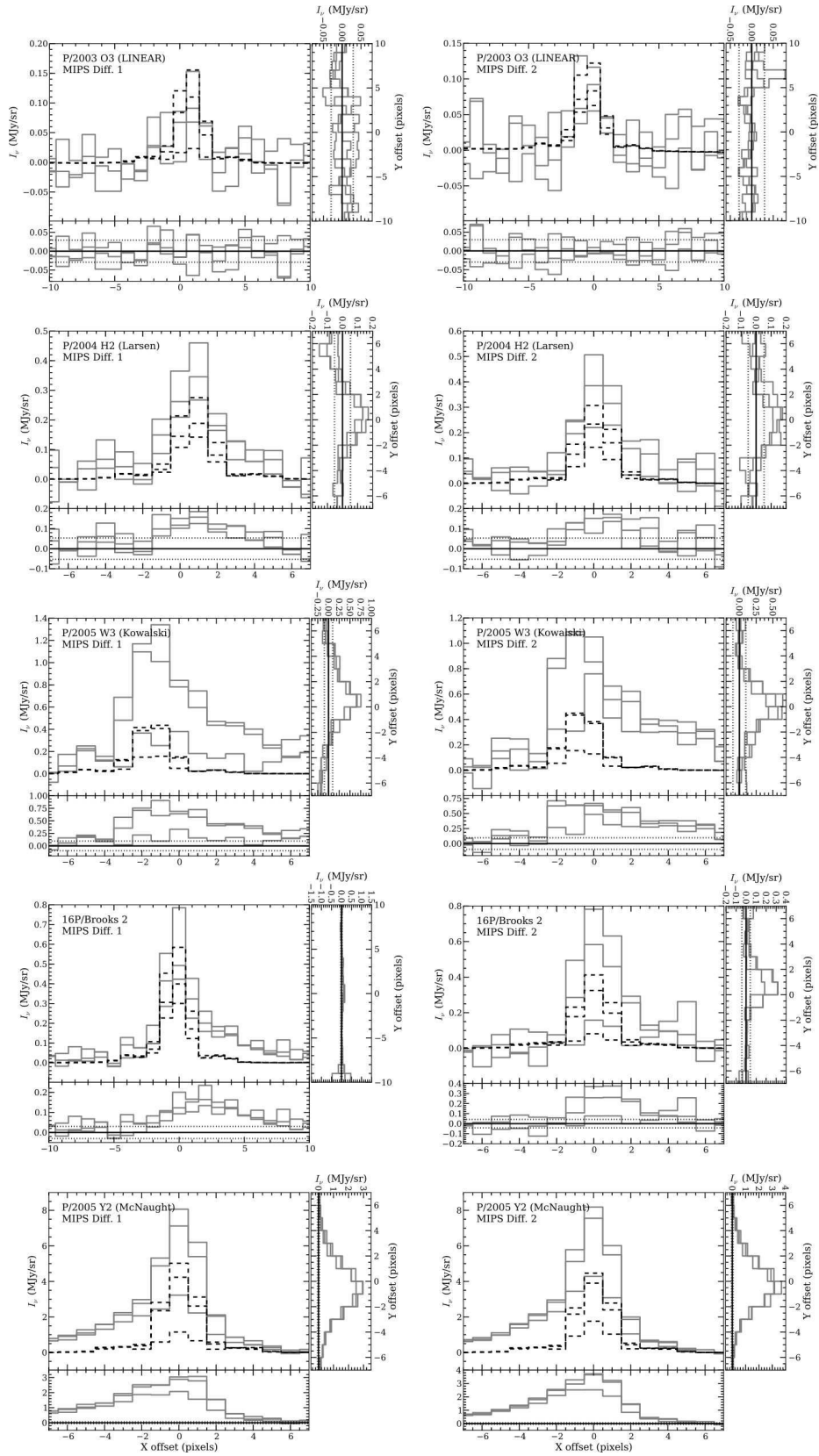


Figure 5 continued, caption after end of figure.

Figure 5. Sample of surface-brightness profiles from ten comets in our survey. The first five pairs of panels are from five IRS-observed comets, with profiles from the “blue” and “red” PU images (one panel for each). The second five pairs are from five MIPS-observed comets, with profiles from the two shadow-subtracted visits (one panel for each). The name of the comet is given in each panel in the upper-left. A variety of coma brightnesses and nucleus-to-coma contrasts is shown. In each panel, there are three plots. The largest plot shows three line cuts through the image in the x-direction; these are the solid grey lines. The plot also shows three line cuts through the best-fitting PSF in the x-direction; these are the black dashed lines. The cuts come from the row that has the pixel with the comet’s centroid, the row above that, and the row below that. The plot below the largest plot shows residuals in the line cuts after subtracting the best-fitting PSF from the image; the solid horizontal black line marks a residual of zero, and the horizontal dotted lines indicated  $\pm 1\sigma$ . The plot to the right of the largest plot is similar in that it shows residuals, except it shows y-direction line cuts.

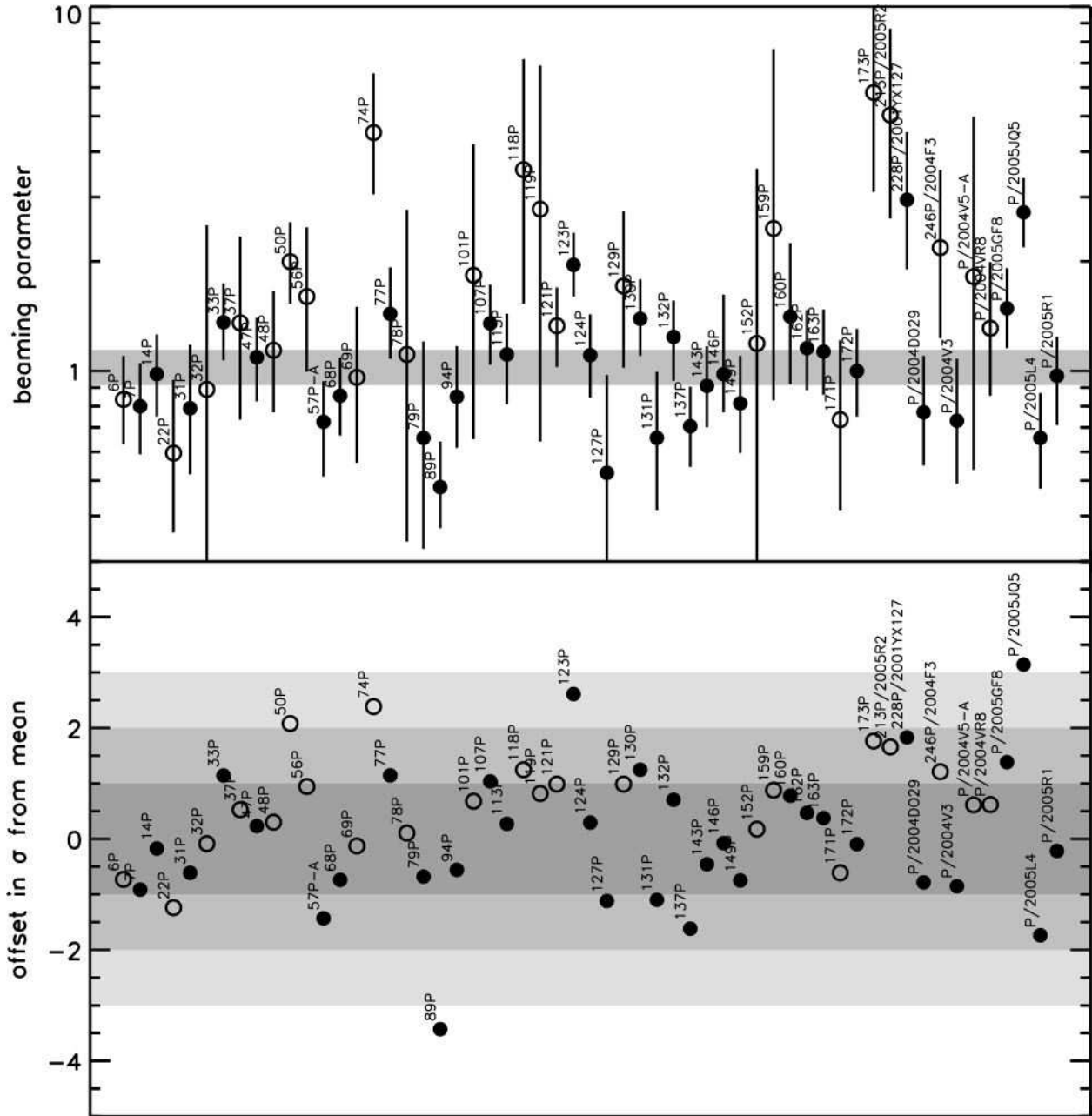


Figure 6. Graphical representation of the 57 beaming parameters reported in Table 4. The top panel is a scatter plot of the points, with each point labeled with its comet. Filled circles indicate comets for which there was no discernible dust coma; unfilled circles are for comets that showed some coma (i.e. those underlined comets in Table 2). Error bars are effectively  $1\sigma$ . The grey rectangle is vertically centered on the mean beaming parameter,  $\bar{\eta} = 1.03$ , and represents the  $1\sigma$  range of the error in the mean,  $\pm 0.11$ . The bottom panel shows the offset of each point from  $\bar{\eta}$  in terms of its own  $\sigma$ . The (dark,middle,light) grey rectangles represent offsets of  $(1,2,3)\sigma$ . Given the wide variety of error bars in the top panel, the bottom panel makes it easier to see that there is good clustering of our measured  $\eta$ , and only two outliers.

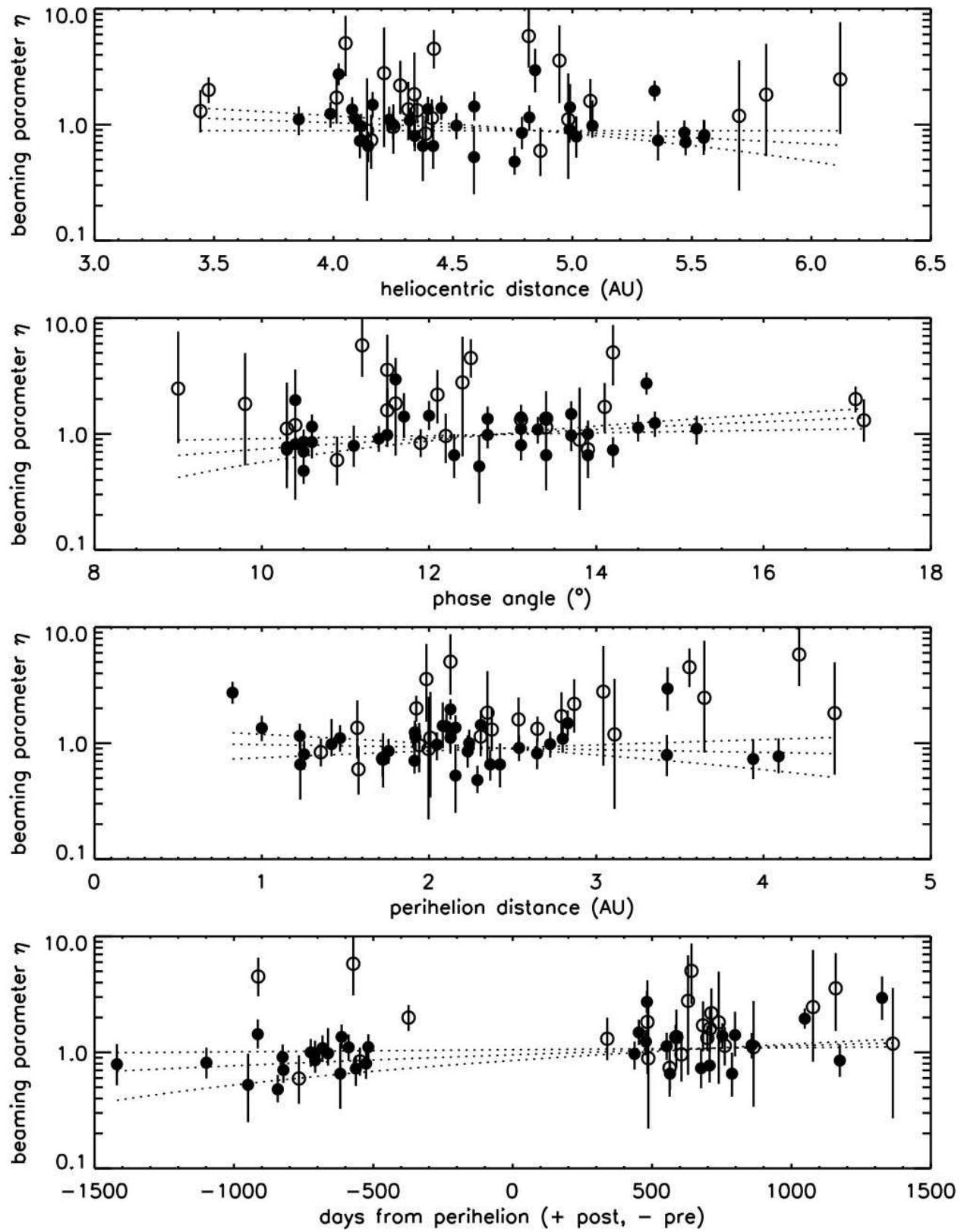


Figure 7, caption after end of figure.



Figure 7. Search for trends of  $\eta$  with various significant quantities, as discussed in §4.1. All 57 beaming parameters from Table 4 are plotted vs. heliocentric distance, phase angle, perihelion distance, and days from perihelion. Filled circles indicate comets for which there was no discernible dust coma; unfilled circles are for comets that showed some coma (i.e. those underlined comets in Table 2). The three dotted lines in each panel represent the best-fitting line to the data and the lines corresponding to  $\pm 1\sigma$  range in slope and intercept (see Table 6 for slopes).

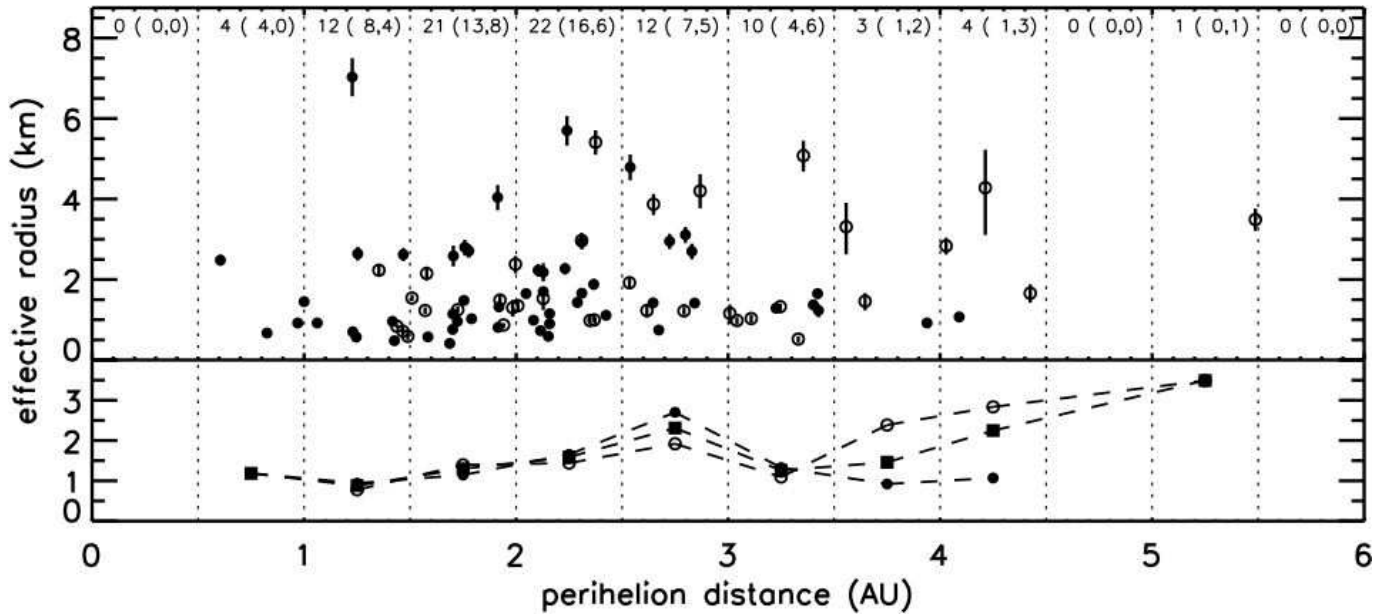


Figure 8. Top panel: scatter plot of all 89 radii vs. each nucleus’s perihelion distance. Error bars are plotted for all points, though some errors are smaller than the symbol used. Filled circles indicate comets for which there was no discernible dust coma; unfilled circles are for comets that showed some coma (i.e. those underlined comets in Table 2). Numbers at the top of the plot of the form “ $m(n,p)$ ” indicate the number of nuclei within each 0.5 AU-wide bin ( $m$ ), the number of comets without discernible dust in that bin ( $n$ ), and the number of comets with dust in that bin ( $p$ ). Bottom panel: Median values of the radii within in each bin. Squares indicate medians of all nuclei within each bin; filled circles, of comets without discernible dust; open circles, of comets with dust.

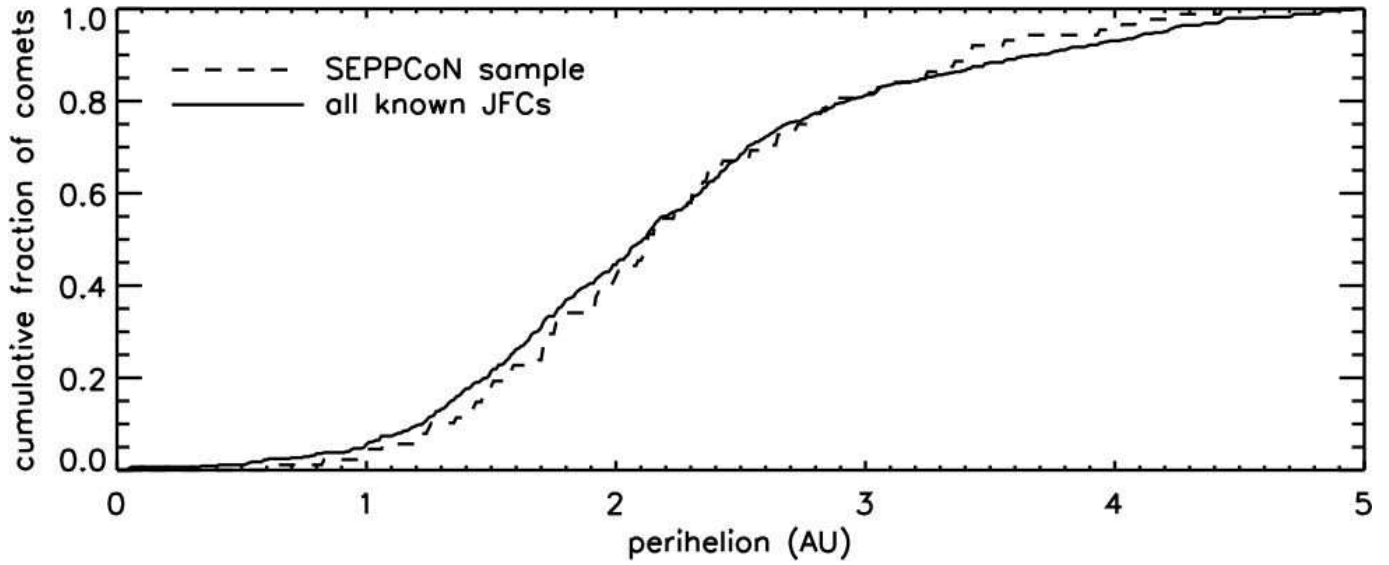


Figure 9. Comparison of the cumulative perihelion distribution of our 89 detected SEPPCoN JFCs (dashed curve) and all 450 JFCs (solid curve) that were known at time of writing. The curves match well, indicating that our sample’s perihelion bias is no different than the overall one that is present in the JFC discovery rate.

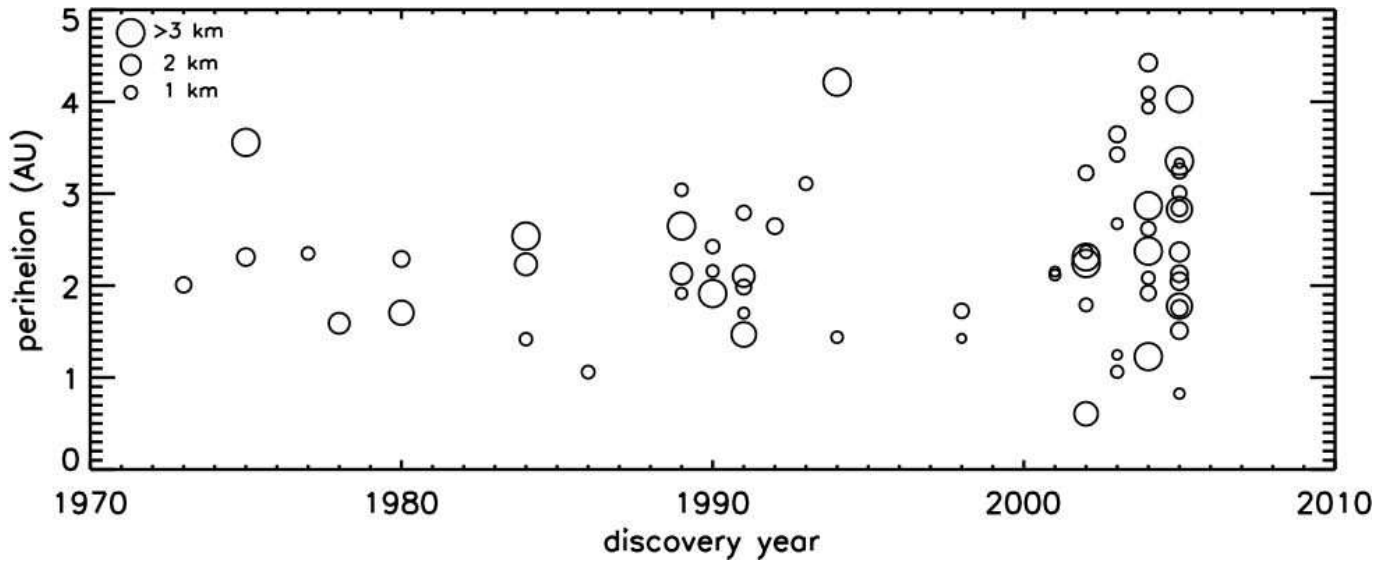


Figure 10. Scatter plot of discovery year and perihelion distance for the 98 nuclei considered here (i.e. the 89 from our survey plus nine reliable estimates from the literature). For clarity we have left out the 32 such comets discovered before 1970 and the 1 comet (P/2004 A1) with perihelion over 5 AU. The symbol size is tied to the radius of the nucleus. Many of our large nuclei ( $\sim 3$  km and larger) and several such nuclei at low perihelion were discovered only recently.

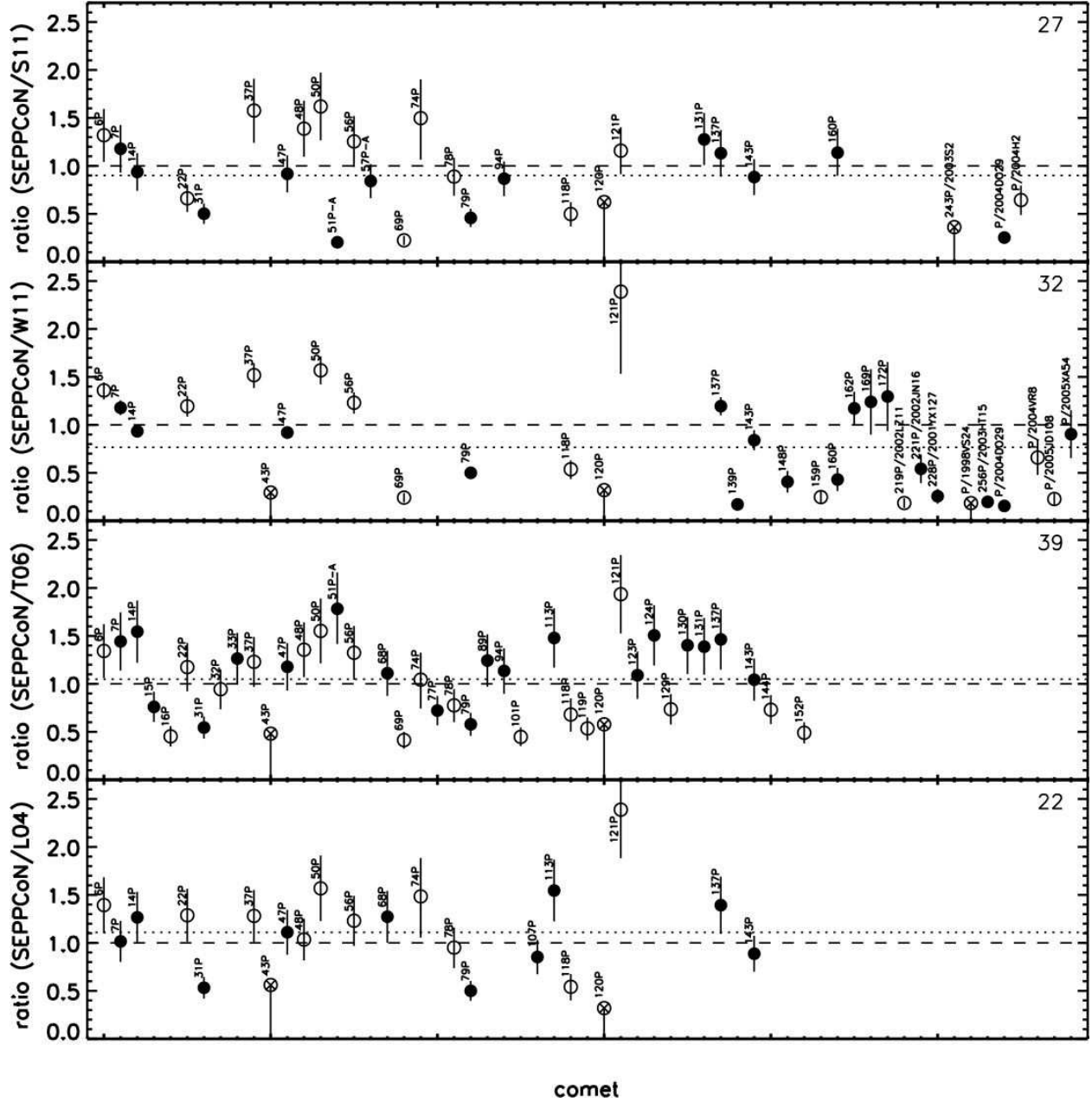


Figure 11. Plots showing the ratio of our radii in Table 7 to those reported in previously-published compilations: (from top to bottom) Snodgrass et al. (2011; S11), Weiler et al. (2011; W11), Tancredi et al. (2006; T06), Lamy et al. (2004; L04). Fifty-nine of our SEPPCoN comets appear at least once in these works. Error bars are propagated from an assumed 20% error (in the case of S11, T06, and L04) or the reported error (in the case of W11). The same comet is at the same abscissa value across all panels. Filled circles indicate comets for which there was no discernible dust coma; unfilled circles are for comets that showed some coma (i.e. those underlined comets in Table 2); crossed circles are for comets that we did not detect. Number in the upper right of each panel indicates the number of comets that overlap with that particular work. Horizontal dashed line indicates unity; horizontal dotted line indicates the average ratio of the points in that panel.

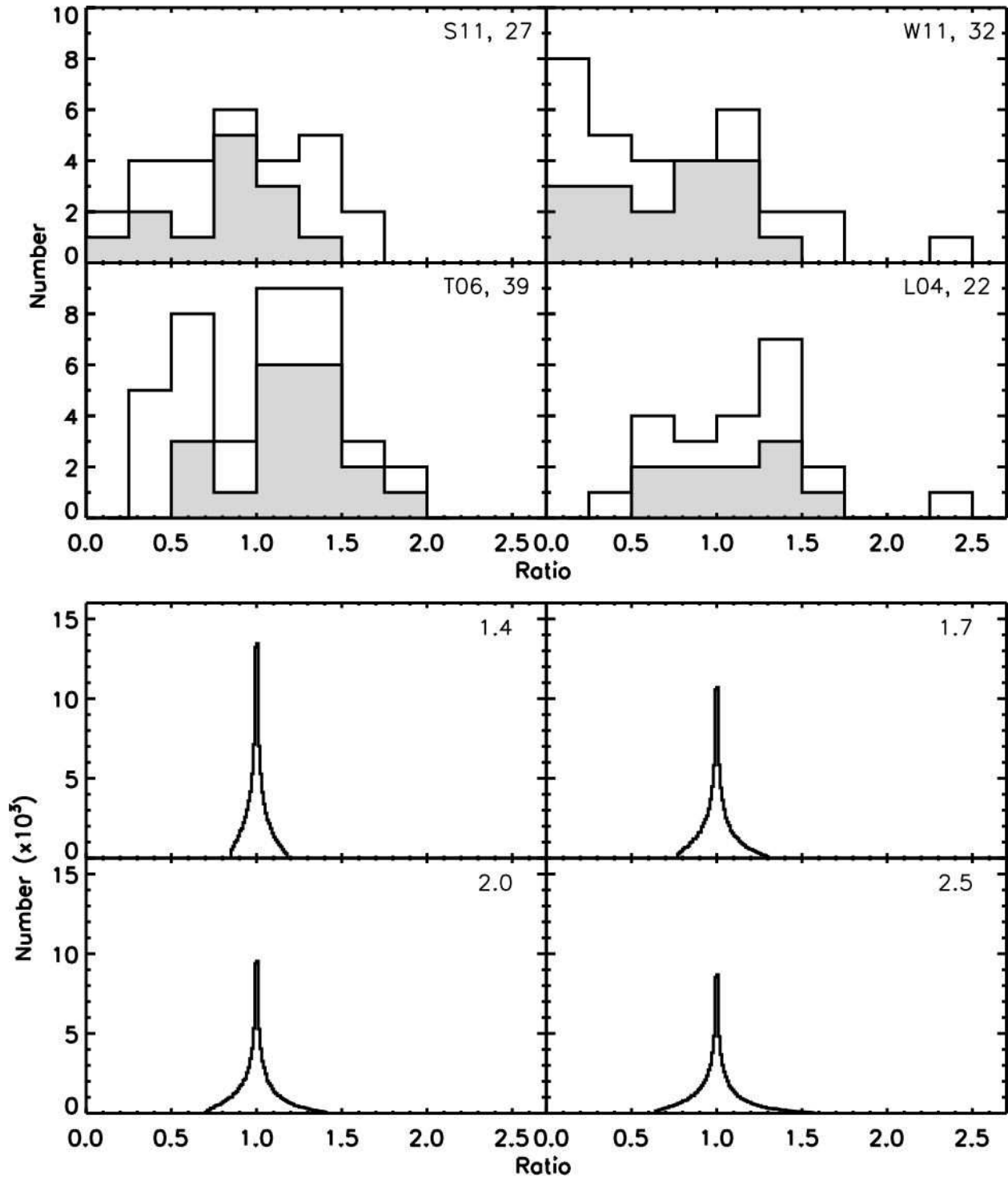


Figure 12. Histograms of measured and expected ratios between two snapshots of radii. Top half: four panels that give the histograms to the panels in Fig. 11. White histogram is for all the comets; grey histogram is for the comets for which there was no discernible dust. Bottom half: four panels that show the expected histograms given the axial ratio listed in the upper right corner of each panel. We note the differences between the character of the histograms in the top and bottom halves.

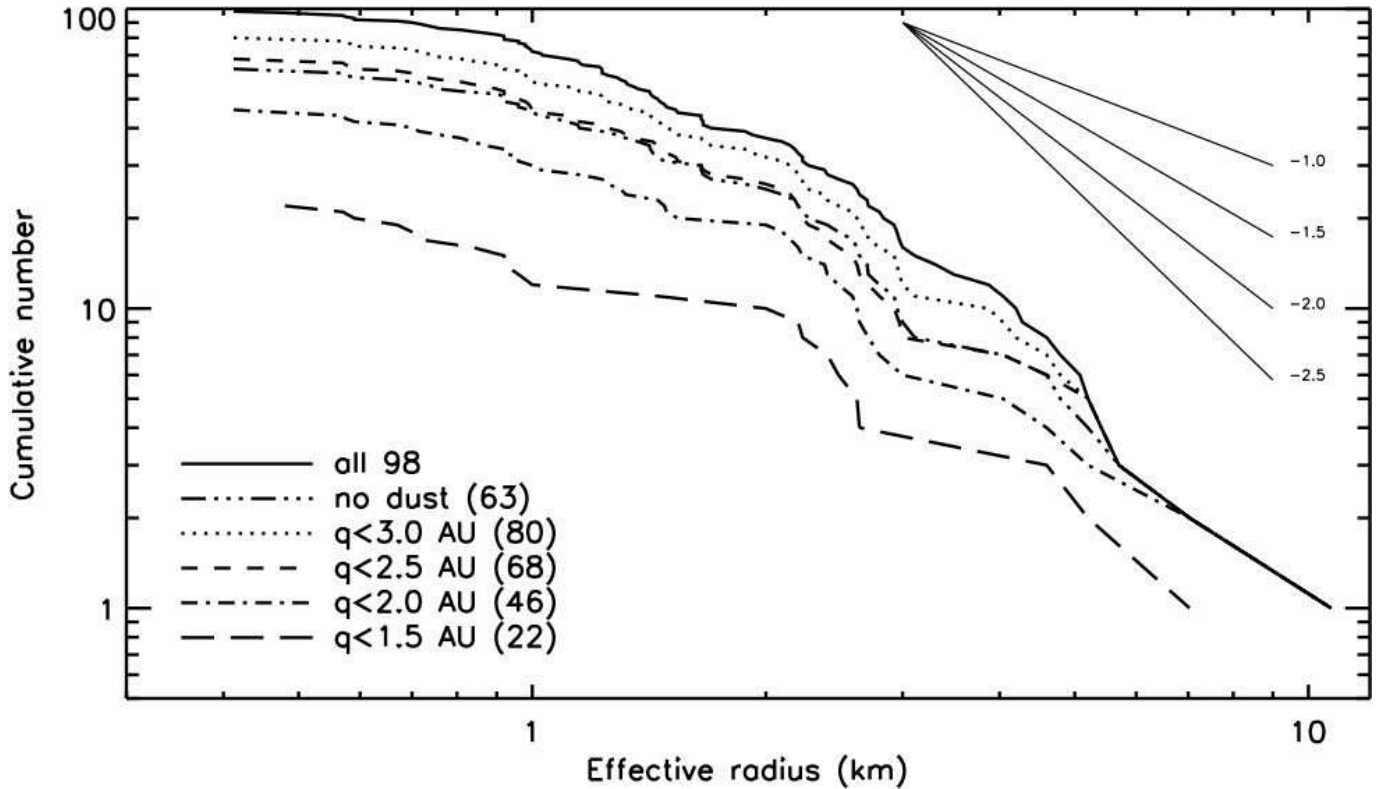


Figure 13. Observed cumulative size distributions (CSDs) of JFCs. To create each curve, the list of radii was sorted and the cumulative number was incremented by one at the radius of each nucleus in that sorted list. Individual points are not shown for clarity. The overall CSD (“all 98”) includes the 89 comets reported here plus nine others from the literature for a total of 98. Separate curves break down the CSD by perihelion distance. Also shown is the CSD (“no dust”) if we included only the 54 SEPPCoN comets that did not show discernible dust plus the nine others from the literature for a total of 63. Straight diagonal lines in the upper right correspond to different (labeled) power-law slopes. The slopes of the CSDs themselves are given in Table 9 and §4.4.

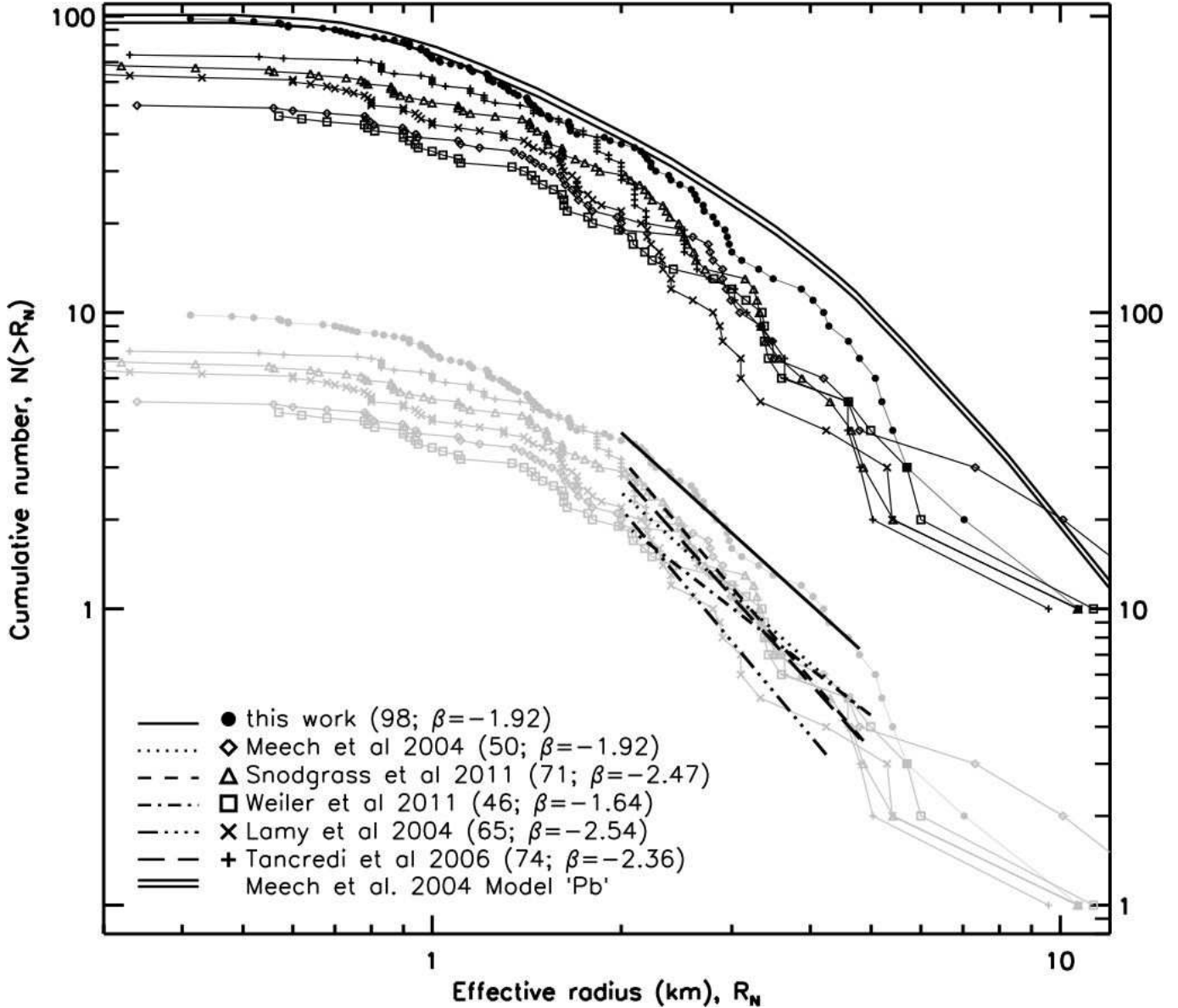


Figure 14. Comparison of our CSD with previous results. The top set of data curves shows six CSDs, including ours and the ones from L04, T06, W11, S11, and Meech et al. (2004). Also plotted here, with a double solid line, is model ‘Pb’ from Meech et al. (2004), the model that fit their CSD best. The bottom set of curves shows the same CSDs in grey – just displaced by a factor of 10 – underneath simple power-law fits to each of the CSDs over the range of  $2 \text{ km} < R_N < 5 \text{ km}$ . This is simply to help lead the eye in the general trend of the CSDs, and shows how ours has a similar overall shape. (It is *not* meant to show a *definitive* answer on the slope of each CSD.) The numbers in parentheses in each line of the legend indicate how many comets were included in the plot and the slope of the power-law fit in that 2-5 km range. We note that the ordinate’s left axis should be used with the top set of curves, and the right axis should be used with the bottom set of curves.